PTYS 594A: PLANETARY GEOLOGY FIELD PRACTICUM

K/T Boundary

28 September - 1 October 2006

Table of Contents

PtyS 594a: PLANETARY FIELD GEOLOGY PRACTICUM
Fall 2006: K/T Boundary Itinerary

Thursday, September 28

8:00 AM: Depart from the LPL loading dock. Proceed on Cherry to Speedway, and west on Speedway to Oracle, turn left and go north on Oracle. Drive north on State Highway 77 towards Globe and Show Low. Stop at the pullout on the south rim of the Salt River Canyon, where **Catherine Neish** will talk about spheroidal weathering and we will look at the exposed volcanic layers.

11:15 AM: Continue along Highway 77 through several exposures of unconsolidated gravels. 17.9 miles from the canyon stop, there is a pullout with a side road where we will stop for lunch.

12:30 PM: Depart lunch and continue along Highway 77. Turn right along Route 60 just after Show Low.

1:30 PM: Enter the Springerville Volcanic Field. 64.8 miles from the rim gravels pullout, we will pull off onto a side road near several cinder cones where **Jade Bond** will talk about the rim volcanism of the Colorado Plateau.

1:45 PM: Depart the volcanic field and continue through Springerville and into New Mexico. Stop for gas in Quemado.

3:30 PM: Continue towards Pie Town. Turn north in Pie Town and proceed towards chez Melosh along dirt roads.

5:00 PM: Arrive at Jay's cabin and camp. **Ellen Germann-Melosh** will give a fireside chat about the history of the Santa Fe trail.

Friday, September 29

8:00 AM: Depart camp and proceed north along a dirt road to Highway 117, where we will turn right and travel north through El Malpais National Monument.

9:00 AM: Stop at the pullout for La Ventana, a natural arch in the sandstone. **Colin Dundas** will talk about joints in rocks. We will then continue along Highway 117 to the Sandstone Bluff overlook.

9:30 AM: Arrive at the overlook, where there is a good view of McCarty's Flow. **Eric Palmer** will talk about recent basaltic volcanism at El Malpais National Park.

9:45 AM: Continue towards Grants, turn right on I-40 and drive towards Albuquerque. Along the way there are many mesas with a variety of mass wasting features. We will continue through Albuquerque, take the exit for I-25 and travel north towards Santa Fe.

12:00 PM: Arrive at Santa Fe, where we will take Exit 276B and follow Route 599. After mile marker 6, take a left turn; turn left at the T intersection, proceed 1.3 miles south, and turn right on Caja del Rio. Follow this for 2.8 miles, turn right on Camino del Rey and pick up Barb Cohen.

12:15 PM: Return to Route 599. We will head for a lunch stop near the shatter cone site. Take Rt. 599 all the way north (14 mi), take the exit towards Santa Fe (right lane), and immediately get into far left lane. Take left exit towards plaza/downtown/museums, and get in the left lane. At the traffic light, take a left onto Paseo de Peralta and stay left. At the second traffic light turn onto Bishop's Lodge Road. At traffic light turn right onto Artist Road (Route 475) and note the mileage. The site is 5.9 miles down Artist Road, but we will travel 7.1 miles to a nice lunch stop and turnaround area.

1:30 PM: Depart lunch and return down Route 475. 1.2 miles along we will stop at the pullout, where **Sam Stevenson** will talk about shatter cones and the recognition of impact craters. We will then retrace our route down Artist Road, turn left onto Bishop's Lodge, and turn right onto Paseo de Peralta. We will go through 3 traffic lights, and at 4th light (T junction) take a left onto St. Francis. Stay in left 2 lanes and take St. Francis back to I-25, return to I-25 and drive towards Las Vegas (the New Mexico version).

3:15 PM: Stop for gas and a bathroom break in Las Vegas.

5:00 PM: Stop at exit 435 and drive over to the pullout on the west side of the freeway. Here there is a good view of a large dike, and **Mandy Proctor** will talk about the mechanics of lava ascent. We will then continue north on I-25.

5:45 PM: Arrive in Trinidad, Colorado. Take exit 13B on Main Street. Turn right, then turn left onto Nevada Ave. Turn left onto Animas, and then left onto Prospect. Follow CO Route 12 to Trinidad Lake State Park campground. We may need to stop at the visitor's center, which is 0.6 miles further down the road, but to get to the campsite we take the turn for the boat launch and follow this road across a dam. Just on the far side of the dam is the turn and a gate. We will go through the gate and camp at the group campsite.

<u>Saturday, September 30</u>

8:00 PM: Depart camp. We will spend the day at several K/T layer sites. One of these is the Sierra Madre (?) railroad cut (unscouted). Directions to other outcrops:

Return to the main road (CO route 12), ~1.3 mi.
Turn left onto main road, proceed 6.0 miles west.
Turn left onto bridge to Long's Canyon.
Proceed 1.2 miles to the Madrid East exposure along the side of the road (~13 min from campsite). This is a very good exposure.
Continue on road to Long's Canyon. After 1.9 miles there is a left turn towards Long's Canyon and a parking area a short way down the road.
From here there is a short walk to an extremely long exposure. Talks here or at the railroad cut will include, in some order:
Impact ejecta deposition in the atmosphere and the double layer **(Tamara Goldin)**
Physics of impact cratering—events near the crater **(Kat Volk)**
Global seismic effects of the Chicxulub impact **(Jason Barnes)**
Structure of the Chicxulub impact crater **(Priyanka Sharma)**
The environmental effects of large impacts **(David Choi and Brian Jackson)**
Paleobotanical evidence for the K/T impact **(Diana Smith)**
The K/T and other impact boundaries around the world **(Dave O'Brien)**
Impacts on the Earth: Comets vs. asteroids and the present status of the NEO search **(David Minton)**
Physics of asteroid deflection **(Rory Barnes)**
This may also be our lunch site.

3.1 miles back to CO 12, turn right.
Retrace route back to Trinidad, enter I-25 southbound (9.5 mi).
Proceed 2.2 miles south, take Exit 11.
Cross to east side of I-25, take frontage road south.

Proceed 2.6 miles south from turn onto frontage road.

The site (Starkville site) is just past the end of the paved road and is good for sampling, with a little digging. **Please take samples here rather than at other sites, since other sites are used by ongoing scientific research! This site gets more traffic and is no longer used much.**

2.6 miles north back to I-25.

Go south on I-25 to exit 452 (Raton, New Mexico), ~19 miles south of Starkville.

Turn right at the exit.

Follow this road until turning left on 1st Street.

Go under an underpass, turn right immediately on the other side

Turn left on Moulton St.

Go 0.5 miles, turn left on Hill St. at the end of the pavement.

Follow Hill Street up the hill. Bear left at the Goat Hill intersection.

0.3 miles along.

0.5 miles from this junction is a pullout with the K/T layer.

(This site is a poor exposure, so we will probably skip it, but it is included for reference)

3:00 PM: Depart from the outcrops by this time and head south on I-25 towards Santa Fe.

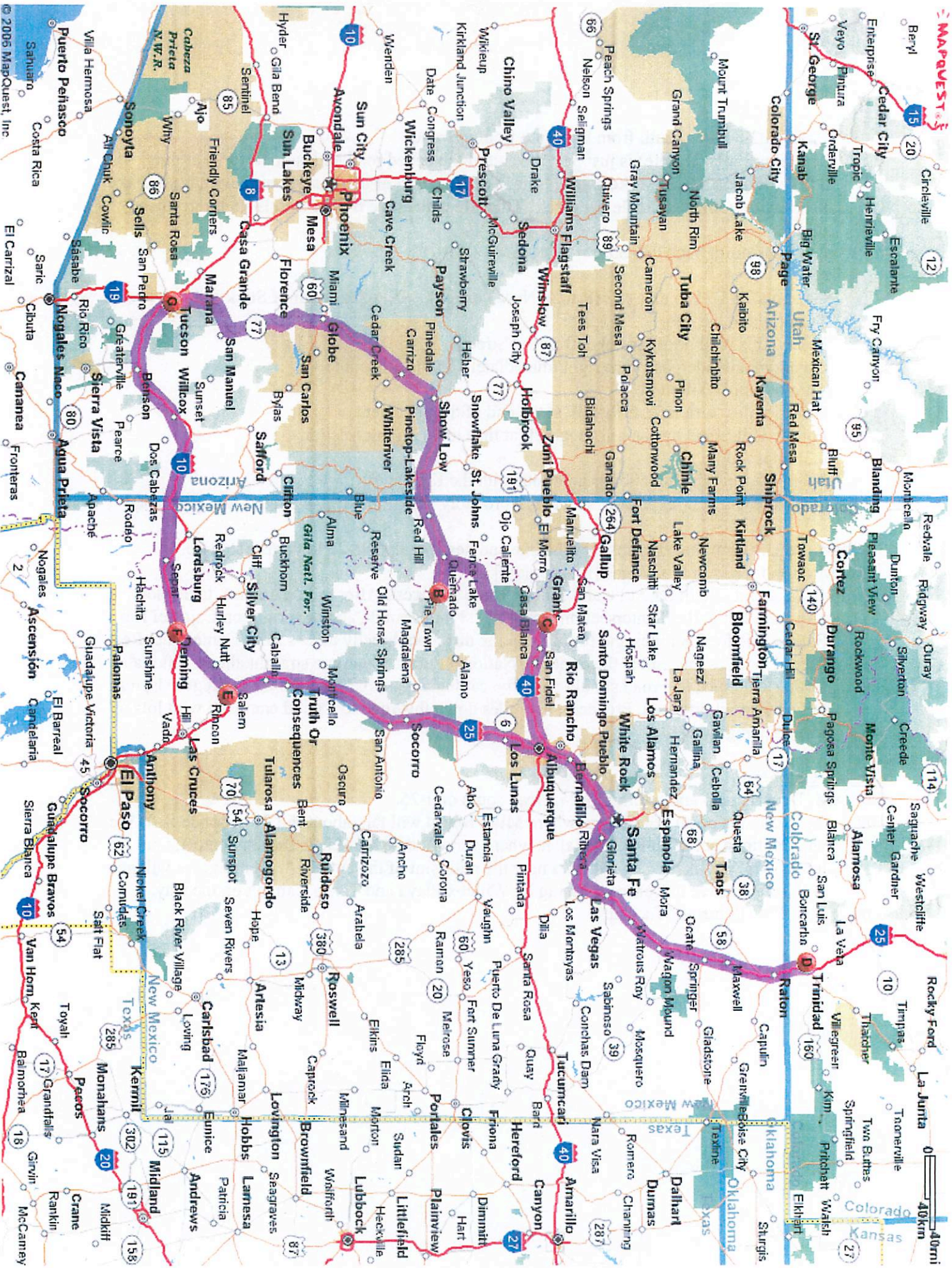4:30 PM: Stop for gas in Las Vegas [if necessary].

6:00 PM: Take exit 276 in Santa Fe and follow Route 599 west. After mile marker 6, take a left turn; turn left at the T intersection, proceed 1.3 miles south, and turn right on Caja del Rio. Follow this for 2.8 miles and turn left on the dirt road directly across from Camino del Rey. After 1.3 miles this enters the Santa Fe National Forest. Continue straight ahead. After a further 1.0 miles this road should pass two cattleguards. ~0.8 mi from the cattleguards, turn left on a small dirt road. Proceed ~0.4 miles down this road to a good campsite with lots of level, open ground.

Sunday, October 1

8:00 AM: Depart camp and return to I-25. Head south on I-25.

10:00 AM: Rest area north of Socorro, where **Mike Bland** will talk about the Rio Grande Rift. We will continue south on I-25 to Hatch, where we will take the Hatch-Deming cutoff. Our lunch stop will likely be a rest area near the midpoint of the cutoff. At Deming, we will get on I-10 and drive to Tucson, passing by Willcox Playa and Texas Canyon on the way.

5:00 or 6:00 PM: Return to Tucson.

Continue on Page 21

San Rafael

LAGUNA INDIAN RESERVATION

San Fidel Villa de Cubero

Chief Rancho

Anzac

McCartys

Acomita

ALBUQUERQUE

A

Alaska West Village

NE BDY

Sand Corner

Tinaja

CIBOLA NATIONAL FOREST

Aragon

El Morro

Quartz Hill

Paxton Springs

San Rafael Mesa

Jose Ignacio Canyon

Galla Peak

Cerritos Margaritas

Ice Cave & Bandera Crater

ZUNI MOUNTAINS

EL MALPAIS NCA

La Ventana Ridge

McCarty Mesa

EL MALPAIS NCA

El Malpais Nat Mon & NCA

Grants Lava Flow

Mesa Negra

Deep Spring

B

Mesa Encantada

EL MALPAIS NCA

El Malpais Nat Mon

EL MALPAIS NATIONAL MONUMENT
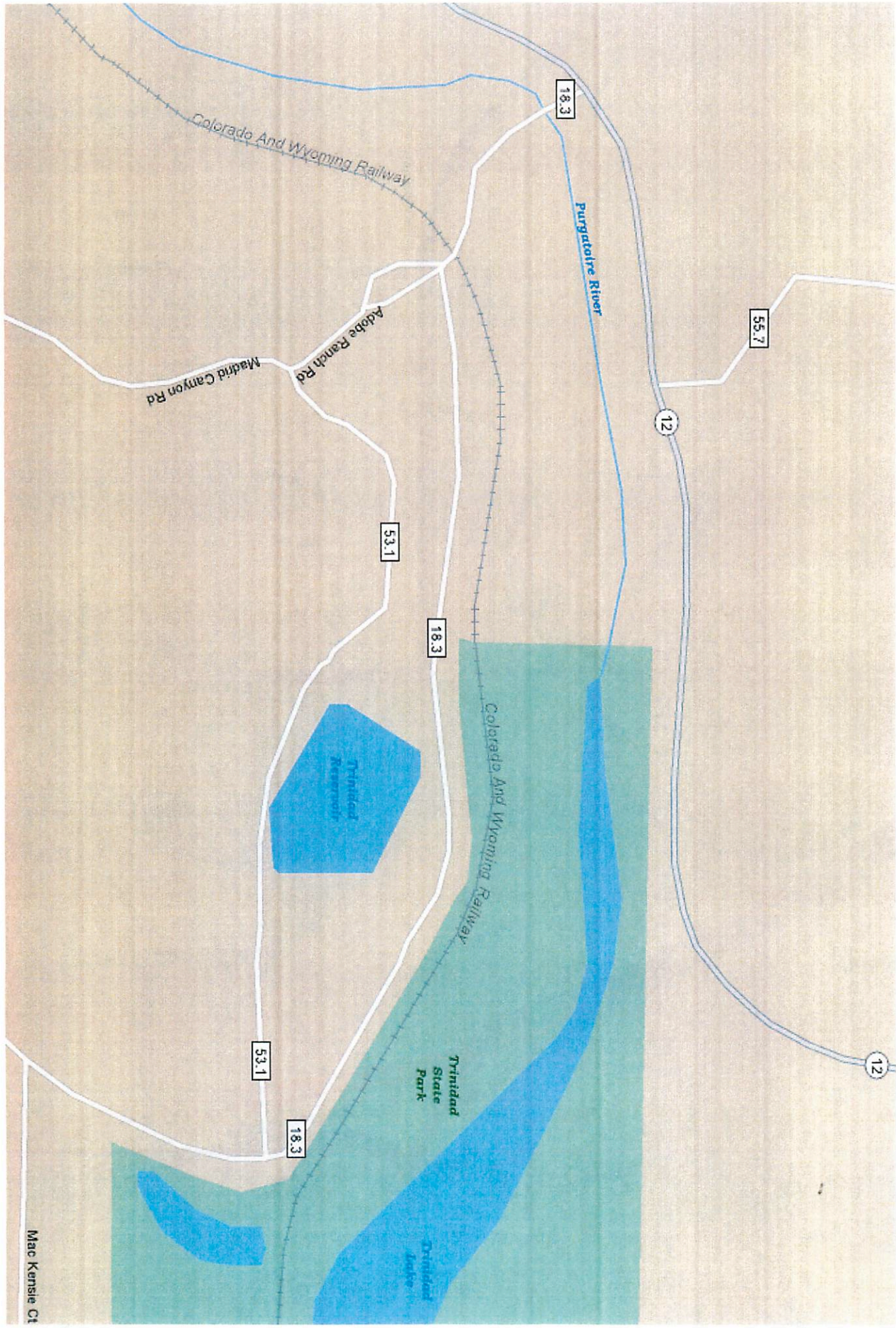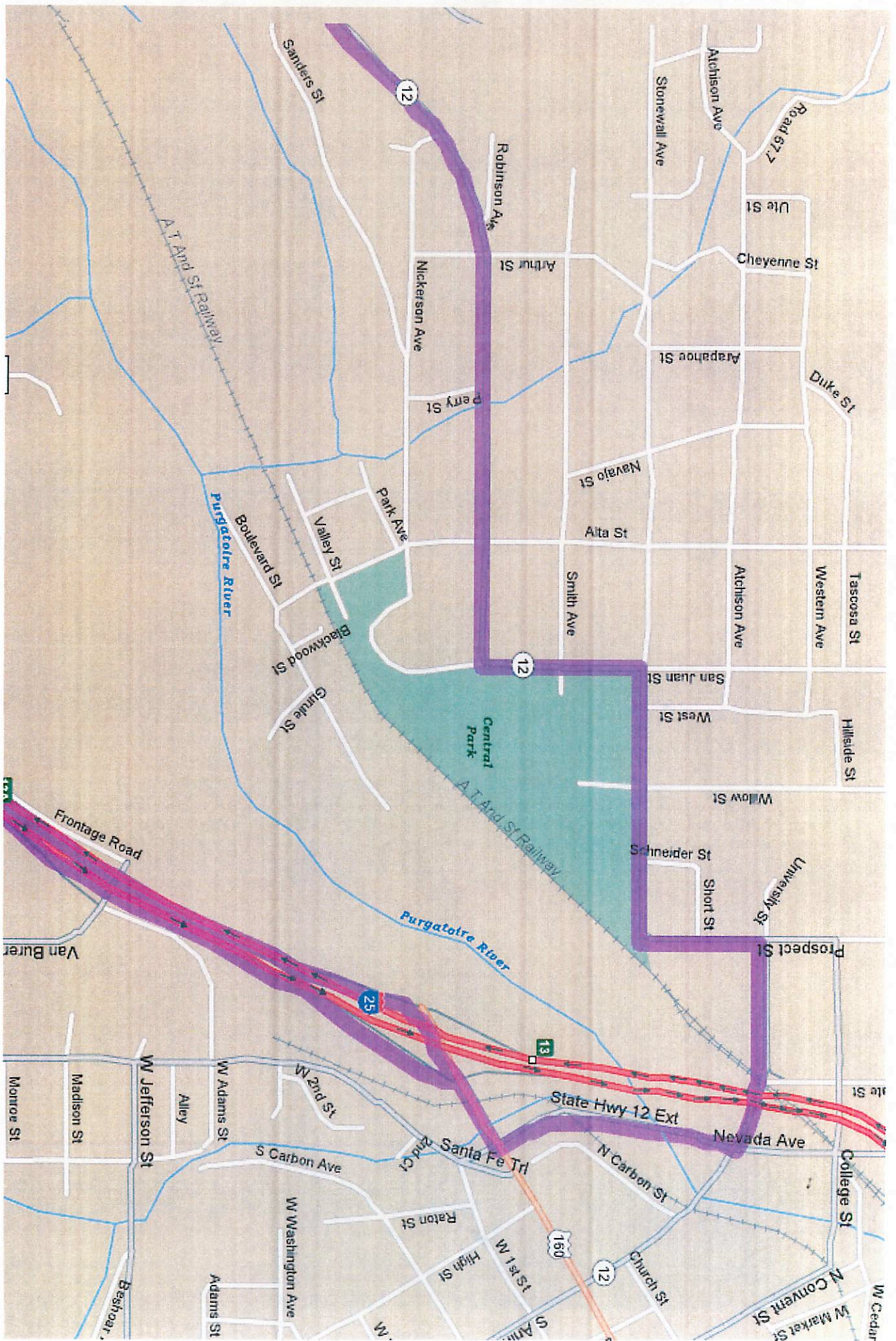
Zuni–Acoma Trail

AIR

NORTH CEBOLLITA MESA

Acoma Pueblo

Sky Spring

Acoma Pueblo

CONTINENTAL DIVIDE

THE MALPAIS

La Ventana Natural Arch

AIR

Kow-ina Ruins

ACOMA INDIAN RESERVATION

C

West Malpais Wilderness

Cerro Alto

EL MALPAIS NATIONAL CONSERVATION AREA

CEBOLLITA MESA

WINDMILLS

Cerro Brillante

PLAINS

Cebolla Wilderness

Cebollita Peak

D

EL MALPAIS NCA

El Malpais NCA

LAGUNA INDIAN RESERVATION

Cerro Pinto

EL MALPAIS NCA

Broom Mountain

NORTH

Blue Water

117

E

CIBOLA CO

CIBOLA CO

CATRON CO / SOCORRO CO

Willow Spring

Dulces Spring

Rio Salado

Wiley Spring

ABNIR

F

CONTINENTAL DIVIDE

Lehew

GRAVEYARD RD

ALAMO BAND NAVAJO IND RES

G

Tres Lagunas

603

CIBOLA NATIONAL FOREST

Madre Mountain

Silver Spring

GALLINAS MOUNTAINS

Pie Town

60

DATIL MOUNTAINS

Chavez Spring

H

Blue Spring

WINDMILLS

Mangas

Allegros Mountain

CONTINENTAL DIVIDE

Pine Park

Swingle Spring

Continue on Page 37

1" = 4.7 mi (7.6 km)

©DeLorme

Datil

SOCORRO

12

60

29

Colorado And Wyoming Railway

Purgatoire River

18.3

55.7

12

Madrid Canyon Rd

Adobe Ranch Rd

53.1

18.3

Colorado And Wyoming Railway

Trinidad Reservoir

Trinidad State Park

Trinidad Lake

53.1

18.3

12

Mac Kensie Ct

Trinidad
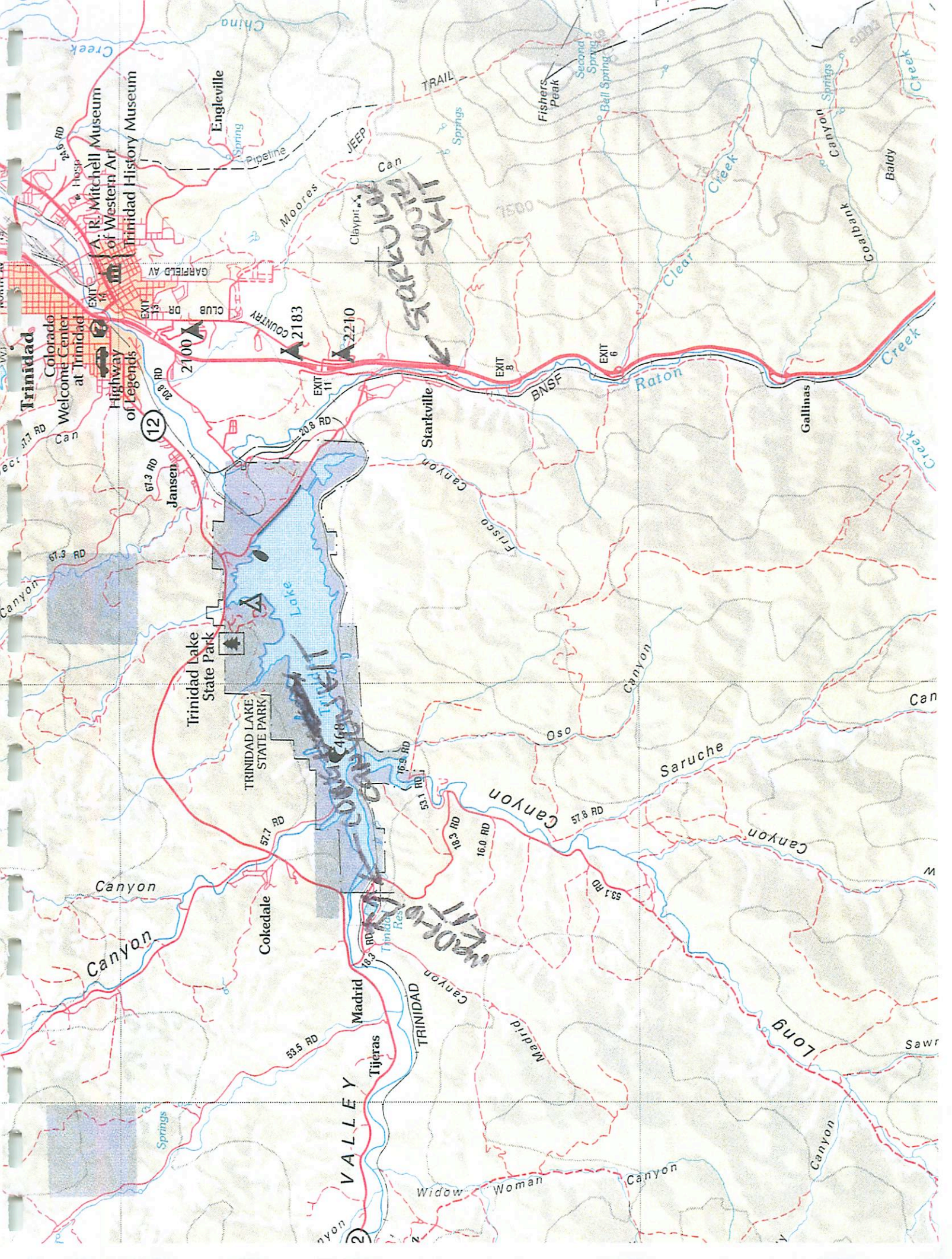
Colorado
Welcome Center
at Trinidad

A. R. Mitchell Museum
of Western Art

Trinidad History Museum

Englevile

Highway
of Legends

Jansen

Trinidad Lake
State Park

TRINIDAD LAKE
STATE PARK

Cokedale

Canyon

Canyon

Madrid

Tijeras

VALLEY

Starkville

Raton

BNSF

Saruche

Canyon

Canyon

Canyon

Long

Fishers
Peak

Baldy

Coalbank

Gallinas

Oso

Creek

Clear

Creek

China

Creek

EXIT 6
EXIT 8
EXIT 9
EXIT 11
EXIT 13
EXIT 14

246 RD
57.7 RD
61.3 RD
61.3 RD
20.8 RD
20.8 RD

GARFIELD AV
CLUB DR
COUNTRY

53.5 RD
53.1 RD
18.3 RD
16.0 RD
16.9 RD
53.1 RD
57.8 RD

2100
2183
2210

7500

JEEP
TRAIL
Pipeline
Spring
Moores
Claypit

Frisco Canyon

Bell Spring
Second
Springs
Springs

Lake

Trinidad
Res.

TRINIDAD

Widow Woman Canyon

Madrid

Canyon

Sawm

Springs

12
2

Spheroidal weathering:
An old favourite

by K/T Neish

Spheroidal weathering is a type of chemical and mechanical weathering that creates rounded rocks. Below is a brief description of the processes that form the rounded rocks, and examples of such exposures.

Step 1: Joint formation

Spheroidal weathering occurs when jointed rocks are exposed to chemical weathering by water. Joints are thought to be formed when a mass of rock experiences a drastic reduction in overlying pressure. When this pressure is removed, the rock mass begins to expand upward, forming lines of fractures. These fractures (or joints) split the rock into blocks that are approximately cube-like in shape (Figure 1a).
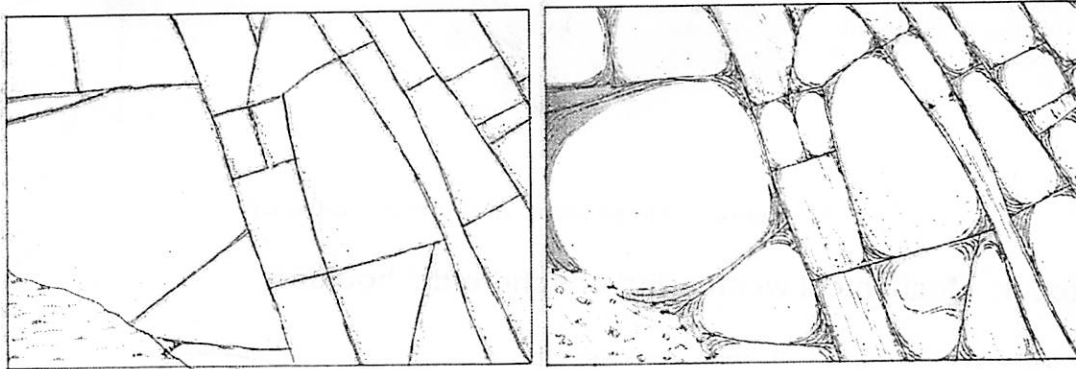

Figure 1: Sketches showing the evolution of spheroidal boulders. (a) Rock cut by a joint system. (b) Preliminary stages of spheroidal weathering.

Step 2: Chemical weathering of the rock surface

As rainwater falls to the earth, it dissolves carbon dioxide, becoming a weak solution of carbonic acid, H_2CO_3. As this water penetrates joints in the rock, it reacts with the minerals there. For example, potassium feldspar reacts with hydrogen ions to produce potassium ions, kaolinite (clay) and silica:

$$2KAlSi_3O_8 + 2H^+ + H_2O \rightarrow 2K^+ + Al_2Si_2O_5(OH)_4 + 4SiO_2$$
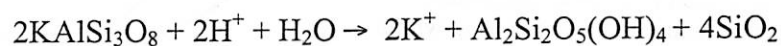
In this way, rock is converted into less-resistant clay, which can then be eroded away. Why then do the rocks become rounded? Since angular edges expose a greater amount of surface area than flatter surfaces, the corners weather faster, becoming rounded (Figure 2). The sphere is the geometric form that has the least amount of surface area per volume. Once the block attains this shape, it simply becomes smaller.

Figure 6.5
Geometry of sphe-
roidal weathering.

A. Solutions that oc-
cupy joints separating
nearly cubic blocks of
rock attack corners,
edges, and sides at
rates that decline in
that order, because the
numbers of corre-
sponding surfaces are
3, 2, and 1. Corners
become rounded;
eventually the blocks
are reduced to spheres.

B. Energy of attack
has now become dis-
tributed uniformly
over the whole sur-
face, so that no further
change of form can
occur.

Attack on three sides

Attack on two sides
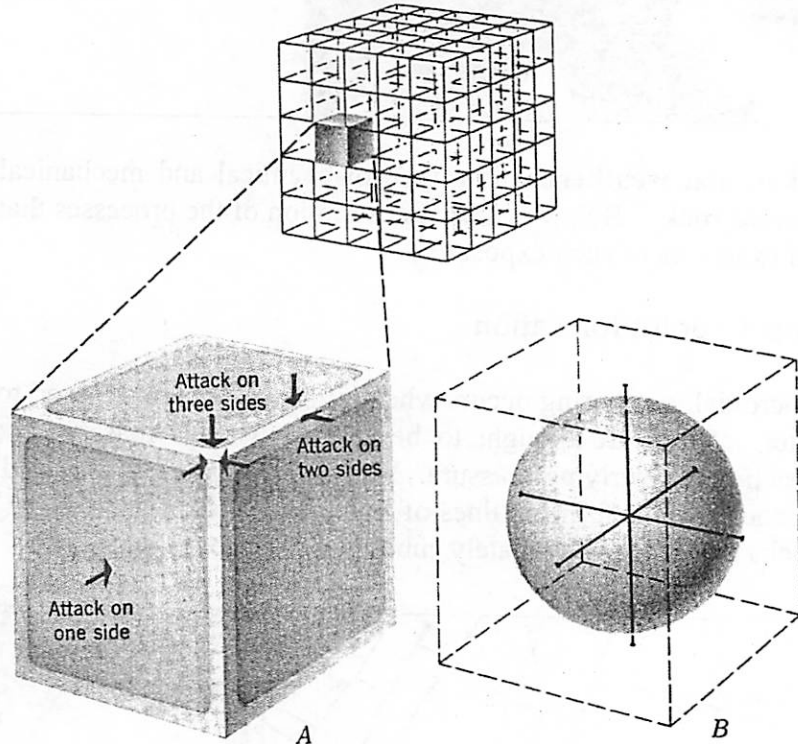
Attack on one side

A

B

Figure 2: The geometry of spheroidal weathering.

Step 3: Mechanical weathering of spheroidal boulders

Erosion of the decayed rock exposes the rounded boulders. This allows chemical weathering to penetrate deeper into the rock. As the feldspar weathers to clay, the rock increases in size, exerting an outward force that causes concentric layers of rock to break loose and fall off the unweathered core like an onion skin (Figure 3).
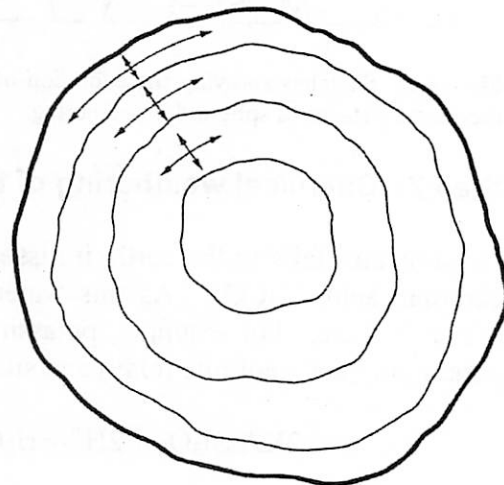
Figure 3: A cross section through a spheroidally weathered boulder showing the stresses set up within the rock.

Unlike joint formation, these shells develop from pressures set up within the rock by chemical weathering. This is an example of chemical weathering producing forces large enough to cause mechanical weathering.

Certain types of rock are more vulnerable to spheroidal weathering than others. Igneous rocks such as granite, diorite, and gabbro are particularly suspectible because they contain a large fraction of feldspar, which produces minerals of larger volume when chemically weathered.

The process of spheroidal weathering is generally slower than other types of weathering. It becomes especially slow at lower temperatures, since low temperatures inhibit the chemical breakdown of feldspar. Thus many granitic mountain peaks are jagged and craggy rather than rounded (Figure 4).
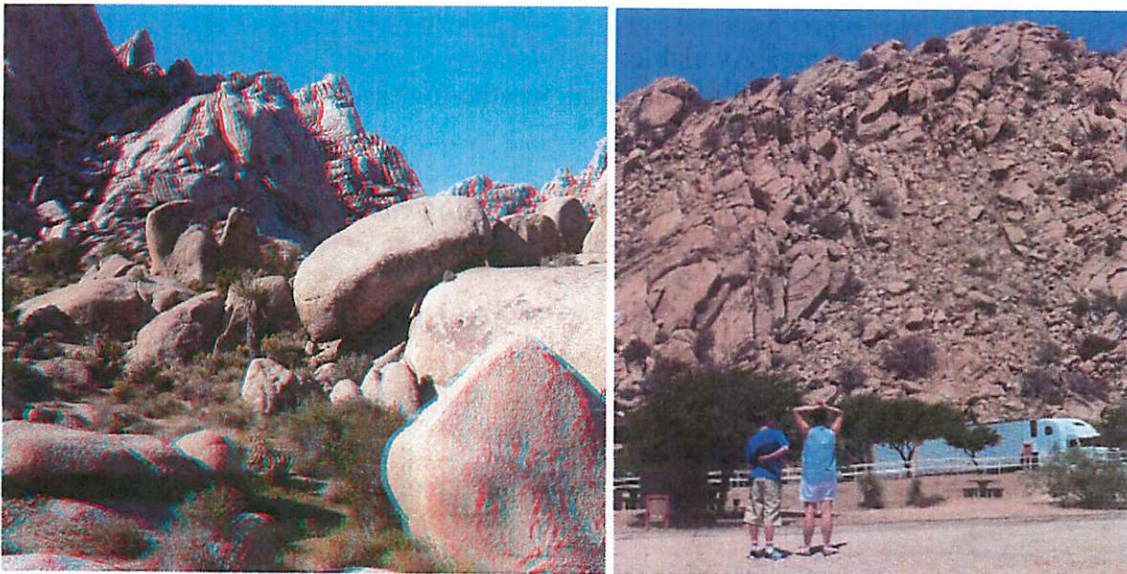

Figure 4: Examples of spheroidal weathering. (a) A 3D look at spheroidally weathered boulders in the Granite Mountains of Mojave National Preserve (which you may remember from the Death Valley trip). (b) The site of earlier field trip talks on spheroidal weathering - Texas Canyon on I-10 east of Tucson.

Planetary connection

Hints of spheroidal weathering have been seen on Mars by the Spirit Rover (Figure 5). If the spheroidal pattern in Figure 5 is indeed due to spheroidal weathering, it would indicate that the basalt has been exposed to groundwater, lending evidence to a wet Martian past.

Figure 5: A basaltic block on Mars that shows what might be spheroidal weathering. Taken in Gusev Crater by the Spirit Rover on Sol 103.

References

- Beyer, R. 2001. 'Spheroidal weathering in Texas Canyon, AZ' in D. O'Brien and F. Ciesla (Eds.) *Southern New Mexico Planetary Geology Field Practicum.* Tucson, AZ: Lunar and Planetary Laboratory Press.

- Flint, R.F. and Skinner, B.J. 1974. *Physical Geology: Second Edition.* New York: John Wiley & Sons.

- Hamblin, W.K. 1973. *The Earth's Dynamic Systems: Second Edition.* Minneapolis: Burgess Publishing Company.

- Leet, D.L., Judson, S., and Kauffman, M.E. 1982. *Physical Geology: Sixth Edition.* Englewood Cliffs, New Jersey: Prentice-Hall.

- *Spheroidal weathering.* Available: http://en.wikipedia.org/wiki/Spheroidal_weathering [accessed 20 September 2006].

- Tarbuck, E.J. and Lutgens, F.K. 1997. *Earth Science: Eighth Edition.* Upper Saddle River, New Jersey: Prentice-Hall.

14

Rim Volcanism of the Colorado Plateau
By Jade Bond

Colorado Plateau:

The Colorado Plateau is a region of high standing, relatively undeformed crustal material surrounded by highly deformed areas (Rocky Mountains, Basin and Range Province) (Foos, 1999). Estimated as being at least 500 million years old, the Colorado Plateau covers more than 130,000 square miles (336,700 km²), making it larger than each of the U.S. states except for Alaska, Texas, California, and Montana (Fig. 1). Elevations on the plateau range from 3,000 to 14,000 feet (914m to 4267m), with an average elevation of approximately 6,500 feet (2km).

During the Late Cretaceous, this area was located near sea level, resulting in the region being dominated by sedimentary units. The area later underwent epeirogenic uplift (uplift without significant deformation or mountain building) starting approximately 25 Ma with most of the uplift occurring in the past 5 million years (Sahagian et al., 2002).
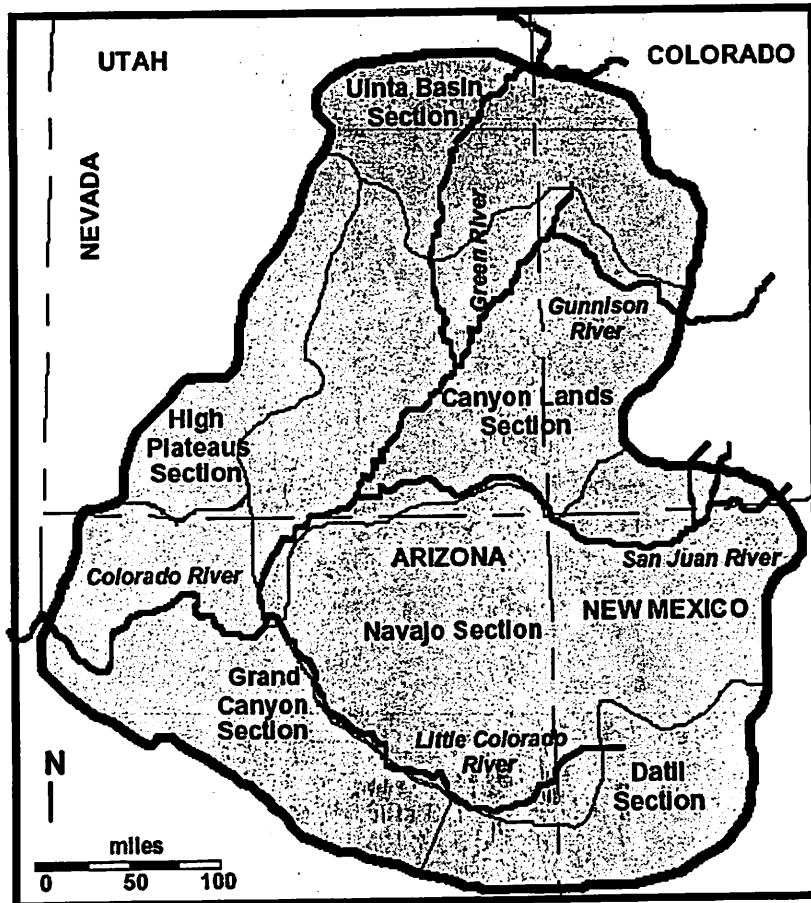
Figure 1: Map of the main provinces of the Colorado Plateau (Foos, 1999)

Volcanism on the Colorado Plateau:

Although dominated by sedimentary units, there is some volcanism located within the Colorado Plateau. During the Oligocene (~25 Ma), magmas migrated upwards through faults in the basement rocks of the plateaus. This produced 2 types of igneous features: laccoliths and lava flows and cinder cones.

Laccoliths are an igneous intrusion that has been injected between two beds of sedimentary rock at shallow depths. Overtime, the weaker sedimentary units are eroded away, leaving the igneous rock exposed, often as a ridge or mountain. Those on the Colorado Plateau (e.g. Henry, La Sal, and Abajo Mountains) have an intermediate composition and were intruded during the Oligocene to Miocene period (20-30 Ma).

Most recent igneous activity, however, is located on the rim of the Colorado Plateau (Fig. 2). Lava flows and cinder cones have been deposited along much of the rim of the plateau within the last 6 million years and some are very recent (see Eric Palmers handout for more

information). The San Francisco field, located north of Flagstaff, is one example of such a rim volcanism. Generally the older rim volcanics tend to be more andesitic in composition while the younger ones are basaltic in composition.
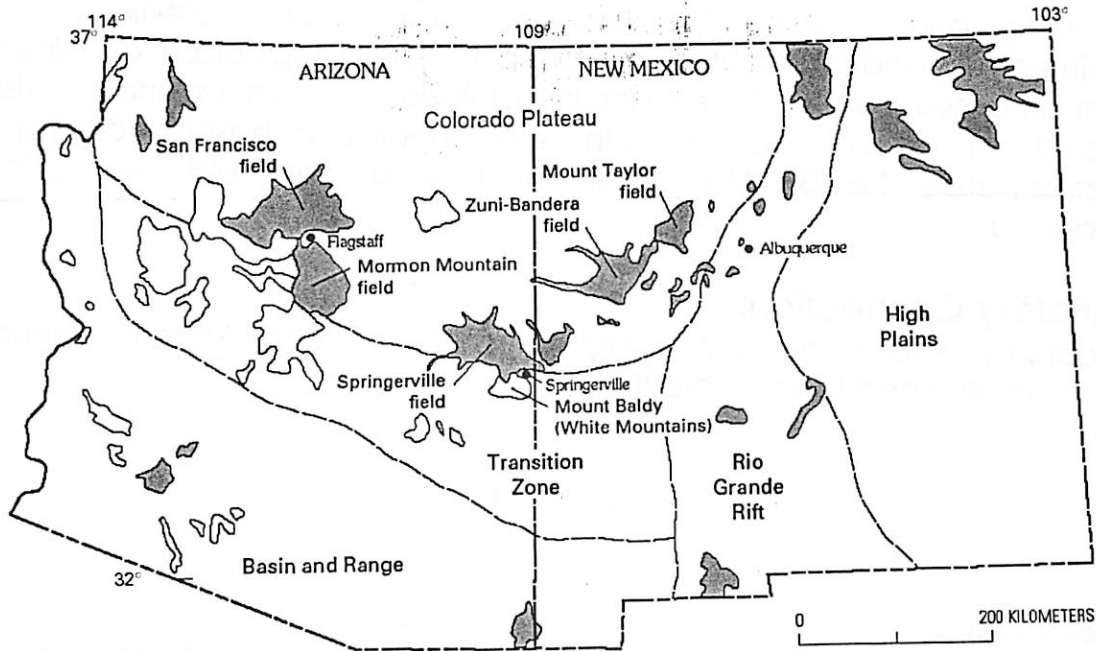

Figure 2: Distribution of volcanic fields on the Colorado Plateau. Shaded areas represent volcanic rocks of Pliocene to Holocene age (<5 Ma); outlined areas represent, volcanic rocks of Miocene or older age (>5 Ma).

Springerville Volcanic Field:
The Springerville Volcanic field is the southernmost of the rim volcanic fields, stretching across the transition zone from the Colorado Plateau to the Basin and Range Province. Located on the Arizona – New Mexico border, it covers approximately 3,000 km², making it the third largest volcanic field in the continental United States (after the San Francisco and Medicine Lake Fields). The Springerville field contains over 400 cinder cones and many flows. Most of the field is between 2.1 and 0.3 million years old with six dated flows having older eruptions of 2.94 Ma, 3.1 Ma, 6.6 Ma, 7.6 Ma, 8.66 Ma and 8.97 Ma (Condit et al., 1993). Additionally, regional alignments of the cinder cones have been observed to parallel

the rim of the Colorado Plateau, suggesting that this alignment reflects the structural margin of the plateau.

The majority of the mapped area is composed of alkalic basaltic rocks (poor in silica and rich in sodium), usually olivine phyric basalts. The chemical evolution of the field can be traced through the ages of the various eruptions. Initially, the eruptions consisted of theoleiitic basalts (olivine-poor, and dominated by clinopyroxene, plagioclase and iron). Over time, we can trace the decline of theoleiitic basalts and the rise instead of alkalic basalts with the theoleiitic basalts declining approximately 1.67-0.97Ma when the bulk of the field was being produced.

Planetary Connection:
Volcanism is known to occur throughout the Solar System. Mars, Io, Venus . . . do I really need to say more?!

References
Condit, C. D., Crumppler, L.S. & Aubele, J. C., 1993. Lithologic, age group magnetopolarity and geochemical maps of the Springerville volcanic field, east-central Arizona. http://geopubs.wr.usgs.gov/i-map/i2431/i2431pamphlet.pdf

Foos, A., 1999. Geology of the Colorado Plateau. http://www2.nature.nps.gov/geology/education/foos/plateau.pdf#searc h=%22geology%20of%20the%20colorado%20plateau%20foos%22

Sahagian, D., Proussevitch, A. & Carlson, W., 2002. Timing of the Colorado Plateau uplift: Initial constraints from vesicular basalt-derived paleoelevations. *Geology*, 30, 9, 807-810.

Joints in Rocks
Colin Dundas

Definition: A joint is a fracture in rock with small, dominantly opening (mode I) displacement, as opposed to a fault where shearing occurs.

Some authors refer to "shear joints" with some shearing displacement. Pollard and Aydin (1988) consider these to be faults, and assert that "the concept of shear joints is sheer nonsense."
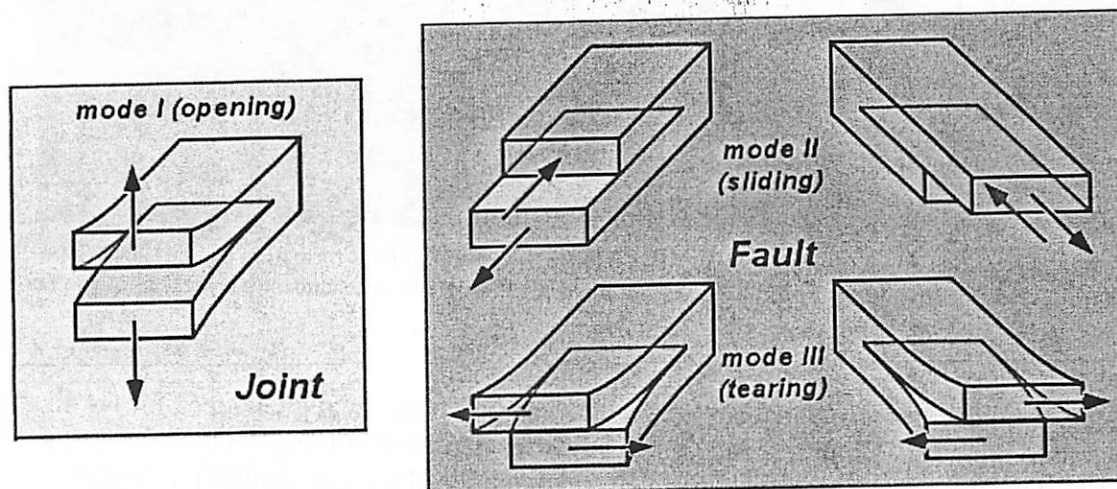

Figure 1: Rock fracture modes (from www.naturalfractures.com)

Why do these matter?

Jointing is a common mode of rock fracture which can create regular zones of weakness. This can affect the erosion of the surface, since there will often be enhanced erosion along joint sets by wind or streams. Joints may also break up large rock bodies into small pieces which are more readily transported. At depth, they can also influence groundwater flow. Tectonically, joints are important as indicators of the state of stress which formed them, and also can later be turned into faults since it is easier to slip along a preexisting break than to form a new one.

Field Observations

Fresh joint surfaces have several interesting features. Joints may initiate at discontinuities or flaws in the rock which locally concentrate the stress. Hackle marks (small three-dimensional structures on the joint surface) commonly form radiating plumose structures around the origin. Rib marks are similar to hackles but form at right angles to them, indicating former positions of the joint edge. These can be used to determine the direction of joint growth.

Joints can have a variety of types of intersection and interaction depending on the conditions of formation. For instance, joints forming near each other affect the local stress field and deflect each other. Joints usually form an ordered joint set in a body of rock with (approximately) regular geometry. In layered rock individual joints are frequently confined to a particular layer, with a joint spacing roughly equal to layer thickness, but this is not always true.
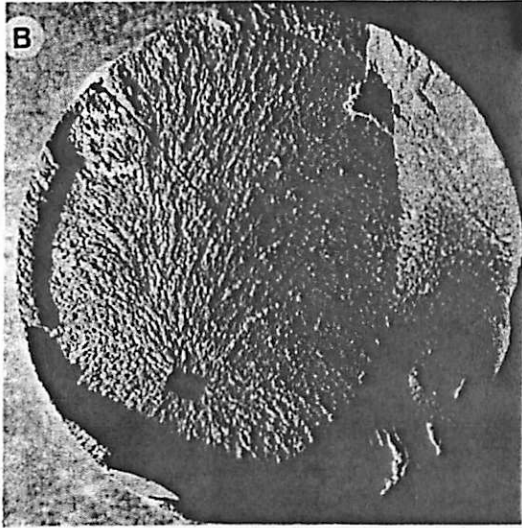
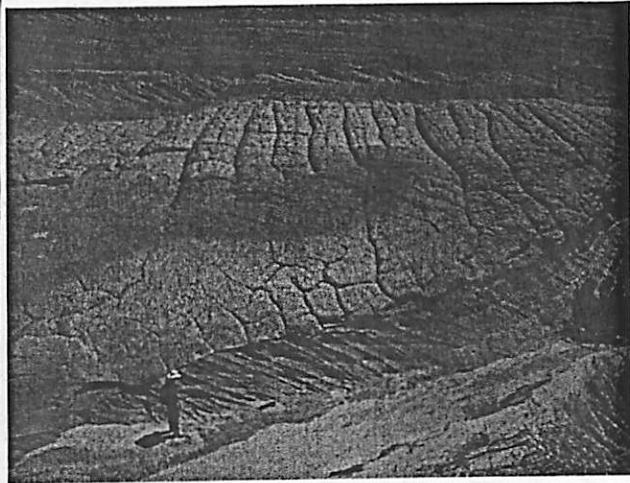**Figure 2:** Plumose structure around joint origin. (From Pollard and Aydin 1988)

Figure 3: Control of joint formation can be subtle; here joints have formed in one sandstone layer but not another.

Mechanics

Joints form due to extensional stresses, which can be caused by regional tectonics or local effects like fluid pressure. (Compressional mode I stresses do different things). Once formed, a crack relieves the stress in the rock for some distance around it (the stress shadow). A bigger joint has a larger stress shadow. This determines the minimum joint spacing and the proportion between joint spacing and layer thickness, and eventually results in fracture saturation, where strain is accommodated only by widening existing fractures. However, this breaks down if the joints are curved or there is significant fluid pressure (Bai and Pollard, 2000; Bai et al., 2000).

Hobbs (1967) provided a commonly used model of joint formation termed the stress-transfer model, with a strong layer coupled to weaker layers with welded boundaries. This can produce a constant joint spacing (Narr and Suppe, 1991). Unfortunately, like most theories of joint formation this has difficulty explaining fracture saturation, and instead predicts ever-increasing fracture density with increasing strain (reviewed by Bai and Pollard, 2000). This may have been resolved by numerical models which predict compression between joints, producing a minimum joint spacing (Bai and Pollard, 2000).

There's lots of math and numerical modeling associated with these...check the references.

Joints on other planets

Joints should form in appropriate stress conditions in rocks on any planetary body. They are fine-scale features, but might be observable in remote-sensing data through their influence on topography, erosion, etc. For instance, the location of closely spaced, regular yardangs in the Medusa Fossae Formation on Mars could be controlled by the location of joints (Bradley et al., 2002). Also, the same basic physics applies to the formation of columnar joints in basalt (Mars, Venus, Moon, Vesta, Mercury, Io) or other cooling volcanic rocks, periglacial polygonal terrain (Mars), and mud cracks (Mars?).
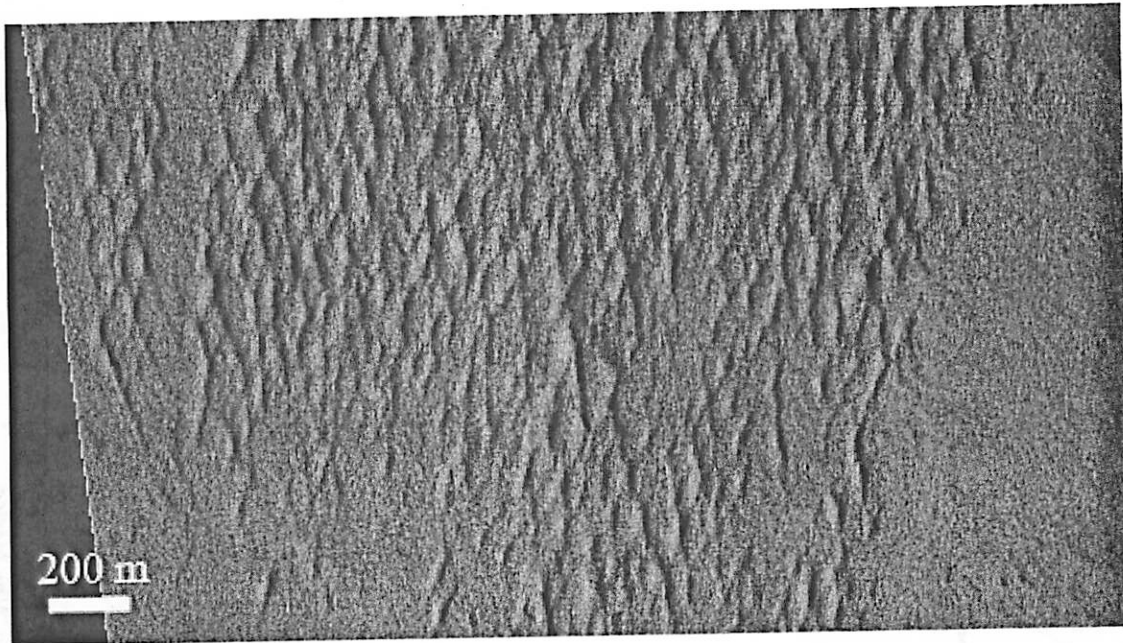
Figure 2: Joint-controlled yardangs in the Medusa Fossae Formation?

References:
Bai, T., Pollard, D. D., 2000. Fracture spacing in layered rocks: a new explanation based on the stress transition. Journal of Structural Geology 22, 43-57.

Bai, T., Pollard, D. D., Gao, H., 2000. Explanation for fracture spacing in layered materials. Nature 403, 753-756.

Bradley, B., A., 3 others, 2002. Medusa Fossae Formation: New perspectives from Mars Global Surveyor. Journal of Geophysical Research 107 (E8).

Hobbs, D. W., 1967. The formation of tension joints in sedimentary rocks, an explanation. Geological Magazine 104, 550-556.

Lachenbruch, A. H., 1961. Depth and spacing of tension cracks. Journal of Geophysical Research 66 (12), 4273-4292.

Narr, W., Suppe, J., 1991. Joint spacing in sedimentary rocks. Journal of Structural Geology 13, 1037-1048.

Pollard, D. D., Aydin, A., 1988. Progress in understanding jointing over the past century. Geological Society of America Bulletin 100, 1181-1204.

El Malpais-Zuni Volcanic Activity
Eric E. Palmer

Figure 1. Geologic map of El Malpais and surrounding area, New Mexico.
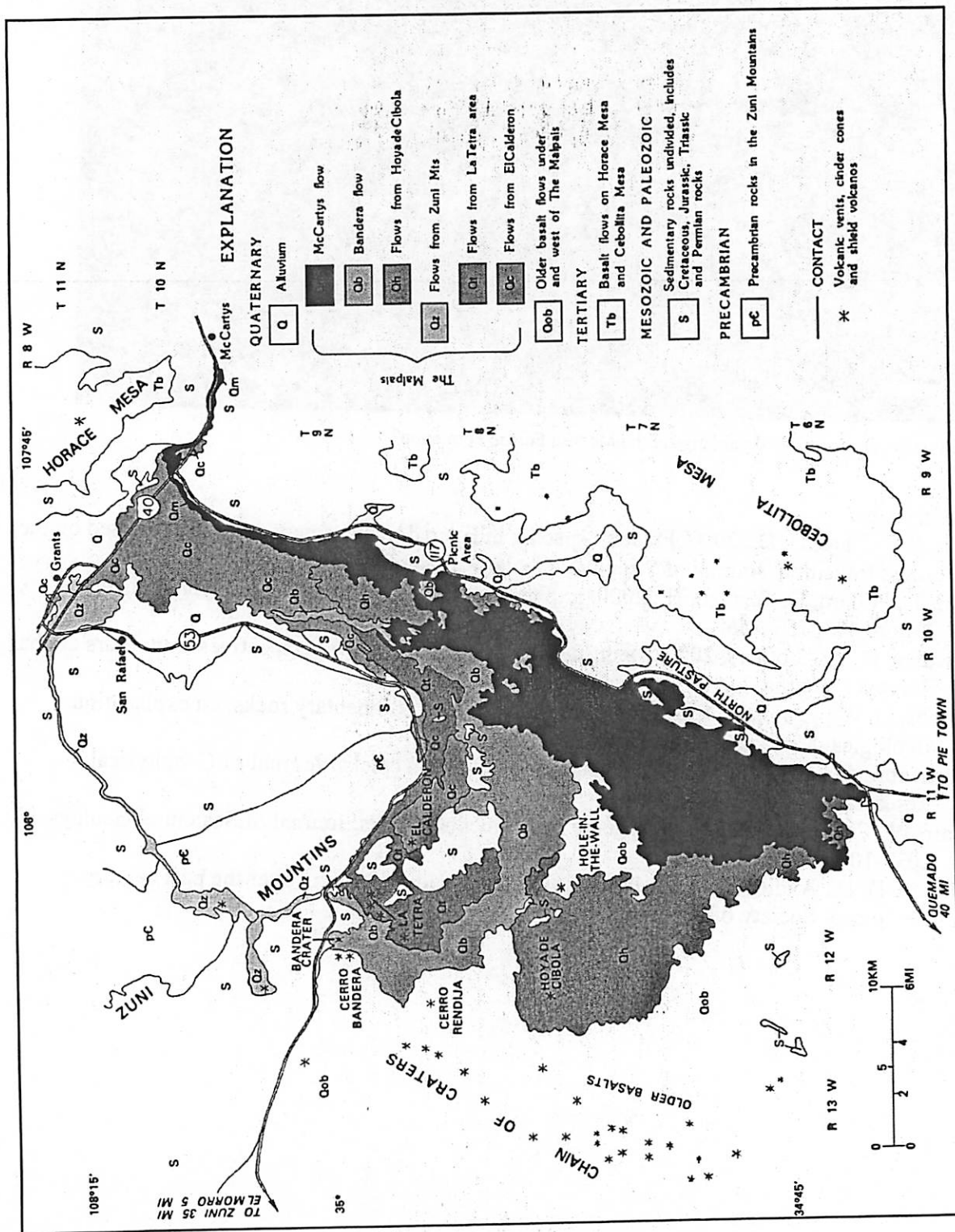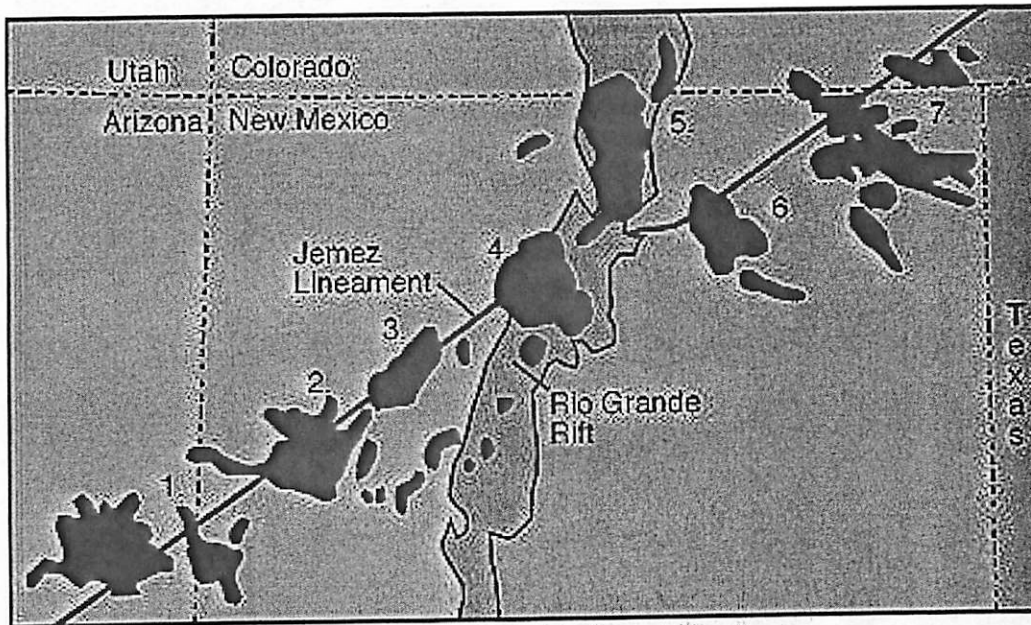
The El Malpais lava flows are just on the edge of the larger Zuni-Bandera lava field. The zuni-Bandera lava field is part of the Jemez volcanic lineament as seen in the Figure.

The Zuni-Bandera lava field covers an area of 2,460 square kilometers and a thickness 20 to 60 meters of lava. Around 100 km³ of lava was erupted from 74 vents that tend to be aligned along faults and fissures. The ages of the flows are from between 0.7 m.a. to 3.0 k.a. (very young)

Its volcanic activity is marked by cinder cones, spatter ramparts and cones, small shields, maars, and collapse pits. Lava flows exhibit pahoehoe, aa, and block surface textures and are extremely long, up to 90 km.

There are many lava tubes, up to 28.6 kilometers long. Other surface morphologies indicative of tube-fed lava characterize some of the flows and include pressure ridges, tumuli, linear squeeze-ups, grooved lava, and collapse pits [3].

Geochemical data from some of the lava flows

	Bluewater	Laguna	McCartys	Twin Craters	Bandera [4]
SiO_2	51.62	50.23	51.48	48.86	44.47
TiO_2	1.25	1.53	1.41	1.44	3.04
Al_2O_3	15.13	14.50	15.18	14.84	15.22
Fe_2O_3	11.49	1.82	11.87	12.48	4.39
FeO	N.A.	9.27	N.A.	N.A.	8.42
MnO	0.16	0.17	0.16	0.17	0.15
MgO	7.42	9.45	8.29	9.15	9.30
CaO	9.30	8.83	9.11	8.87	8.80
Na_2O	2.60	2.91	2.78	2.81	3.38
K_2O	0.42	0.77	0.69	0.74	1.60
P_2O_5	0.15	0.22	0.19	0.22	0.58
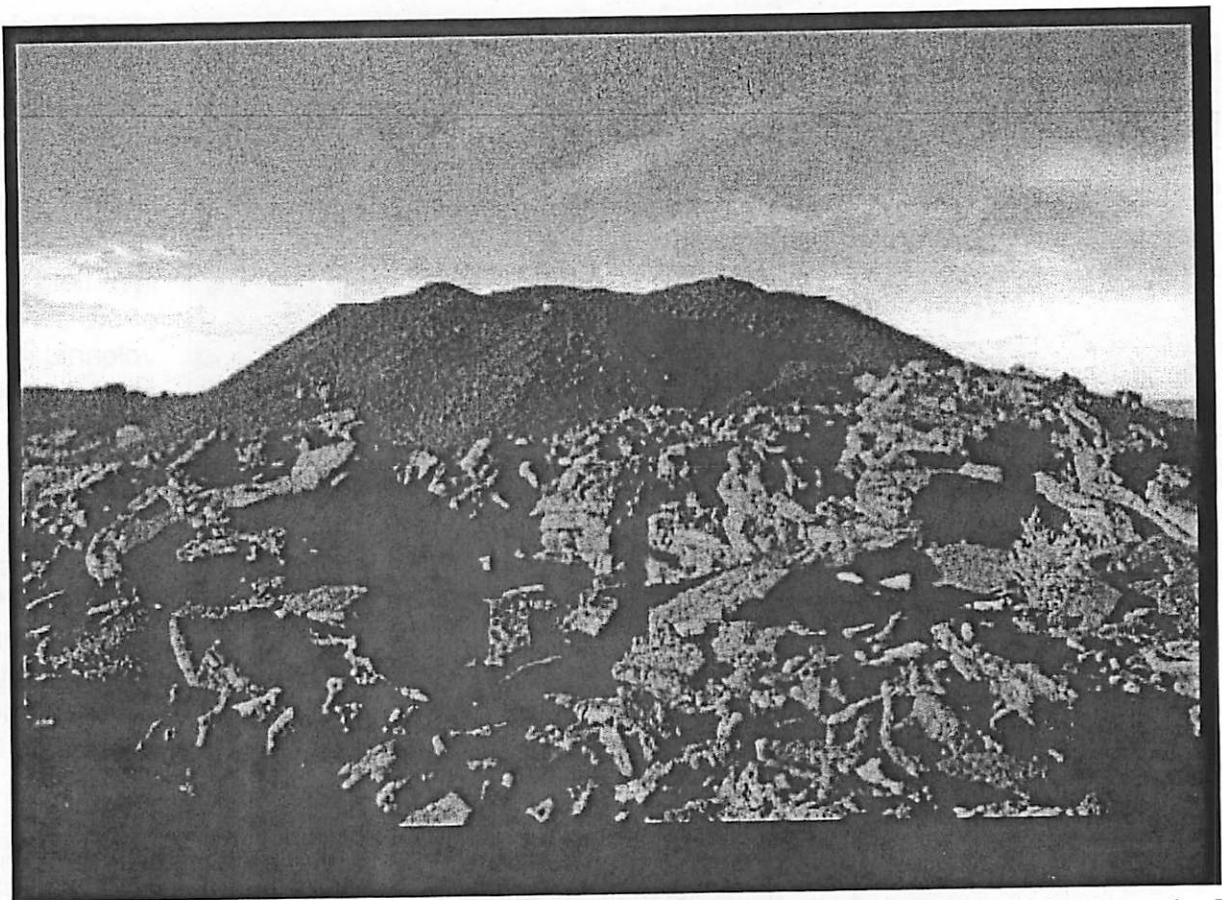
The vent area of the McCartys lava flow, El Malpais-Zuni-Bandera Field. Photo by L. Crumpler [1]

McCartys Flow

McCartys flow is the youngest basalt flow within the Zuni-Bandera volcanic field, about 3,000 years based on C14 dating. Its source is a small cinder cone about 8 m high sits on top of a broad shield. The lava flowed a long distance (8 km to the SW to over 40 km NNE) due to the low amount of silicon (see geochemical data) which has a low viscosity. It is on top of some older basalts of the Zuni-Bandera volcanic field and Holocene alluvium.

The lava is vesicular (lots of holes) and has many small crystals in it (phenocrysts) making it a porphyritic basalt. These crystals are mostly plagioclase between 0.2 and 1.5 cm. However further from the vent, there is an increase in the amount of mafic phenocrysts you will find (basically, small olivine crystals). This shows that the last lava erupted (nearest to the vent) was becoming more silicon rich. [3]

Bandera Crater Flow

Further to the west is the most interesting geologic area of El Malpais. The Bandera crater flow is the largest (about 150m high and 1 km in diameter) of a whole series of cinder cones called the "Chain of Craters". There is a short hike to its summit where you can see bedding of

Lapilli and variations in the cinders from red to black matching the changing amount of Fe to Mg in the lava. Bandera crater and lava flow erupted around 10,000 years ago.

If you go there, or look at an aerial photo, you would note that most of these craters (to include Bandera) breach to the SW. During eruption, the prevailing winds in this region cause the NE crater to become high, but the cinders that will make up the SW will be blown downwind, making a lower, but wider wall. Typically, these cinder cones will fill up with lava, making a lava lake. The lower SW walls typically breach, as can be seen with most of these craters.

The basaltic nature of the lava created many lava tubes, the longest of which extends from the breach in Bandera's crater wall. The lava tube runs for about 29km to the south and creates a set of caves. One cave, known as the Ice Cave, was used as a source of ice for the nearby towns. However, now the cave is a tourist attraction displaying ice columns and green ice. They claim that the ambient temperature never goes above 31 degrees F.

The lavas are vesicular near the surface with nephenline normative composition. There are both crustal and mantle xeonliths (rocks taken from the side walls of the lava vent) as well as some anorthclase megacrysts - $(K,Na)AlSi_3O_6$, a sodium rich feldspar.

NAME	VENT	TYPE OF FLOW	AGE [3]
McCartys	McCartys shield	Pahoehoe sheet flows, aa	2,500-3,900
Bandera	Bandera Crater	Aa and tube fed pahoehoe	9,500-10,900
Cerro Hoya	Cerro Hoya shield	Pahoehoe sheet flows	
Lava Crater	Lava Crater shield	tube fed pahoehoe	16,000
Lost Woman Crater	Lost Woman cin cone	Channel & tube pahoehoe	
Twin Craters	Twin Craters cin cone	Channel aa & tube pahoehoe	15,800-17,800
Laguna	El Calderon		33,400
Bluewater flow	El Tintero cin cone		35,600-79,000
Candelaria	Cerro Candelaria	aa	
El Calderon	El Calderon cin cone & shield	Aa & pahoehoe	115,000
Zuni Canyon	Paxton Springs cin cone	Channelized aa	> Bandera, < Bluewater
Oso Ridge	Oso Ridge cin cone	Aa	> Zuni Canyon, < El Calderon
Plagioclase lava	South Rendija shield	Pahoehoe sheet	
Cerro Rendija	Cerro Rendija shield	tube fed pahoehoe	
Cerro Encierro	Cerro Encierro shield	tube fed pahoehoe	
Ramah Navajo			7.65 million years
Fence Lake flow	unknown		0.6-0.7 million years
North Plains basalts	unknown		0.6-0.7 million years

[1] Crumpler, L.S. and Aubele, J.C. Volcanoes of New Mexico: An abbreviated Guide for Non-specialists. New Mexico Museum of Natural History and Science, 1801 Mountain Road NW, Albuquerque, NM 87104

[2] http://vulcan.wr.usgs.gov/Volcanoes/NewMexico/description_new_mexico_volcanics.html

[3] http://geoinfo.nmt.edu/tour/federal/monuments/el_malpais/zuni-bandera/background.html

[4] Laughlin, et al. Field-trip guide to the geochronology of El Malpais National Monument and the Zuni-Bandera Volcanic Field, NM. Los Alamos National Laboratory, Los Alamos, New Mexico 87545

[5] http://volcano.und.edu/vwdocs/volc_images/north_america/mccartys_flow.html

Shatter Cones and Impacts

Samantha Stevenson

Shatter cones are fracture features which have been demonstrated to be associated with impacts. As their name indicates, they appear conical in shape, and occur on size scales from centimeters to meters. This makes shatter cones the only shock-metamorphic feature known to occur on scales larger than the microscopic.
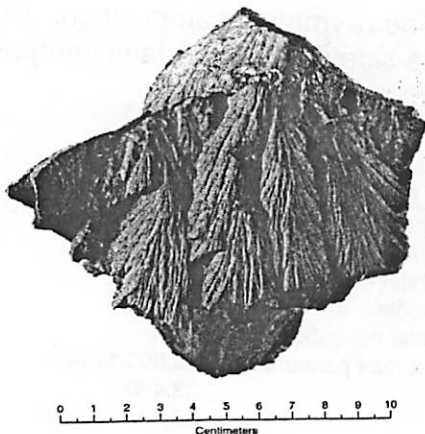
Shatter cones form when the shock wave from an impact encounters a heterogeneity (typically a mineral inclusion) within the underlying rock. The wave is scattered off of these inclusions, which can result in the above patterns of interlocked cones. Each cone is believed to result from an individual scattering event.

Shatter cones are observed in all kinds of target rocks: everything from sandstone and shale to carbonates and crystalline rocks. However, the most well-formed examples occur in finer-grained rocks, especially carbonates.

## Shatter Cone Morphology

How do you know when you're looking at a group of shatter cones? The LPI impact handbook (French et al.) summarizes the main features to look for:

- Striations along the surface of the cones, often indicating shock radiation divergent from the axis of the cone.

- Groups of cones branching off from one another (parasitic cones) are common as well.

- The apparent orientations of the cone axes are often random due to post-impact modification (though cone axes can be shown to have originally pointed toward the source of impact – see below).

In most cases, complete cones are not observed. It is much more common to see either partial cones or topless cones – the tops sustain the most damage due to passage of the shock wave.
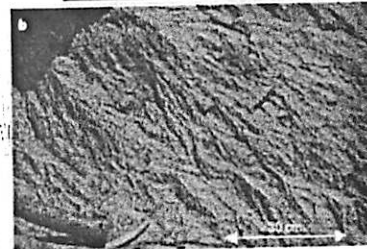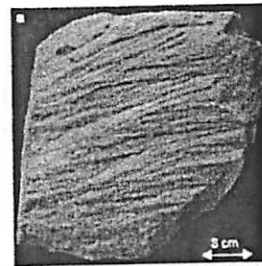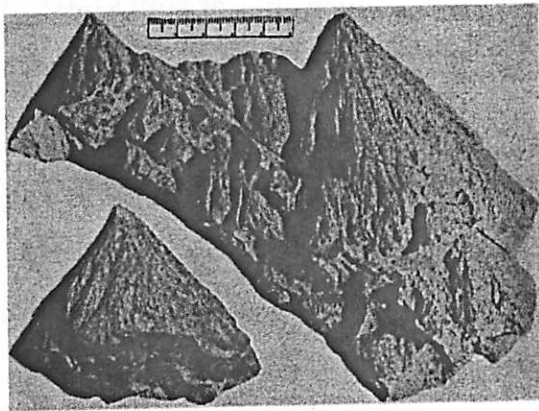
Shatter Cone Formation

Shatter cones form as a result of tensional stresses caused by the propagation of the spherical shock wave associated with the impact. The wave is passing through a non-uniform material - so it scatters off of inclusions in the rock, which creates a region of higher stress. The material then fractures in the conical pattern which we observe.
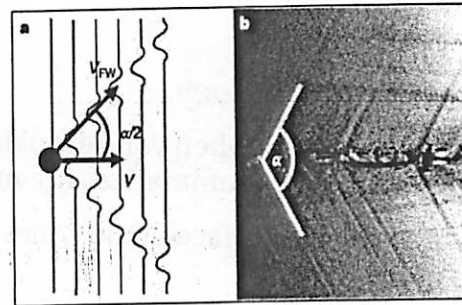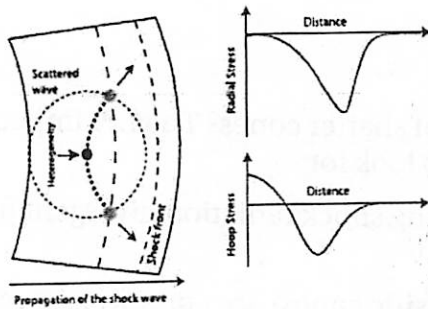
Left: the model of Baratoux & Melosh. A tensional wave is generated when the main shock wave encounters an inclusion. This wave interacts with the main shock wave, resulting in fractures along a conical surface.

Right: the model of Sagy et al. Tensional stresses cause a "fracture front" to propagate through the rock – when this front scatters off an inclusion, "front waves" are created, forming uniform striations.

When craters resulting from experimental TNT explosions (i.e. Roddy & Davis 1977) are examined, it is found that shatter cones are only present in regions that were subjected to a limited range of pressures. The minimum pressure at which shatter cones have been observed is 2 GPa. The high-pressure limit is less certain, and is somewhere between 6 and 30 GPa.

Shatter Cones and Impacts

Shatter cones are accepted as a good indicator of an extraterrestrial impact. Several field studies have demonstrated that when observed shatter cone features at a given site are rotated to their pre-impact orientations, the apices of all cones point towards a single central location, which can be extrapolated to lie above the level at which the cones are found. This indicates that the source of the shock was external to the rock formation.

The figure on the following page demonstrates the various fracture features you might expect for a typical central-uplift type crater.
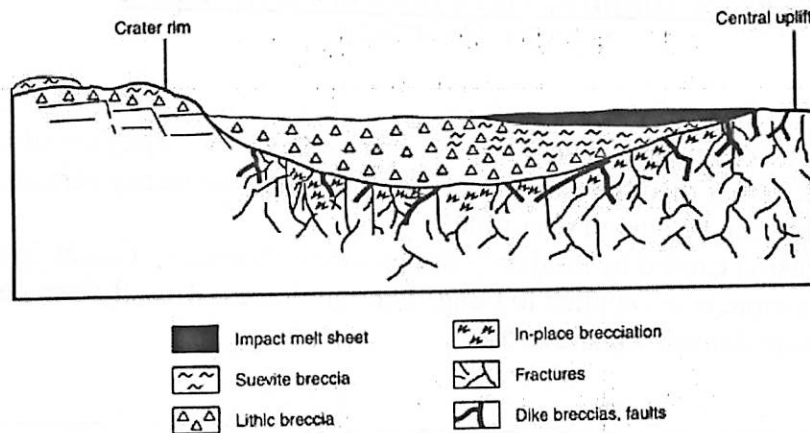
Fig. 3.13. Complex impact structure: locations of impactite types. Schematic radial cross section across a complex impact structure of the central-uplift type, from the central uplift (right) to the outer, downfaulted rim (left). (Vertical scale is exaggerated.) The subcrater parautochthonous rocks, exposed in the central uplift, are highly fractured and brecciated and may contain distinctive shock features such as shatter cones. These rocks may also contain widespread pseudotachylite breccias and dike-like intrusive bodies of allogenic breccias and impact melts. Larger and thicker subhorizontal units of allogenic breccias and melts occur as an annular unit of crater-fill material that covers the parautochthonous rocks between the central uplift and the rim. The bulk of these crater-fill deposits consist of melt-free lithic breccias, with lesser amounts of melt-bearing suevite breccias. The melt component in the crater-fill deposits becomes more abundant toward the center and upward, and a discrete layer of impact melt (solid black) may occur at or toward the top of the crater fill. (Modified from *Stöffler et al.*, 1988, Fig. 12, p. 290.)

In known impact features, shatter cones are often found in the centrally uplifted regions (for larger craters) and occasionally near the epicenter of the impact for smaller craters. Typically, however, shatter cones are most common further from the impact center, in locations consistent with the observed limited pressure range described above.

References

Baratoux & Melosh 2003, EPSL, v. 216, p. 43

Dietz 1960, Science, v. 131, no. 3416

Roddy & Davis 1977, "*Impact and Explosion Cratering*", p. 715

Sagy, Fineberg & Reches 2004, JGR, v. 109, B10209

Sagy, Reches & Fineberg 2002, Nature, v. 418

French 1998, "*Traces of Catastrophe*", Lunar & Planetary Institute

Dikes vs. Diapirs: Mechanics of Lava Ascent
MANDY PROCTOR
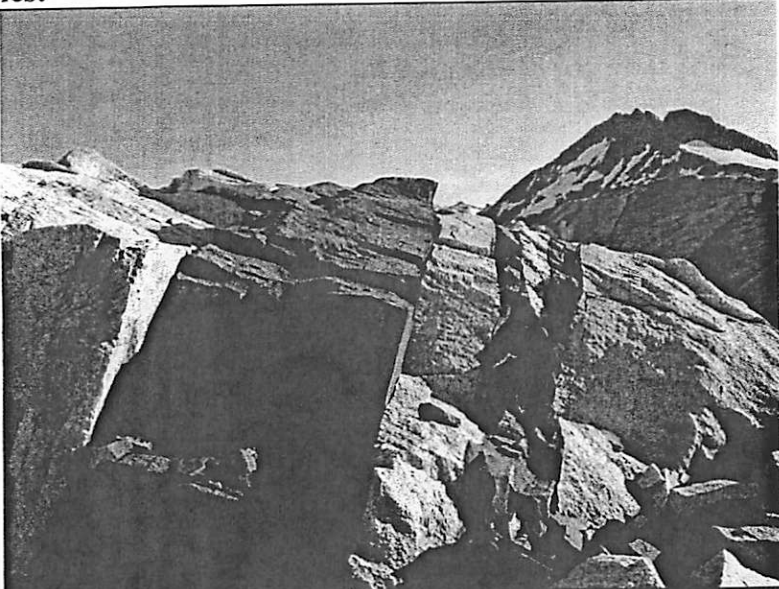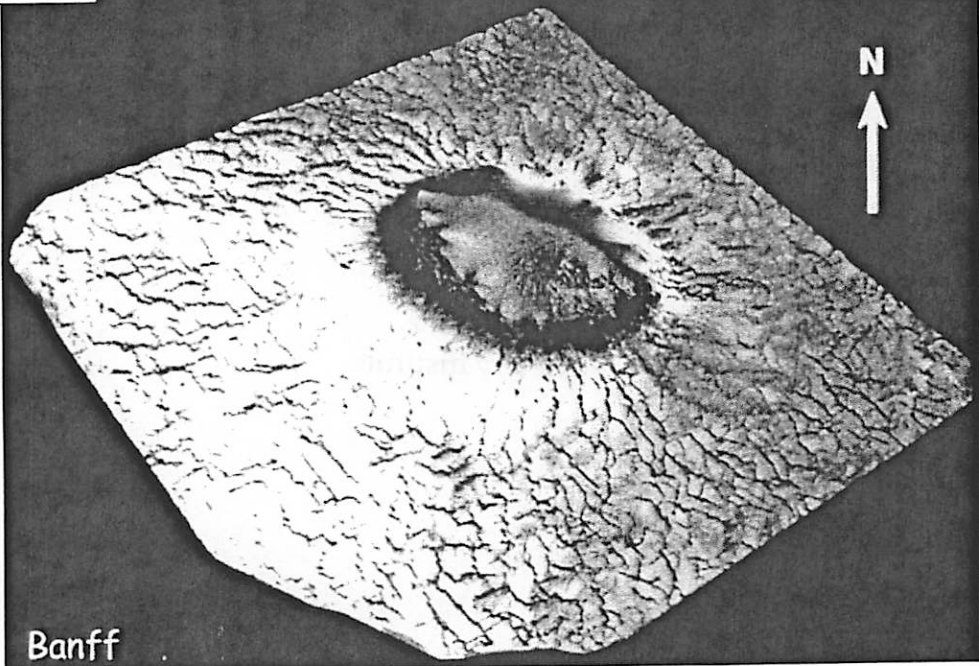
Definitions:

Dike: An intrusion of igneous material into a surrounding rock. They are usually much longer and higher than they are thick. Normally they are nearly vertical after creation, but can be altered over time.

Diapir: An intrusion caused by buoyancy or pressure differences. Can be igneous, but the term is more often applied to things like salt domes. Usually intrude vertically through more dense rock above them.

Examples:

Example of a basalt dike cutting through a lighter rock (granite or sandstone).

Note: Dike is very thin.

Schematic of a salt dome diapir.

Note: The diapir is not as thin as the dike.

Banff

Formation:

Fig. 1. Schematic diagram illustrating idealized end-member cases of (a) (geophysical) diapir intruding viscous host rock and (b) dike intruding elastic host rock. Material in host rock along diapir axis rises with diapir, but vertical displacement of material adjacent to dike is negligible. Dike thickness greatly exaggerated.
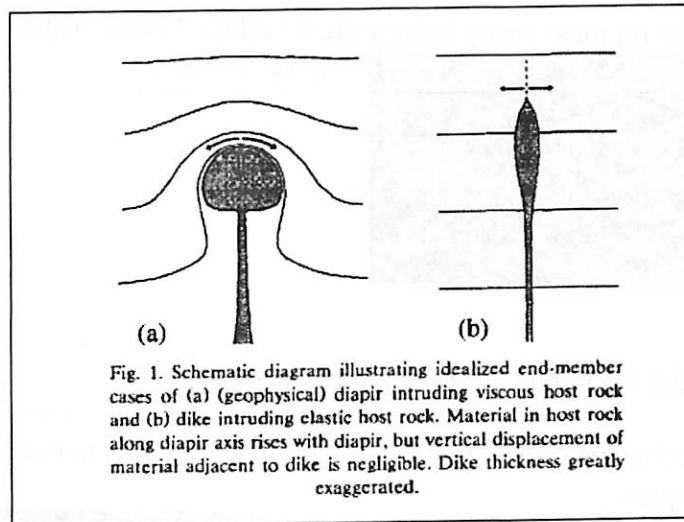
Dike

PLUTONS & VOLCANIC LANDFORMS

Volcanic Cone
Flow   Dike
Laccolith
Sill
Pluton
Batholith

Formation of a Dike:
1. Magma is forced upward from below.
2. Breaks through surface rock, but does not flatten out.

Diapir

Centrifuge stress

$\rho 1$
$\rho 2$
$\rho 3$

Formation of a diapir:
1. Several density layers, bottom layer is less dense (will rise).
2. Surface layers get bent as the less dense material forces them upwards.

Planetary Connection:

Dikes seem to be on most rocky solar system bodies, Venus, Mars, Moon, Io

Dike on Mars

Diapirs may exist on Venus, Mars, Io and Enceladus.

Deformation on Enceladeus caused by ice diapirs.
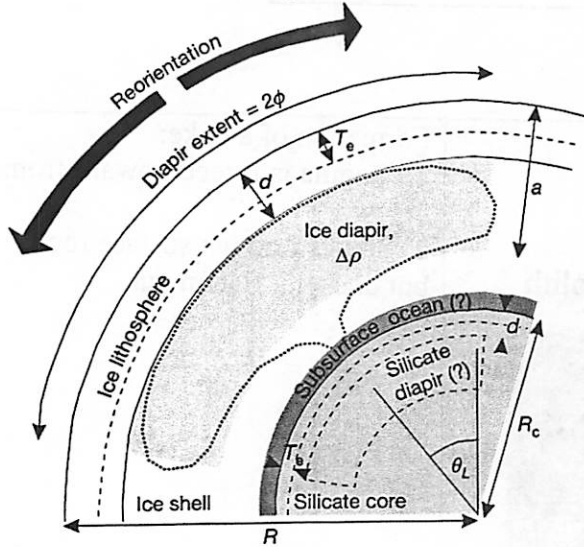
Diapir on Venus
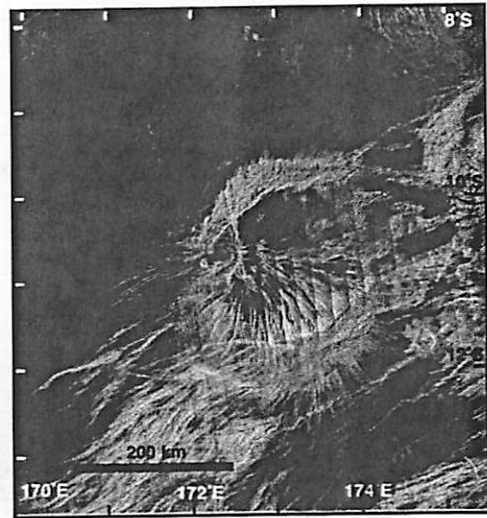
References:

Diapir-induced reorientation of Saturn's moon Enceladus. Francis Nimmo and Robert T. Pappalardo

Dikes vs. Diapirs in viscoelastic Rock. Allan M. Rubin.

LUCEU, Ecology of the Mississippi River Delta Region
http://www.loyno.edu/lucec/mrdsalt.html

A Brief Field Guide to
The K/T boundary in the Raton Basin,
New Mexico and Colorado

By Tamara Goldin

Compiled based largely on the USGS website http://esp.cr.usgs.gov/info/kt/index.html
and the Izett 1990 (GSA Special Paper 249) detailed report

On this fieldtrip we will be visiting several K/T boundary sections, the first three near our campground in Trinidad, Colorado and the fourth near Raton, New Mexico.

1) Madrid East
2) Long Canyon
3) Starkville South
4) Raton Pass

The locations of these sites (along with other Raton basin K/T boundary sections) are marked on this map (from Izett 1990):

SYMBOL   LOCALITY

BER	BERWIND CANYON
MAD	MADRID
MADE	MADRID EAST
MADN	MADRID NORTH
MR	MADRID RAILROAD
SVN	STARKVILLE NORTH
SVS	STARKVILLE SOUTH
CCN	CLEAR CREEK NORTH
CCS	CLEAR CREEK SOUTH
RAT	RATON
CLC	CLIMAX CANYON
SUG	SUGARITE
SS	SUGARITE SOUTH
CAN	CANADIAN RIVER
NP	NORTH PONIL
GAL	GALINAS
CAR	CARMEL and LONG CANYON
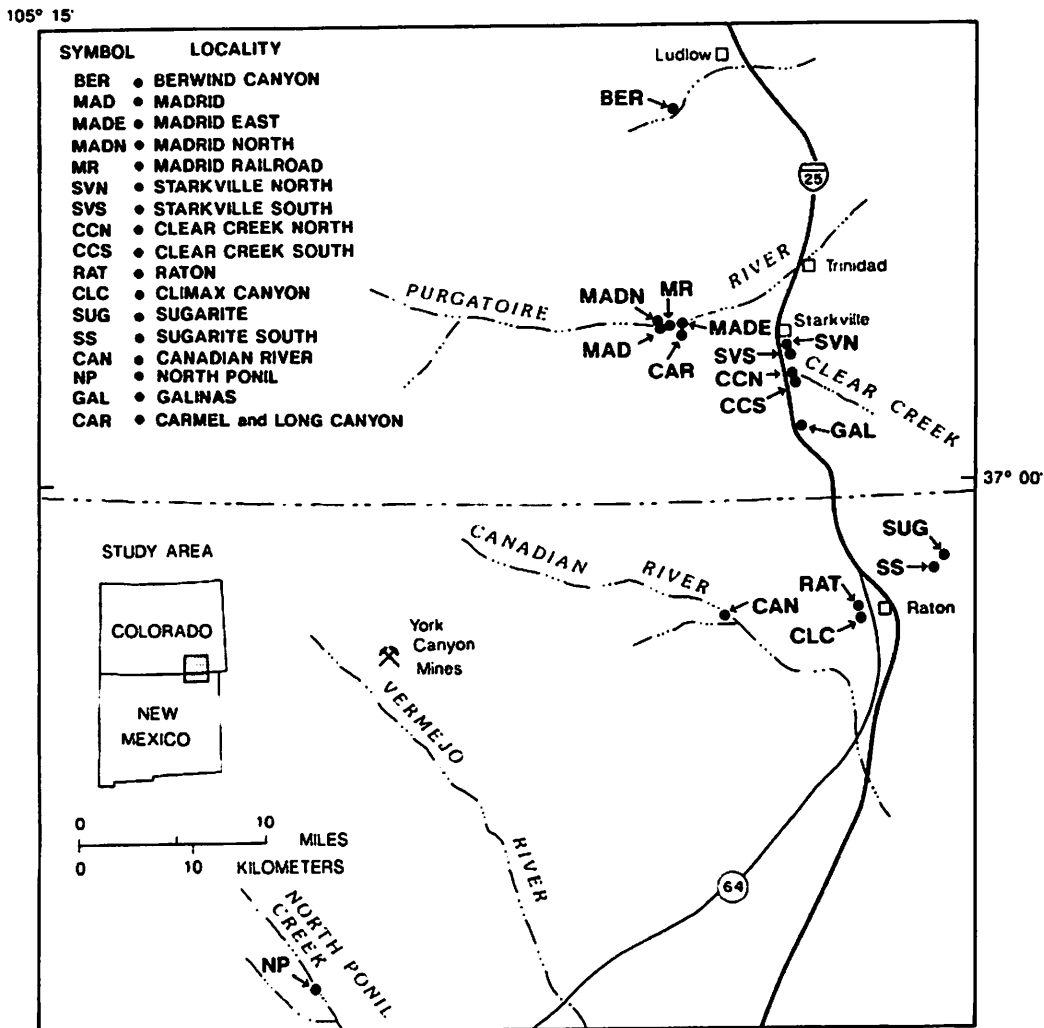
Overview of Geology

The Raton basin is a large asymmetric syncline extending from Huerfano Park, CO to ~~Cimarron, NM. A series of continental sedimentary rocks of upper Cretaceous to~~ lowermost Paleogene age, representing the retreat of the Western Interior Cretaceous seaway, fill the basin. From oldest to youngest these rocks include:

1) **Pierre Shale** (marine)
2) **Trinidad Sandstone** (marginal marine)
3) **Vermejo Formation** (nonmarine)
4) **Raton Formation** (nonmarine, *contains K/T boundary*)
5) **Poison Canyon Formation** (non marine)

AGE	FORMATION NAME	GENERAL DESCRIPTION	SYMBOL	APPROXIMATE THICKNESS IN FEET
PALEOCENE	POISON CANYON FORMATION	SANDSTONE--Coarse to conglomeratic; beds 15-50 ft thick; interbeds of yellow-weathering, clayey sandstone. Thickens to west at expense of underlying Raton		500+
PALEOCENE	RATON FORMATION	Formation intertongues with Poison Canyon Formation to the west. UPPER COAL ZONE--Very fine grained sandstone, siltstone, and mudstone with carbonaceous shale and thick coal beds. BARREN SERIES--Mostly very fine to fine grained sandstone with minor mudstone, siltstone, carbonaceous shale, and thin coal beds. LOWER COAL ZONE--Same as upper coal zone; coal beds mostly thin and discontinuous. Conglomeratic sandstone at base; locally absent		0?-2100 K-T BOUNDARY
UPPER CRETACEOUS	VERMEJO FORMATION	SANDSTONE--Fine- to medium-grained; also mudstone, carbonaceous shale, and extensive, thick coal beds. Local sills		0-380
UPPER CRETACEOUS	TRINIDAD SANDSTONE	SANDSTONE--Fine- to medium-grained; contains casts of *Ophiomorpha*		0-300
UPPER CRETACEOUS	PIERRE SHALE	SHALE--Silty in upper 300 ft. Grades up to fine-grained sandstone. Contains limestone concretions		1800-1900

(from the USGS online guide)
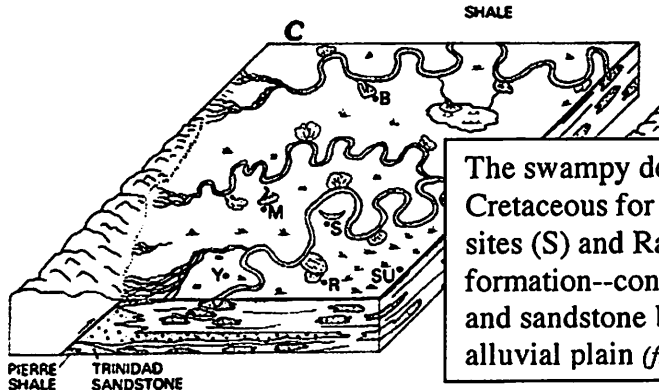
The swampy depositional setting at the end of the Cretaceous for the Madrid sites (M), Starkville sites (S) and Raton site (R). The Raton formation--consisting of coal, mudstone, siltstone, and sandstone beds-- was deposited on an upper alluvial plain *(from USGS online guide)*.

What does the K/T boundary look like?

In North American localities of continental depositional origin, including the Raton basin, the K/T boundary layer actually consists of a couplet of layers. The upper layer ("fireball layer") correlates with the global boundary layer and rests sharply on top of a lower claystone layer ("ejecta layer" or "K/T boundary claystone"). On this trip, we will discuss the debate over the origin of this dual-layered structure.

The **lower ejecta layer** is easiest to spot. It is a band of light grayish claystone 1- to 2-cm thick. It's light color stands out against the surrounding dark rocks. It's lower contact, according to Izett (1990), sometimes appears gradational whereas its upper contact with the fireball layer is sharp.

The **upper fireball layer** is quite thin (~5 mm) and thus is not so visible at a distance. It is the darker laminated shaley material above the boundary claystone (and below the coal which is commonly seen above the K/T boundary in the Raton basin). Only the fireball layer contains an extraterrestrial component.

Here's a photo of a polished slab from the Clear Creek North site (Izett 1990):
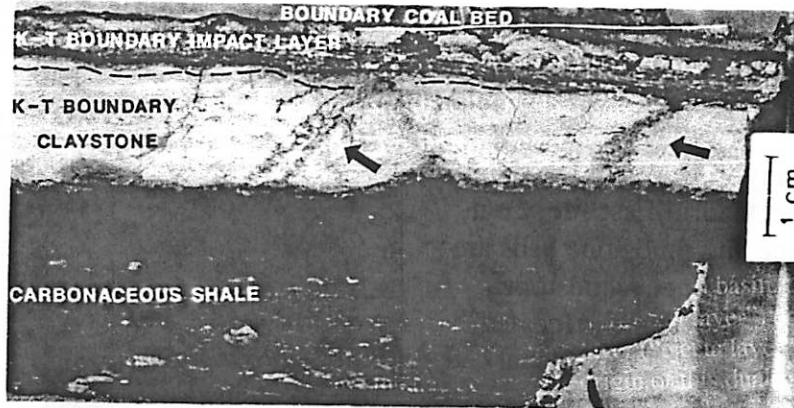
A comparison of stratigraphy showing iridium measurements (ppb) at four Raton sites (Izett 1990)
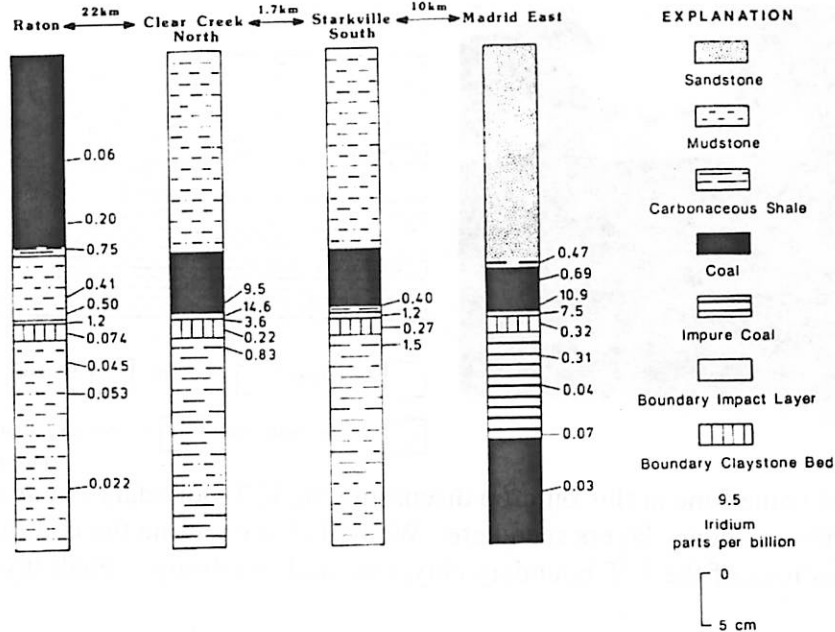
Figure 15. Stratigraphic diagram showing amounts of iridium (ppb) in K/T boundary rocks of the

Stop 1: Madrid East

There are several Madrid sites, which lie along/near the Purgatoire River. Leaving the campsite, we will drive past Cokedale, site of the large Asarco coal waste pile (the mine closed in 1946). After we drive across the new bridge over the river, we will cross the railroad tracks. Upstream along these railroad tracks the K/T boundary outcrops for several hundred meters (this is the **Madrid Railroad** locality). We will stop a little further along the road, where the K-T boundary is exposed in a steep roadcut (the Madrid East locality).

The K-T boundary claystone lies beneath a thin coal bed that is directly overlain by a prominent sandstone bed. The stratigraphy here is similar to what we will see at the Long Canyon site a couple miles from here. We will stop at Madrid East for an introduction to the K/T boundary and a first peek at the biggest celebrity of all impact layers and proceed on to Long Canyon.

Stop 2: Long Canyon

The Long Canyon site is an extended version of the Madrid East site. Coal, shale, siltstone and mudstone beds are overlain by a prominent sandstone ledge. The K/T claystone is located below the thin (few cm-thick) coal bed, which is directly below the sandstone. The sandstone makes the K/T boundary claystone easy to spot.

(from USGS online guide)
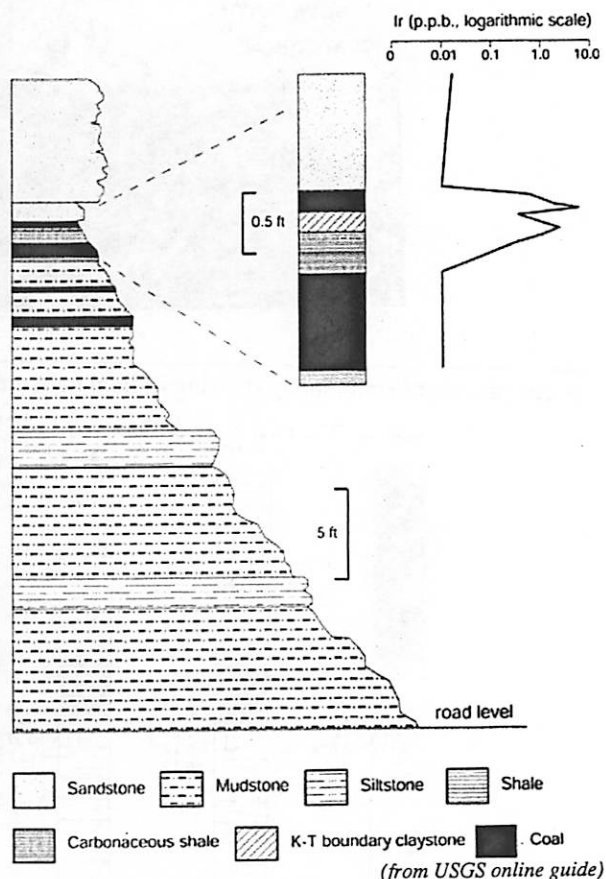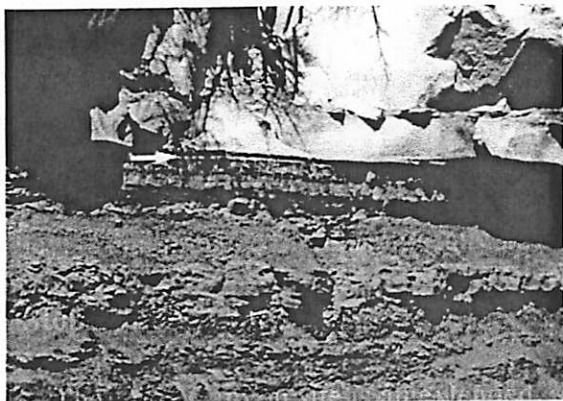
We will spend some time at this outcrop discussing the K/T boundary event and formation of the boundary layers seen here. We will also examine the continuity and thickness variations of the K/T boundary claystone and overlying fireball layer along this outcrop.

Stop 3: Starkville South

The Starkville sites lie in outcrops along the I-25 near Starkville (not so good for group discussion, but it's still loads of fun playing with K/T dirt!). Proceeding along the service road, we will pass by the Starkville North locality, which is now obscured by a landslide. This was the first recognized K/T boundary locality in Colorado. 1/4 mile down the road is the Starkville South site. In 1984, a team from the Smithsonian collected a 2.5-ton sample of the boundary interval for archival purposes. The 'road' we will walk along, just stratigraphically above the boundary, was made during this excavation. It's not the prettiest K/T boundary site around because it has been heavily sampled, but this means we can go crazy sampling it too!

Here the K/T boundary lies above carbonaceous shale and below a 5-cm thick coal bed. The boundary is located ~2 m above the thick point-bar sandstone at the base of the outcrop. Again, we see the couplet of impact layers at the boundary: the 2-cm thick whitish kaolinitic claystone (ejecta layer) below with a 5-mm thick, dark kaolinitic shale (fireball layer) above.
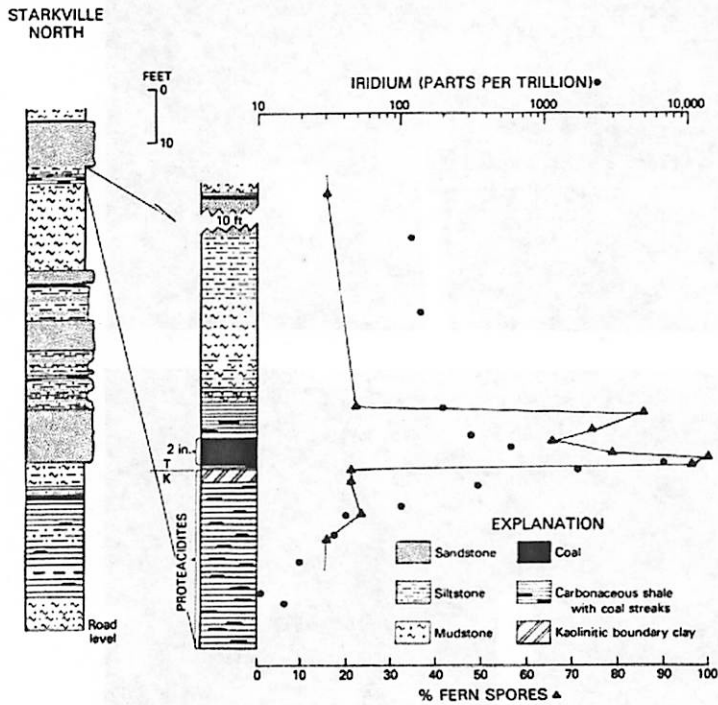
Left: stratigraphic column and Ir measurements at Starkville North (the South site is only slightly different)

Below: Photographs of the Starkville South site

(from the USGS online guide)
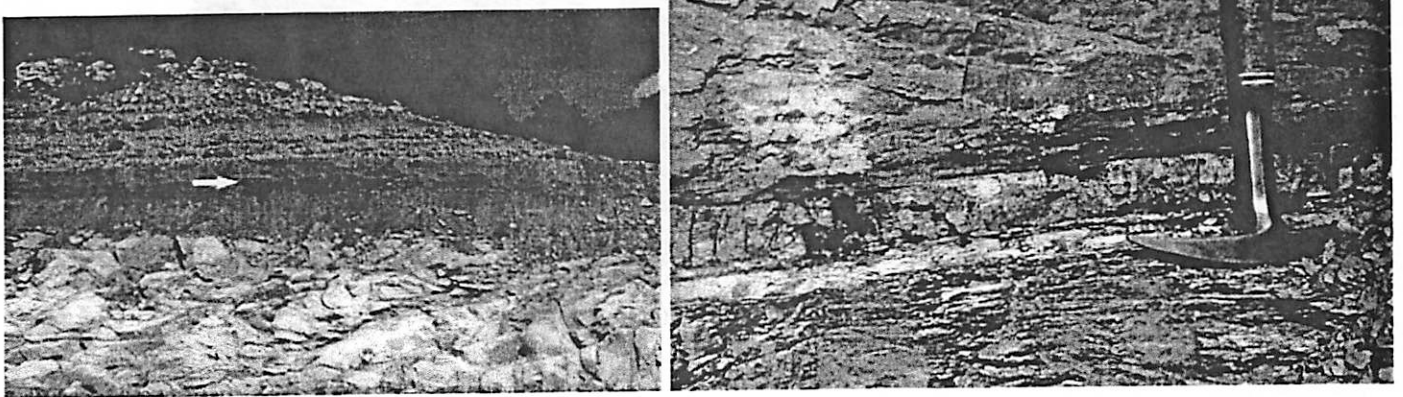
Stop 4: Raton Pass

The Raton site is on top of a saddle on Southwell Mountain Road, just west of Raton, where the K/T boundary is exposed in a roadcut. This is where the Iridium anomaly was first discovered (in the fireball layer) in the Raton basin... hence the lovely (but ailing) sign. The K/T boundary occurs within a detrital claystone sequence and, unlike most other Raton basin localities, is not directly beneath a coal bed. The K/T boundary claystone can be found ~8 inches below the uppermost coal bed. The coal zone observed here appears to correlate with that mined at Sugarite, another K/T boundary locality.

Note the position of the coal bed above the K/T boundary claystone layer. Knife blade is points to the top of the boundary claystone. *(from USGS online guide)*

Impact ejecta deposition in the atmosphere ...and the double layer in the Raton basin

By Tamara Goldin

Basics of impact ejecta deposition

- **Where does the ejecta come from?**
  - VAPOR PLUME—target + projectile
  - EJECTA CURTAIN--target
- **Where does the ejecta end up?**
  - Ejecta blanket
  - Proximal vs. distal ejecta

The excavation flow generated following impact. Note expanding vapor plume and ejecta curtain (from Melosh 1989).

(http://jeff.medkeff.com/astro/lunar/geology/01_crater.htm

- **Impact ejecta deposition**
  -On airless bodies...
  - The vapor plume expands, recondenses and falls back on ballistic trajectories
  - Ejecta curtain material is ejected and deposited ballistically
    - **"Ballistic Sedimentation"** (see figure to right)

(based on Oberbeck 1975)

Ejecta deposition & the double layer
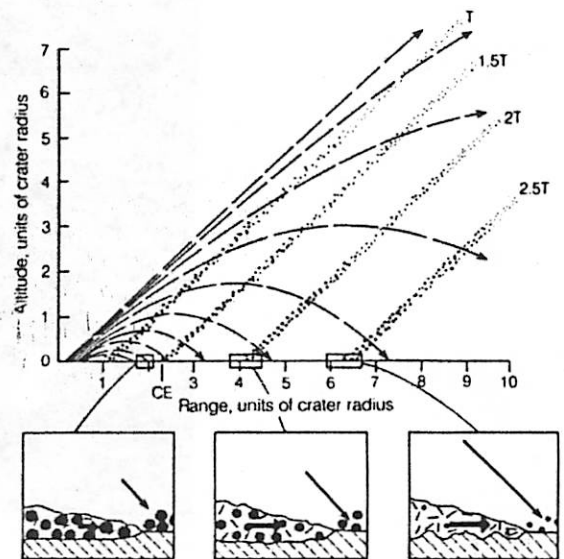
Atmospheric Interactions
Earth has an atmosphere
(so we can't treat ejecta deposition as a ballistic problem)

We can make a couple general statements:
- Impact layers from large impacts, such as Chicxulub, are found throughout the stratigraphic record. Some of these layers, like the K/T boundary layer, are global in distribution.
- Large impact events are thought to result in environmental disturbances leading to potentially catastrophic consequences

This leads to two big questions:
1) *How do terrestrial impact layers form?*
2) *What do these layers tell us about the environmental consequences of large terrestrial impacts?*

Understanding the interactions between the falling impact ejecta (of vapor plume and ejecta curtain) and the atmosphere is key to answering both these questions (*...and so I toil away my days trying to figure this out using an extra-fun code called KFIX-LPL*).

Some facts about the global K/T boundary layer:
-fairly uniform thickness (~3 mm) worldwide
-composed of uniform-sized (250 μm) crystalline spherules of basaltic composition
-the **"fireball layer"** (thought to represent vapor plume material)—Ir, shocked Qtz
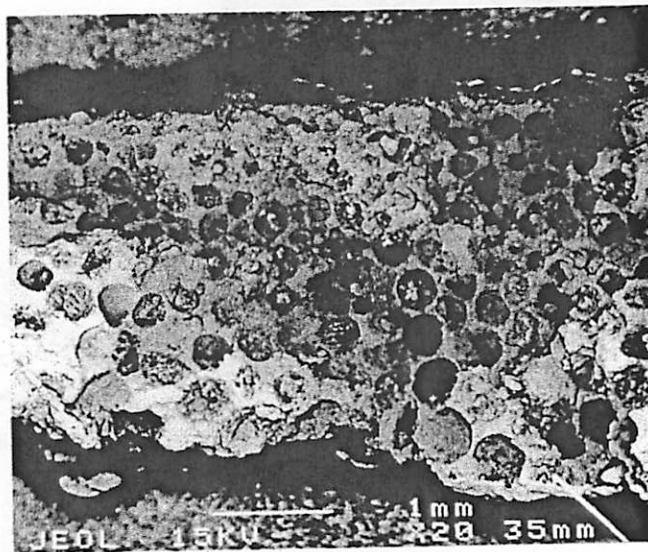
(Smit 1999)

Ejecta deposition & the double layer

Modeling the global fireball layer
(aka the fireball layer according to Tamara)

LIQUID VELOCITY

LIQUID TRACERS

Preliminary Results

Particles fall through thin atmosphere at high velocity

The vertical velocity slows

Particles accumulate in a band and continue to fall

80 min

Preliminary Results

80 min
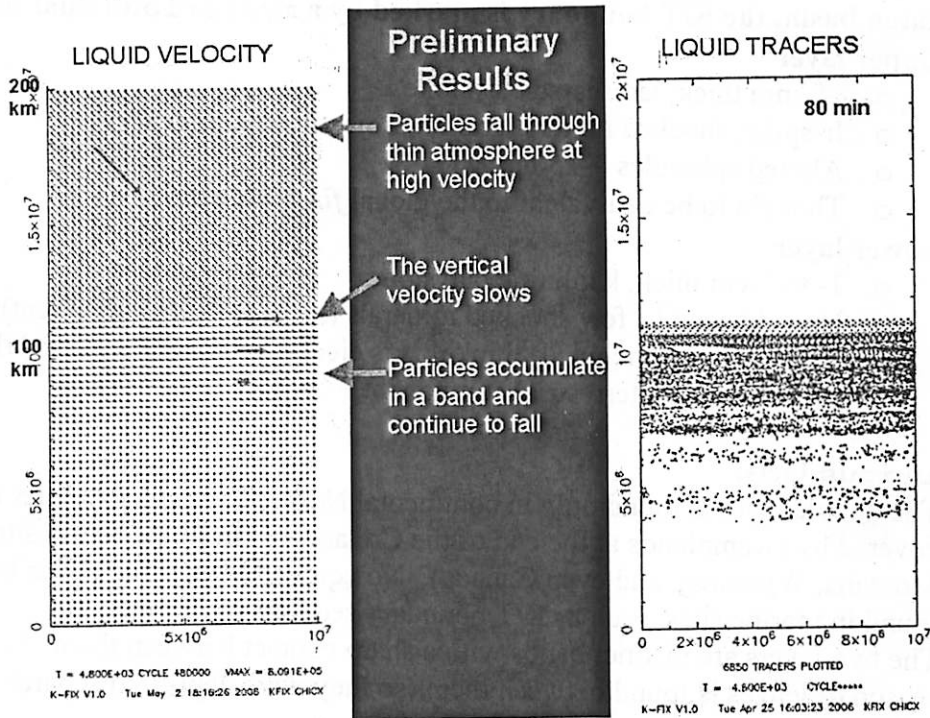
Gas:
- Atmosphere pushed down
- Sharp pressure gradient
- Hot dense lower atmosphere, which expands

Liquid:
- Broad band of droplets
- Densest, hottest near top of layer
- Top of layer corresponds to top of dense air

Ejecta deposition & the double layer
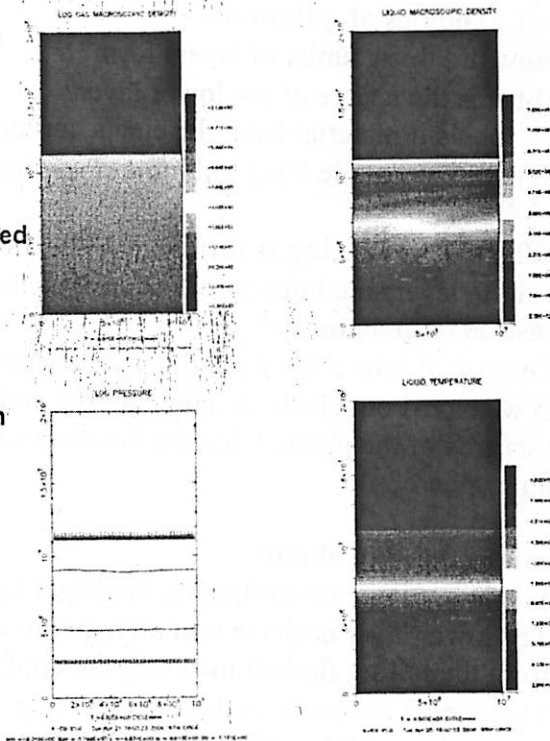
The Mystery of the Double Layer
(insert suspenseful music here)

In the Raton basin, the K/T boundary is marked by a mysterious dual-layer:

- **Upper layer**
  - ~5-mm thick, laminated claystone
  - Ir-spike, shocked mineral grains (projectile component)
  - Altered spherules (~250 μm)
  - Thought to be equivalent to the global *fireball layer*
- **Lower layer**
  - 1- to 2-cm thick, kaolinitic claystone
  - No enhanced Ir, few shocked minerals (no projectile component)
  - Many (myself included) think this is ejecta curtain material and thus contains only a terrestrial component

Some curious facts:

- The double layer is found only in continental North American localities (areas covered by swamplands at the end of the Cretaceous, from the Raton sites up to Montana, Wyoming, and even Canada). No equivalanent of the lower layer is found in marine sites, such as K/T boundary sections in Europe.
- The two layers are distinct bands with a sharp contact between them. Not a single season of leaves is found between them (so they were deposited separately, but quickly)

This leads to oodles of questions:

- How did this couplet of layers form?
- What is the source of the lower layer?
  - Is it material from the ejecta curtain?
- Why is the double layer only found in continental North America and not globally?
- Why are the two layers different? (Why no Ir in the lower layer?)
- If both layers are impact-related, why is the contact between them so sharp instead of gradational?
- Over what time scale were the layers deposited?
- If we have both ejecta curtain material and fireball material being deposited over this area of the globe, what are the associated changes occurring in the atmosphere?

Explanations floating about:

- The lower layer is authigenic; the upper layer is the fireball layer
- The lower layer is ejecta curtain material and was somehow deposited separately from the falling fireball material; the upper layer is the fireball layer
- There are 2 layers, ergo there were 2 impacts

I'll tell you what I think is going on
What do YOU think?

Ejecta deposition & the double layer

42

The Physics of Impact Cratering
Kat Volk

To examine crater formation, the process is broken down into three stages: contact and compression, excavation, and modification.

Contact and Compression

When the projectile hits the ground, it is traveling faster than the speed of sound in the ground material. This results in a shock wave that travels into the ground as well as into the projectile itself, which transfers the projectile's kinetic energy to the ground. This shock wave propagates outward in a hemispherical fashion. As is moves outward, it loses energy because it must cover an area that increases with distance from the impact and because the rock it travels through is heated and deformed. The result of this is an exponential decrease in the shock wave pressure with increasing distance from the impact point (see isobars in figure 3.4 from French p 22). For high velocity impacts, the pressures near the impact point can be in the range of a few tens of GPa to 100 GPa. For comparison, most terrestrial rocks undergo normal elastic and plastic deformation at about 1 GPa (French p 17). The contact and compression stage continues until the projectile is melted or vaporized. This happens when the initial shock wave has traveled from the leading edge of the projectile to the trailing edge to be reflected back to the ground as a rarefaction. This whole process occurs on a timescale of a fraction of a second, depending on the size and speed of the projectile.
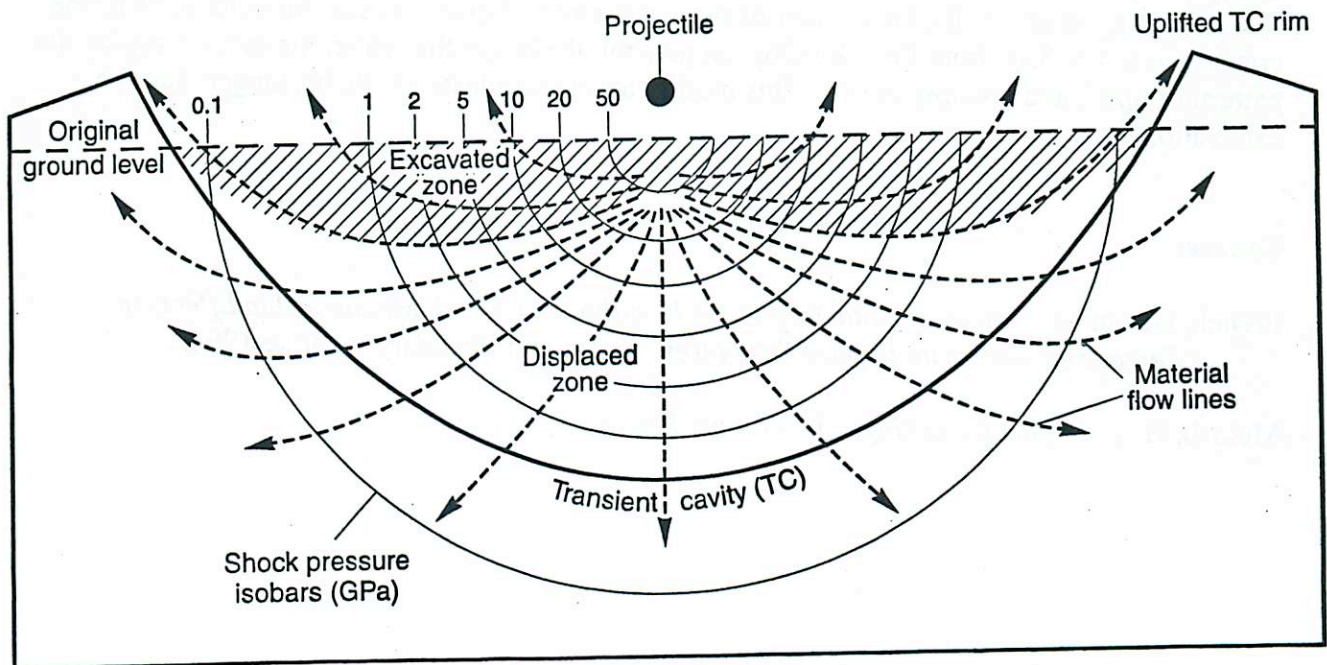
Fig. 3.4. Excavation stage: formation of transient crater. Theoretical cross section showing development of the transient crater immediately after the contact/compression stage. Original peak shock pressures (units in GPa) around the impact point are shown for simplicity as hemispherical isobars (for details, see Fig. 3.2). Complex interactions of the shock wave, the ground surface, and the subsequent rarefaction wave produce an outward excavation flow (dashed arrows) that opens up the transient crater. In the upper part of this region (excavated zone; ruled area), target material is fractured, excavated, and ejected beyond the transient crater rim. In the lower region (displaced zone), target material is driven downward and outward, more or less coherently, and does not reach the surface. This model yields two important geological results: (1) ejected material is derived only from the upper part (approximately the top one-third to one-half) of the transient cavity; (2) because the excavation flow lines in the excavated zone cut across the initially hemispherical shock isobars, ejected material will reflect a wide range of original shock pressures and deformation effects, ranging from simple fracturing to complete melting and vaporization. (Modified from *Grieve*, 1987, Fig. 5; *Hörz et al.*, 1991, Fig. 4.3a, p. 67.)

(French p 22)

Excavation

Once the projectile itself has vaporized, the combined effects of the initial shock wave and the following rarefactions open up the crater. Since the projectile penetrates past the surface of the ground, there are parts of the initial shock wave that propagate upward. When it hits the surface, this portion of the initial shock wave is reflected back into the ground as a rarefaction, which closely follows the initial shock wave. This creates an upward pressure gradient. Near the surface, the stress resulting from this gradient is sufficient to pulverize rock and send it upward in an excavation flow. As the waves travel deeper, the stresses created are no longer large enough to eject material, but instead displaces it outward and downward (see the material flow lines in figure 3.4 from French p 22). These processes cause an expansion of the crater and an uplift of ground material along the rim until the expanding shock wave loses energy and decays into an elastic wave, ending the excavation stage. This stage lasts longer than the contact and compression stage, but still only takes from a few seconds to a minute or so depending on size.

Modification

Once the crater reaches maximum size, and the shock waves have died away, the final shape of the crater is determined by gravity and the characteristics of the rock out of which it is formed. For small craters, gravity dominates this process. Ejected material and material from the crater's rim and walls falls back into the crater, partially filling it and creating a simple impact structure (see figure 3.3 from French p 20-21). Complex impact structures occur for larger impacts. Complex interactions between the shock waves and the rock beneath the crater cause shifts in the rock, resulting in an uplift of the center of the crater and collapse zones in the outer parts of the crater (see figure 3.10 from French p 26). In general, the larger the crater, the more complex the pattern of uplift and collapse zones. This modification stage lasts a little bit longer than the excavation stage

Sources

French, Bevan M. *Traces of Catastrophe: A Handbook of Shock-Metamorphic Effects in Terrestrial Meteorite Impace Structures.* Lunar and Planetary Institute 1998.

Melosh, H. J. *Impact Cratering: A Geologic Process*

Fig. 3.3. Development of a simple impact structure. Series of cross-section diagrams showing progressive development of a small, bowl-shaped simple impact structure in a horizontally layered target: (a) contact/compression stage: initial penetration of projectile, outward radiation of shock waves; (b) start of excavation stage: continued expansion of shock wave into target; development of tensional wave (rarefaction or release wave) behind shock wave as the near-surface part of original shock wave is reflected downward from ground surface; interaction of rarefaction wave with ground surface to accelerate near-surface material upward and outward; (c) middle of excavation stage: continued expansion of shock wave and rarefaction wave; development of melt lining in expanding transient cavity; well-developed outward ejecta flow (ejecta curtain) from the opening crater; (d) end of excavation stage: transient cavity reaches maximum extent to form melt-lined transient crater; near-surface ejecta curtain reaches maximum extent, and uplifted crater rim develops; (e) start of modification stage: oversteepened walls of transient crater collapse back into cavity, accompanied by near-crater ejecta, to form deposit of mixed breccia (breccia lens) within crater; (f) final simple crater: a bowl-shaped depression, partially filled with complex breccias and bodies of impact melt. Times involved are a few seconds to form the transient crater (a)–(d), and minutes to hours for the final crater (e)–(f). Subsequent changes reflect the normal geological processes of erosion and infilling. (French p 20-21)
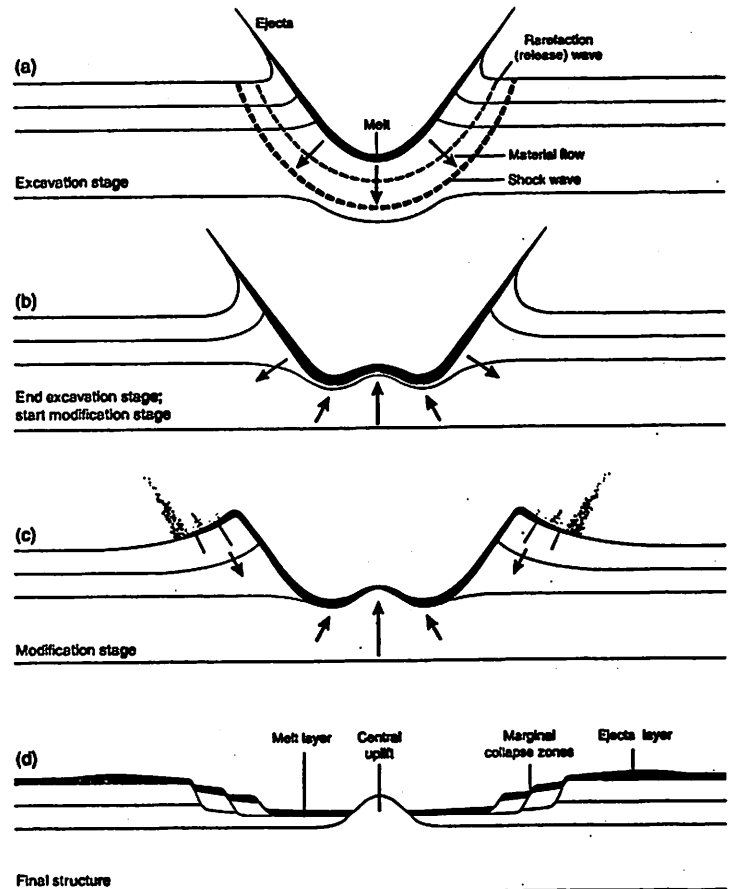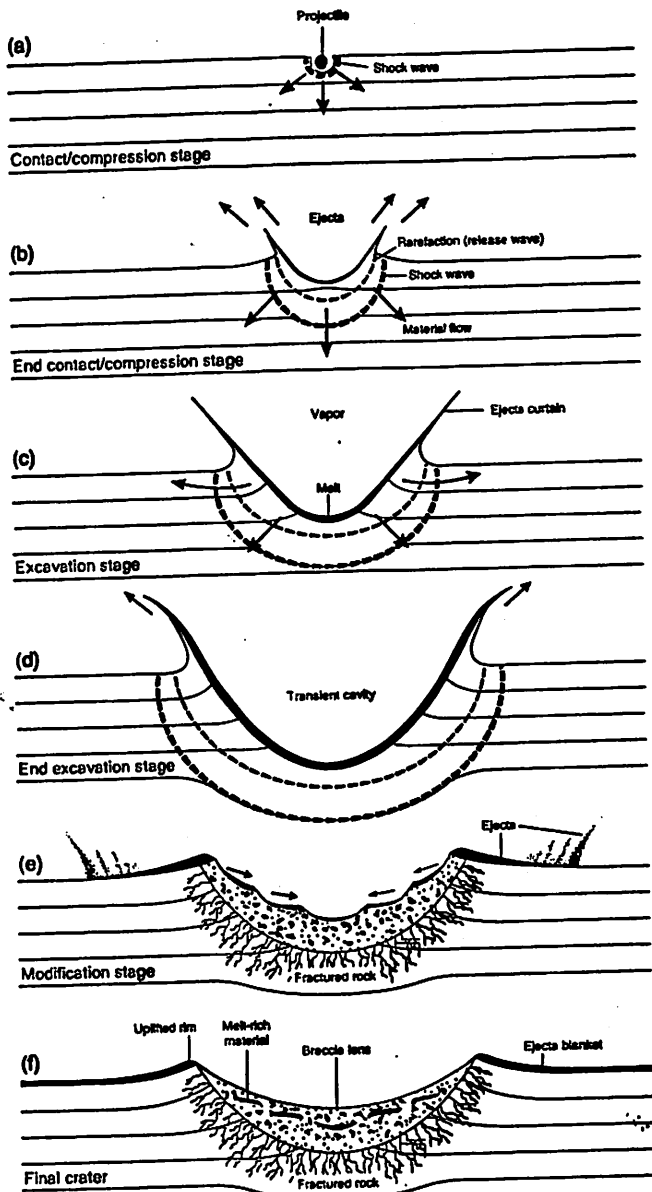
Fig. 3.10. Development of a complex impact structure. Series of cross sections showing progressive development of a large, complex impact structure in a horizontally layered target: (a) formation of a large transient crater by the excavation process is virtually identical to transient crater formation in smaller structures (compare with Fig. 3.3a–d); (b) initial development of central uplift during the subsequent modification stage; (c) start of peripheral collapse, accompanied by continuing development of the central uplift and the thinning and draping of the original melt layer (black) over the uplifted rocks; (d) final structure, which is of the central-uplift type, consists of a central uplift of deeper rocks, surrounded by a relatively flat plain and by a terraced rim produced by inward movement along stepped normal faults. The central uplift is surrounded by an annular deposit of allogenic breccias and impact melt (black), which may be absent from the central peak itself. An ejecta layer (stippled) covers the target rocks around the structure. The diameter of the final structure, measured at the outer rim beyond the outermost fault, may be 1.5–2× the diameter of the original transient crater. This central-peak morphology is observed in terrestrial structures ranging from about 2–25 km in diameter; larger structures tend to develop one or more concentric rings within the crater (for details, see text). (French, p 26)

45

Global Seismic Effects of the Chicxulub Impact

Jason W. Barnes

Department of Planetary Sciences, University of Arizona, Tucson, AZ, 85721

jason@barnesos.net

ABSTRACT

I will discuss the seismic pulse produced by the Chicxulub impact. The pulse was equivalent to an earthquake of magnitude 13 on the Richter scale, and produced 1 meter amplitude surface offsets up to 7000 kilometers away from the impact site. It is now thought that this seismicity induced massive landslides along the eastern margin of North America.

Subject headings: field trip — Chicxulub

1. HANDOUT

On the previous field trip to Raton in spring of 2000, I talked about marine-deposited K/T boundary sequences, including tsunami deposits and crazy, mixed-up layers in the Carribean. Bourgeois et al. (1988) found what they suggested to be a tsunami deposit within a section in Texas dated at the K/T boundary (see Figure 1). The section is a graded sandstone layer several 10s of centimeters thick within a large mudstone. Bourgeois et al. (1988) had hypothesized that an incoming tsunami $\sim$ 100 meters high had entrained rocky material, depositing it out heaviest-particles-first onto the previously existing seabed. Other tsunami-interpreted sites were found in Haiti and similarly proximal Carribean locations (Hildebrand & Boynton 1990; Maurrasse & Sen 1991).

Work in the intervening years has cast doubt on the tsunami interpretation for the source of such deposits. Similar deposits were seen (Norris et al. 2000) (see Figure 2 off the Atlantic coast of the main North American continent. This area should have been shielded from a direct tsunami by the shallow sea that was Florida at the time, hence the discovery of these deposits was inconsistent with the tsunami hypothesis. Similarly, the possible landslide deposits that we saw in fall of 2005 in Baja California could not have been emplaced by a direct tsunami from the impact point (Busby et al. 2002).

It is now thought that such deposits were created via mass wasting, specifically landslides into the sea and entirely undersea density-current landslides, as suggested by Bralower et al. (1998). The landslides are thought to have been triggered by seismic shaking induced by the Chicxulub impact. There is no difinitive evidence of Tsunami to date.

The shock wave that produces planar deformation features, shocked quartz, and shatter cones (see Samantha's talk) propogates radially outward from the impact. The shock wave diminishes in strength as it travels. A few crater diameters away from the impact point, the shock
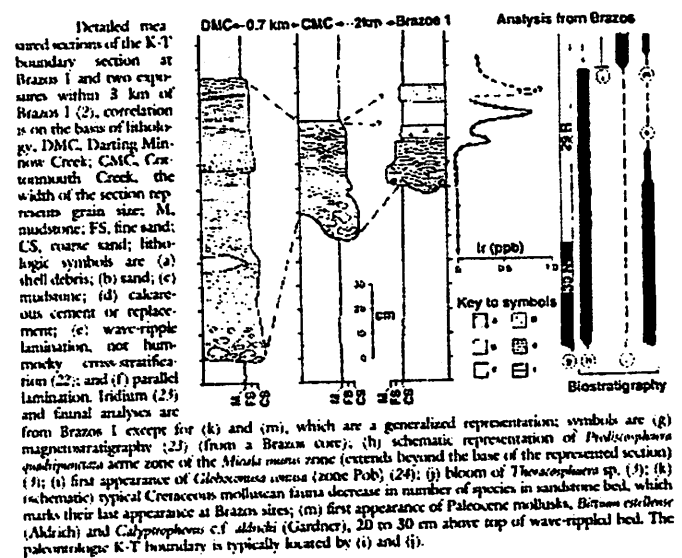
Fig. 1.— Section diagram of seismic-triggered landslide deposits, previously thought to represent tsunami remnants, near the Brazos River in Texas. From Bourgeois et al. (1988).
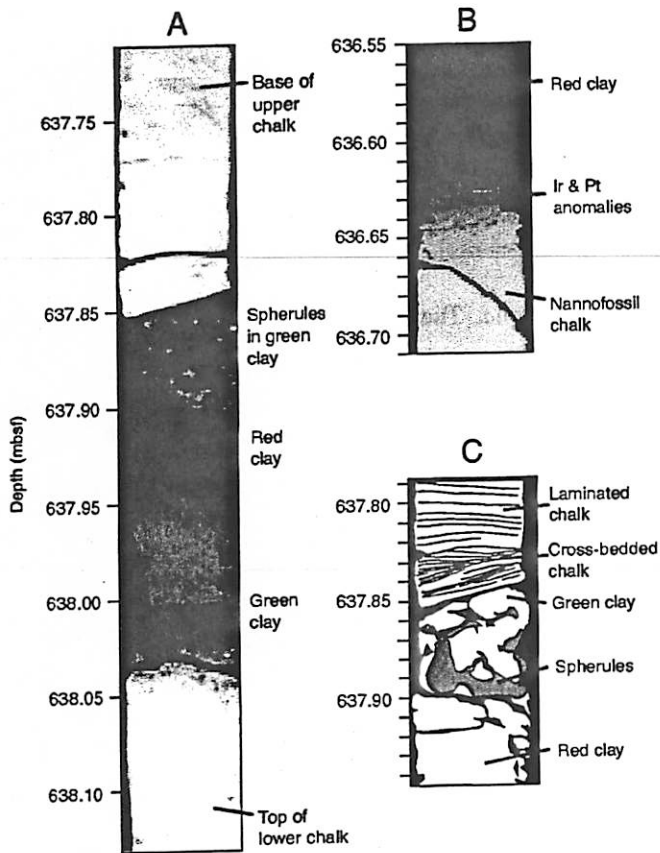
Figure 3. Mass-wasting deposits in Deep Sea Drilling Project Site 386, core 35. A: Interval between gravity-flow chalk deposits (bed 3 in Fig. 2). Light green spherules (impact ejecta) in dark green clay at base of upper chalk firmly ties gravity flow to Chicxulub impact. We infer that red pelagic clay slumped onto lower chalk bed and was buried by second gravity flow of chalk (mbsf, meters below seafloor). B: Overlying red clay. Green color of clay overlying lower chalk bed in A contrasts with situation at top of upper chalk (B, bed 5 in Fig. 2), where red clay accumulated long after organic matter in chalk was oxidized. C: Cross-bedding demonstrates that chalk was deposited as gravity flow. We infer that two chalk beds and intervening clay layer were mass-failure deposits formed by seismic shaking during Chicxulub impact.

Fig. 2.— Section of seismic-triggered landslide deposits in the North Atlantic Ocean off the eastern seaboard. From Norris et al. (2000).
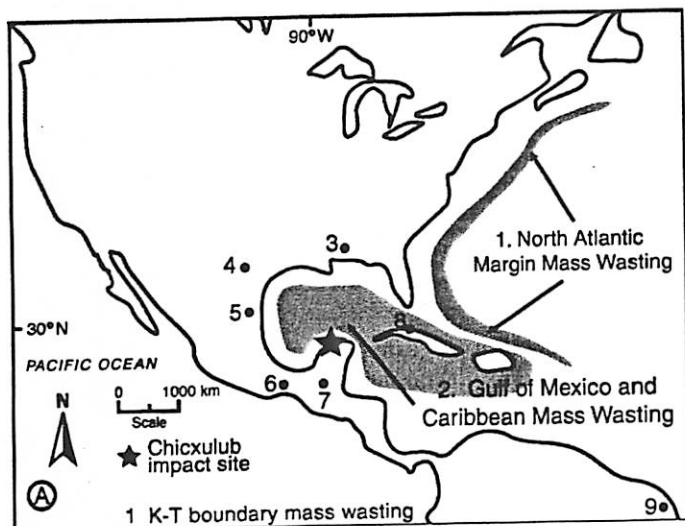
Fig. 3.— Map of mass wasting deposit locations, from Busby et al. (2002).

wave linearly transforms into an ordinary pressure wave — a seismic wave. Estimates of the efficiency of energy transfer into the shock (and subsequently seismic) wave imply an earthquake corresponding to magnitude 13 on the Richter scale (!!!!). A magnitude 10 earthquake is one large enough to be felt all over the world. The Chicxulub-induced seismic event would then have been 1000 times larger than necessary to have planet-wide consequences. The quake would sweep around the planet in about an hour (see Figure ??), wreaking havoc as it went. All dinosaurs that couldn't find a doorframe to hide under would be in serious danger, as would those dinosaurs asleep in their beds, with bookshelves to fall on them.

Boslough et al. (1996) calculate that amplitudes of over 1 meter would be expected for all areas within 7000 kilometers (!!!) of the impact site. Amplitudes in excess of 10 meters should have occurred within a few crater radii of the impact site, heavily affecting the Carribean.

Current thinking is that the unusual marine-deposited coarse-grained sedimentary sequences found at the proximal sea-bed K/T boundary sites represent landslides triggered by this massive seismic event. Such landslides may have continued for days or months after the impact itself, as loosed and newly jointed materials gave way under rain or thermal stress. The time delay explains the presence of work tunnels and other evidence of bioturbation within the landslide K/T deposits.

REFERENCES

Boslough, Chael, Trucano, Crawford, & Campbell. 1996, Geological Society of America, Special Paper 307, 307, 541

Bourgeois, J., Hansen, T. A., Wiberg, P. L., & Kauffman, E. G. 1988, Science, 241, 567

Bralower, Paull, & Leckie. 1998, Geology, 26, 331

Busby, Yip, Bilkra, & Renne. 2002, Geology, 30, 687

Hildebrand, A. R. & Boynton, W. V. 1990, Science, 248, 843

Maurrasse, F. J.-M. R. & Sen, G. 1991, Science, 252, 1690

Norris, Firth, Blusztajn, & Ravizza. 2000, Geology, 28, 1119
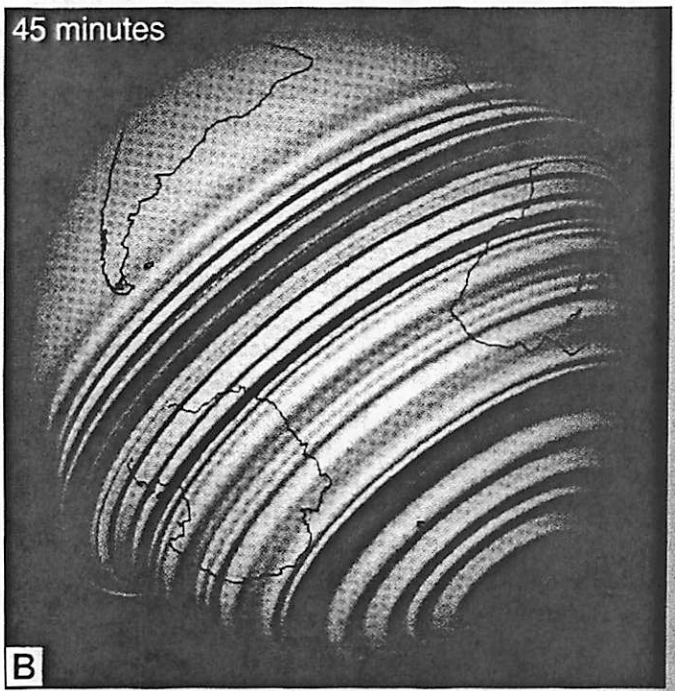
Fig. 4.— P-waves propogating around the world after the
Chicxulub impact, from Boslough et al. (1996).

Environmental Effects of Impact Events: How You are going to Die

Brian "Pestilence" Jackson and David "Famine" Choi

September 2006

Impacts don't kill people, it's the subsequent shock wave and reduction in solar insolation that kills people.
– Jay Melosh's bumper sticker, according to a 1998 LPL Grad Christmas Skit

1 How You will die Quickly

We discuss the short-term effects of an asteroidal or cometary impact. These effects would result in a quick and probably painless death. For our purposes, short-term effects are effects which result from the collision only hours after the impact. Effects which take longer than this to result are considered long-term (see other section). In this paper, we will describe effects as the arise from atmospheric and surface phenomena. First, however, we will briefly describe the physical processes that occur during an impact.

1.1 Synopsis of Impact Processes

Upon entering a planetary atmosphere, an impactor encounters atmospheric drag and ablation. Smaller impactors are slowed to their terminal velocity, while larger impactor velocities are hardly changed by the atmospheric drag. During its passage through the atmosphere, the impactor heats by atmospheric ablation and may evaporate some. The impactor also shocks the atmosphere, increasing local temperatures and inducing shock chemistry. The differential pressure on the front and the back of the impactor can cause the impactor to deform and could completely disrupt the impactor before it strikes the ground. The Tunkguska Event is a prime example of impactor disruption. (For more information, see Turco et al. [1982].)

After successfully passing through the atmosphere, the impactor strikes the surface of the target. The impact strongly compresses and shocks the impactor material and the target surface. Shock waves propogate through the surface and may generate melt. The shock waves can also produce distinctive mineralogies (see Sam Stevenson's talk).

The high pressures in the target and impact material drive the impacted materials at high velocity, and a crater is excavated which generally has a diameter many times larger than the diameter of the impactor. The crater which forms immediately after the impact is called the transient crater. Usually the transient crater collapses some under gravity to form the final crater. Thus the appearence of an observed crater can reflect both impact processes and subsequent surface processes.

1.2 Atmospheric Effects

After the target and impactor material are compressed to high temperatures and pressures, they vaporize, and the hot vapor expands rapidly. This hot ball of expanding gas is called the fireball. The fireball can reach temperatures in excess of 10000K and pressures greater than 100GPa [Collins et al., 2005], but the fireball rapidly cools to the ambient conditions due to expansion and eventually radiation on a timescale of order 1000s [Zahnle, 1990].

Initially the impact fireball is opaque to radiation and cools only by expanding into the ambient atmosphere. However, once the fireball temperature has dropped below some critical temperature, radiation can escape into the surrounding atmosphere. For the Earth's atmosphere, the critical temperature is 2000-3000K,
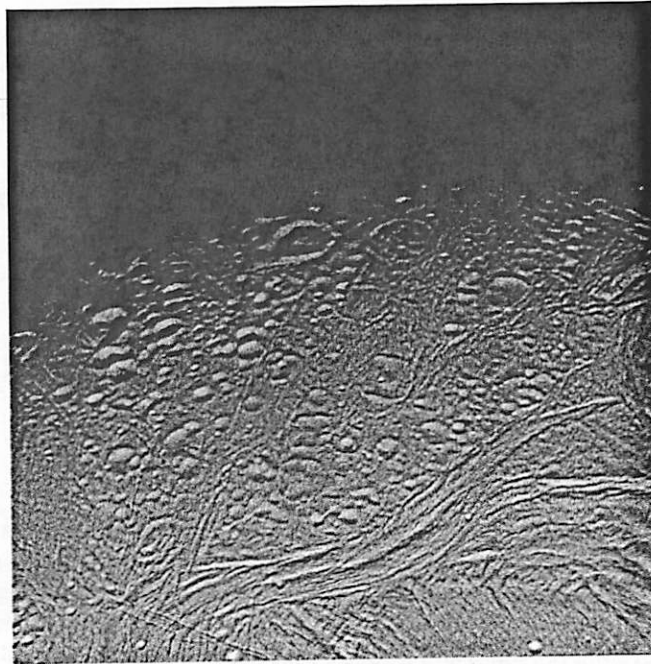
Figure 1: Degraded craters on Enceladus as viewed by Cassini

Figure 2: Trees around the Tunguska "Impact" Site

so the emitted radiation is in the visible and IR [Collins et al., 2005]. This radiation can ignite surrounding materials (like animals or people) and burn the impact site surroundings (such as at Tunguska).

The fireball's radiant flux, Φ, is given by $\Phi = \frac{\eta E}{2\pi r^2}$ where $\eta \sim 10^{-3}$, the radiant efficiency, E the impact energy, and r the distance from the impact. Collins et al. [2005] estimate that a radiant flux of 420 kJ/m^2 can cause third degree burns, equivalent to a fireball of 1 Megaton ($= 4.18 \times 10^{15} J$) viewed from 2 km away.

In addition to radiative consequences, the impact fireball can affect significantly the overlying atmospheric column. If the fireball expands at or near the escape velocity for the target planet, significant atmospheric erosion can occur, but this effect is only important for planets with low surface gravity. Melosh and Vickery [1989] consider erosion of the primitive Martian atmosphere and find that sufficient atmospheric erosion could have occurred to reduce Mars' atmosphere from 1 bar surface pressure to its current value of 6mbar early during solar system history.

The supersonic expansion of the impact fireball also produces an air blast which can knock over trees and damage buildings and other structures (like animals and people). Collins et al. [2005] develop empirical fits from nuclear bomb explosion data of blast wave pressure and wind speed and find that the blast wave pressure drops off as $\sim 1/r^{2.3}$ where r is the distance from the impact center. They also find that the speed of the air blast wave is roughly the speed of sound in the ambient atmosphere. We have reproduced table 4 from Collins et al. [2005] (Figure 3) which describes the damage and blast wave pressure from a 1 kiloton nuclear blast at various distances from the epicenter.

Table 4. Air blast damage.[a]

Distance from a 1 kt explosion (d_l in m)	Over pressure (p in Pa)	Description of air blast-induced damage
126	426000	Cars and trucks will be largely displaced and grossly distorted and will require rebuilding before use.
133	379000	Highway girder bridges will collapse.
149	297000	Cars and trucks will be overturned and displaced, requiring major repairs.
155	273000	Multistory steel-framed office-type buildings will suffer extreme frame distortion, incipient collapse.
229	121000	Highway truss bridges will collapse.
251	100000	Highway truss bridges will suffer substantial distortion of bracing.
389	42600	Multistory wall-bearing buildings will collapse.
411	38500	Multistory wall-bearing buildings will experience severe cracking and interior partitions will be blown down.
502	26800	Wood frame buildings will almost completely collapse.
549	22900	Interior partitions of wood frame buildings will be blown down. Roof will be severely damaged.
1160	6900	Glass windows shatter.

[a]Data extracted from Glasstone and Dolan (1977).

Figure 3: Blast wave pressure from a 1 Megaton explosion and resulting damage

1.3 Surface Effects

In addition to the environmental effects of an impact-shocked atmosphere, there are effects transmitted through the impact surface. A large impact will set off sufficient seismic shaking that nearby structures might suffer considerable damage. For the most part, the kinetic energy of the impactor transfers poorly to seimicity, with an efficiency of order 10^{-4}. If the impactor brings in a lot of energy, however, significant seismic shaking can result from an impact. Collins et al. [2005] relate the energy of an impact and the distance from the impact center to seismic shaking on the Mercalli Intensity scale, a scale which relates the Richter Scale intensity to observed effects. The energy of a seismic event, E, is related to its Richter magntitude, M, by

$$M = 0.67log(E) - 5.87 \tag{1}$$

We have reproduced both the mapping between the Richter and Mercalli scales and the observed effects of the Mercalli Scale. The perceived Richter magnitudes of an impact event decrease as the log of the distance away from the impact center so that for a 1.75 km diameter, rocky impactor with an entry velocity of 20 km/s, San Diego would experience VII-VIII Mercalli magnitude earthquakes (in addition to third-degree burns and severe structural damage from blast winds). We have reproduced the relation between distance and perceived magngitude for large distances ($r > 700km$) below as given in Collins et al. [2005] (Figure 5).

$$M_{eff} = M - 1.66log(r) - 6.399 \tag{2}$$

Table 2. Seismic magnitude/Modified Mercalli Intensity.[a]

Richter magnitude	Modified Mercalli Intensity
0–1	—
1–2	I
2–3	I–II
3–4	III–IV
4–5	IV–V
5–6	VI–VII
6–7	VII–VIII
7–8	IX–X
8–9	X–XI
9+	XII

[a]Based on data from Richter (1958).

Figure 4: Table 2 from Collins et al. [2005]

Generally for large impacts, many people living within a few hundred km of the impact site would die a quick and probably painless death.

2 How You will die a slow, lingering death

We define "long-term" environmental effects as those that occur over timescales ranging from as short as days to as long as years. Whereas most of the short-term consequences of an impact are felt on a "regional" scale (even for an extinction-level event), it is the long-term effects that are typically felt on a global scale and ultimately test which members of the biosphere will adapt and survive, or yield to their fate.

Table 3. Abbreviated version of the Modified Mercalli Intensity scale.

Intensity	Description
I	Not felt except by a very few under especially favorable conditions.
II	Felt only by a few persons at rest, especially on upper floors of buildings.
III	Felt quite noticeably by persons indoors, especially on upper floors of buildings. Many people do not recognize it as an earthquake. Standing motor cars may rock slightly. Vibrations similar to the passing of a truck.
IV	Felt indoors by many, outdoors by few during the day. At night, some awakened. Dishes, windows, doors disturbed; walls make cracking sound. Sensation like heavy truck striking building. Standing motor cars rocked noticeably.
V	Felt by nearly everyone; many awakened. Some dishes, windows broken. Unstable objects overturned. Pendulum clocks may stop.
VI	Felt by all, many frightened. Some heavy furniture moved; a few instances of fallen plaster. Damage slight.
VII	Damage negligible in buildings of good design and construction; slight to moderate in well-built ordinary structures; considerable damage in poorly built or badly designed structures; some chimneys broken.
VIII	Damage slight in specially designed structures; considerable damage in ordinary substantial buildings with partial collapse. Damage great in poorly built structures. Fall of chimneys, factory stacks, columns, monuments, and walls. Heavy furniture overturned.
IX	General panic. Damage considerable in specially designed structures; well-designed frame structures thrown out of plumb. Damage great in substantial buildings, with partial collapse. Buildings shifted off foundations. Serious damage to reservoirs. Underground pipes broken. Conspicuous cracks in ground. In alluviated areas sand and mud ejected, earthquake fountains, sand craters.
X	Most masonry and frame structures destroyed with their foundations. Some well-built wooden structures and bridges destroyed. Serious damage to dams, dikes, and embankments. Large landslides. Water thrown on banks of canals, rivers, lakes, etc. Sand and mud shifted horizontally on beaches and flat land. Rails bent slightly.
XI	As X. Rails bent greatly. Underground pipelines completely out of service.
XII	As X. Damage nearly total. Large rock masses displaced. Lines of sight and level distorted. Objects thrown into the air.

Figure 5: Table 3 from Collins et al. [2005]

52

2.1 Firestorm

As the ejecta from the initial impact re-entered the Earth's atmosphere ballistically, the thermal radiation emanating from the ejecta increased the global radiation flux by nearly two orders of magnitude for anywhere from one to a few hours. This dramatic, sudden, and large increase in the incident radiation was a likely trigger for wildfires that would be ignited essentially world-wide [Melosh et al., 1990].

Essentially, the expansion of the impact plume has a fundamental role in accelerating the ejecta to very fast velocities (comparable to and perhaps even exceeding Earth's escape velocity), and providing a "vent" that shoots ejecta upwards towards space. (Interesting to note is that comets, with their high impact velocities, may enable most of their ejecta to escape into space rather than falling back towards the Earth.) Melosh et al. [1990] make an initial estimate that most ejecta fall back to the Earth at velocities between 5 and 10 km s^{-1}. From a K/T impactor, they estimate that the re-entry of ejecta generated 50-150 kW m^{-2} of power deposition worldwide. (see Figure 6)

A secondary effect of the impact firestorm is the generation of copious amounts of soot, as shown by the presence of soot found at various sites around the world. Though the immediate danger from the firestorm to life would be the burn dangers and the vast spatial coverage of the fires, the long residence time of the soot would have reduced the incident lighting upon the Earth from the Sun, proving detrimental to life dependent on photosynthesis. In addition, the global wildfires could create enhanced amounts of CO_2, CO, CH_4, and N_2O that would perhaps harm the biosphere and affect the climate.

FIG. 1 a, Mass and b, power deposition in the upper atmosphere as a function of time after the ejection of 5×10^{15} kg at speeds between 5 and 10 km s^{-1} from a large impact on the Earth. Deposition rates are shown in three ranges of angle from the impact site.

Figure 6: from Melosh et al. [1990]

2.2 Sub-micron Dust Injection

Sub-micron dust can come from a variety of sources. First, a fraction of the condensing vapor plume will lie in this size range. Second, some of the re-entering ejecta will ablate and fragment into particles in this size range. Last, the shock wave from the impact blast will pulverize the target surface, producing some particles in this size range. It is estimated that about 0.1% of the pulverized rock is introduced into the Earth as sub-micron dust, mainly from studying the size distribution of pulverized rock from nuclear tests and laboratory experiments [Toon et al., 1997]. Also, oceanic impacts with sufficient energy (> 10^5 Mton on average) can produce craters with a significant amount of ejecta and dust, so it is likely that the effects from sub-micron dust are important for nearly all significant impact events. Most of the dust will be lofted into the stratospheric altitudes (or above), even for "small" impacts with energies of 10 to 100 Mton. This has been demonstrated by nuclear tests and large volcanic eruptions. Once the particles are deposited in the stratosphere, they induce vertical motions and shifts in the circulation pattern that enable a global distribution in a timescale of weeks. Whereas small impacts (less than or equal to 10^4 Mton) would produce climate perturbations within the normal annual variability, impacts larger than 10^5 Mton being to have a noticeable effect on the climate. An impact around 10^6 Mton could produce climate perturbations on the order of those experience after the 1815 Mount Tambora volcanic eruption (which produced the so-called "Year Without a Summer" in 1816). Impacts of greater magnitude have the potential of inhibiting photosynthesis and possibly darkening the Earth below the threshold of human vision. Covey et al. [1994] has used a GCM to simulate the climatic effects of a K/T magnitude impact on the present Earth. He finds that the strongest perturbations occur in continental interiors and were frequently below freezing (see Figure 7).
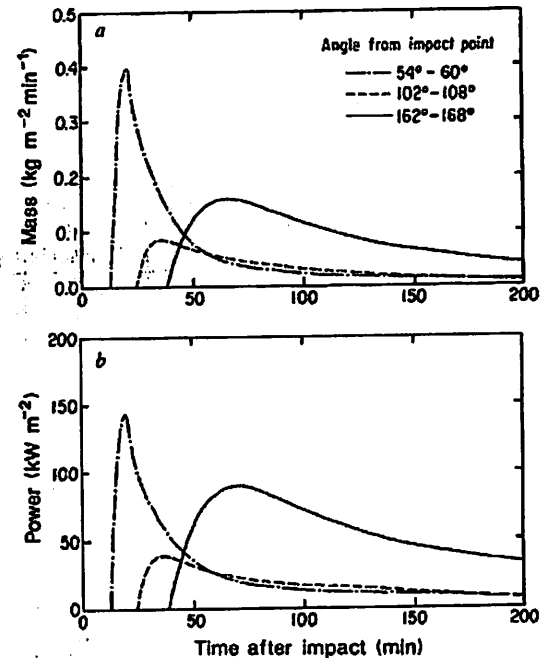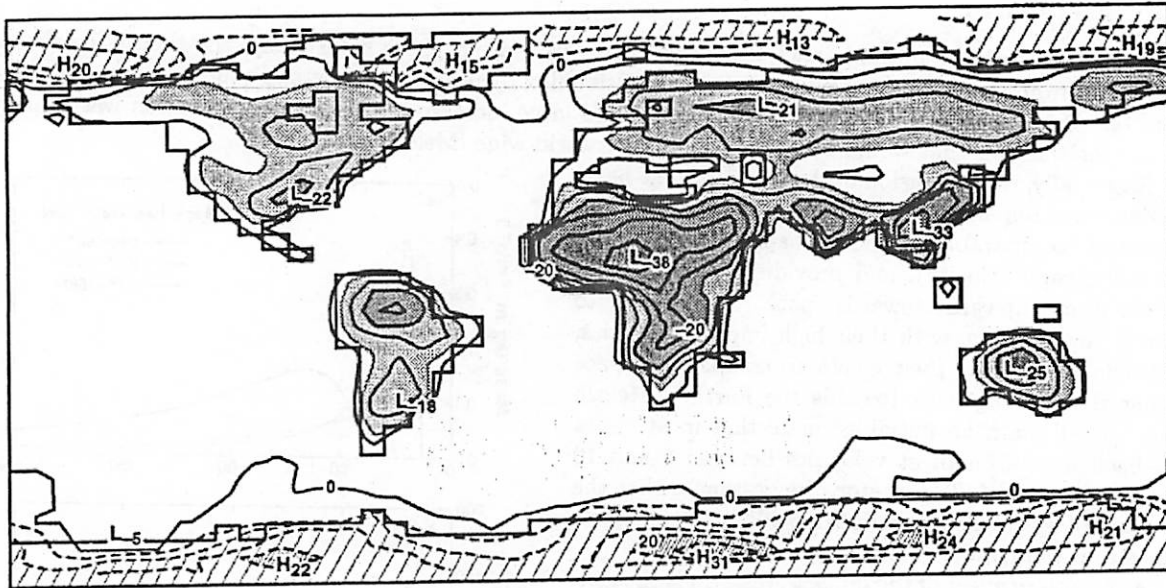
Changes in surface temperature (difference between control and dust-perturbed cases) averaged over 10–20 days after impact in the small-particle scenario of *Covey et al.* [1994]. Contours are drawn every 5 K. Lightly shaded areas are 10–20 K cooler in the dust perturbed cases; darkly shaded areas are more than 20 K cooler; sparsely hatched areas are 10–20 K warmer; densely hatched areas are more than 20 K warmer. In addition to selected contour levels, local maxima (high, H) and minima (low, L) of the temperature change are indicated. Reprinted from *Covey et al.* [1994] with kind permission of Elsevier Science–NL, Sara Burgerhartstraat 25, 1055 KV Netherlands.

Figure 7: from Covey et al. [1994]

2.3 Water Vapor Injection

Although Toon et al. [1997] estimates that a large amount of vaporized and displaced water will be deposited into the upper troposphere and stratosphere from a (likely) oceanic impact, just what exactly will happen to the water vapor and to the climate is somewhat unpredictable. Certainly the resultant water vapor cloud will condense, but the degree of condensation is variable. If the cloud takes several days to condense, the water cloud could be spread over a vast area, but a large fraction may be lost through photolysis. Furthermore, because water vapor radiates well in the infrared, a positive feedback may form where the resultant cooling will result in condensation and more precipitation. Toon et al. [1997] suggests that there is an upper limit to the amount of water vapor in the upper atmosphere of about 250 times ambient. However, there is a strong possibility that enhanced concentrations of water vapor would exist in the upper atmosphere for several years.

The effect of the enhanced water vapor is somewhat unknown, however. The enhancement would certainly strengthen the greenhouse effect, to first-order. However, the formation of ice clouds would either dampen or amplify the warming depending on the optical depth and particle size of the clouds. The warming would also be negated at first by the cooling brought about by any injected dust and soot. Furthermore, the warming would also be affected by the large thermal lag time of the ocean-atmosphere climate system. It is estimated that ambient levels of water vapor would be approached in as short as a few years as water vapor is transported to colder regions of the stratosphere.

2.4 Atmospheric Chemistry - Modification

2.4.1 Nitrous Oxide

The shock waves from the incoming bolide during its original entry into the atmosphere will form NO from atmospheric N_2 and O_2. Additional sources of NO from shock include the ejecta plume (if the plume is ascending with sufficient velocity), and the shock waves from ejecta particles as they re-enter the Earth's atmosphere. Although previous studies [Prinn and Fegley, 1987] estimated that the production of nitric acid rain would be sufficient to acidify global oceans (leading to dissolution of calcite, etc.), Toon et al. [1997] states that the danger is likely not as great, in fact estimating that the acidification of the resulting rain wouldn't be too much different from what is currently exprienced in industrial areas such as the eastern United States and Europe.

The real danger from nitric oxide generation is to the ozone layer. Impacts with energies exceeding 10^5 Mton would generate enough nitric oxide to significantly deplete the ozone layer and render it useless for protecting the biosphere. However, some caveats exist. The formation of nitrogen dioxide, which is strongly absorbing in the near-ultraviolet, from NO would render the change in ultraviolet penetration to the surface to be perhaps negligible. However, once the nitrogen dioxide dissipates (it essentially gets converted into nitric oxide), significantly enhanced levels of UV radiation could reach the surface. This enhancement could be mitigated by sulfate particles and clouds that form in the aftermath of an impact, as will be discussed in the following section.

2.4.2 Sulfur

The impacting population of comets and asteroids have a fairly significant amount of sulfur contained within them, ranging from 3 to 6 percent by weight. Pierazzo et al. [1998] has estimated that the K/T event may have released 40 to 560 Gt of S into the atmosphere, which is many orders of magnitude larger than what has been observed from volcanic eruptions. This sulfur (in the form of SO_2 or SO_3) would react with water vapor in the atmosphere (or water vapor generated or vaporized during the impact event) and produce stable sulfate hazes with long residence times. The resulting hazes would cool the Earth's surface and significantly perturb the climate for numerous years. Toon et al. [1997] estimates that optical depths of 10 or more may persist for up to a decade, because of the delayed oxidation time of the sulfur diox-

Thermal excursions produced by Chicxulub impact event as a function of time. Preimpact ambient temperature is marked with a dashed line.

Figure 8: from Kring [2000]

ide. The climatic impact of the sulfate clouds would be much greater than the dust/soot clouds, but it is unclear whether they would reduce light levels to the point that it would be detrimental to photosynthesis. Although the exact temperature perturbation is uncertain (and is not necessarily linearly correlated with the amount of sulfur added), the large amount of sulfur would take a long time to diffuse out of the atmosphere, meaning that the climate perturbation could last for several years or decades. A good figure depicting the overall temperature perturbation to the atmosphere is shown as Figure 8. [Kring, 2000]

Eventually, the sulfuric acid aerosols will diffuse into the troposphere and precipitate out as acid rain. Although nitric acid has been downgraded as a possibility for acidifying global oceans, sulfuric acid has emerged as a candidate. However, even the large amount of sulfur produced after the K/T event is about an order of magnitude below that necessary to depress oceanic pH to a level harmful to plankton. Nevertheless, the sulfuric acid rain may have been harmful on local scales in terrestrial or shallow freshwater ecosystems.

2.4.3 Other Chemicals

Erickson and Dickson [1987] has stated that the introduction of trace metals from the vaporized impactor (such as Fe, Co, Mn, Al, etc) as atmospheric aerosols could be absorbed into the ocean and be toxic to
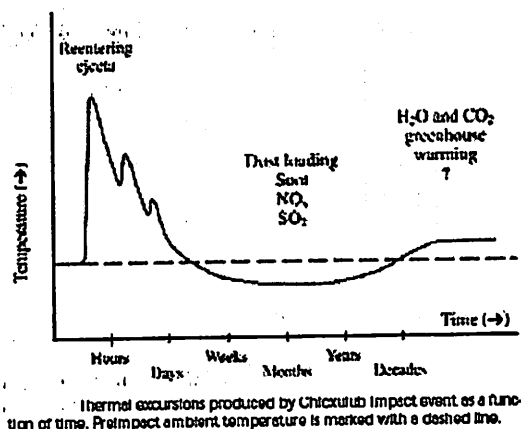
marine life. Also, Toon et al. [1997] and Pierazzo et al. [1998] both cite the injection of carbon dioxide into the atmosphere from vaporizing the target and impactor, and the global wildfires, the exact magnitude of both the total mass of carbon dioxide injected and its effect on the climate system is uncertain.

3 Planetary Connection: Mars

Segura et al. [2002] has published an article speculating on the environmental effects of an impact on early Mars. They state that the largest impacts would have produced "global blankets of hot ejecta" that would subsequently warm the surface. (They state the ejecta would fall back onto the surface extremely hot (~1600 K) because it would not completely cool radiatively. The warming would be sufficient in keeping the surface above the freezing point of water for up to a millenia, and would also cause subsurface ice to melt. The impacts would inject large amounts of precipitable water into the atmosphere, which would help carve out rivers and recharge aquifers. This is their preferred theory for explaining the valley networks on Mars that cut through the heavily cratered southern highlands and formed towards the end of the late heavy bombardment, countering the "classical" theory that an ancient warm and wet Mars generated the valley networks via its greenhouse climate. Instead, they envision a cold and dry Mars, where moist episodes (and opportunities for life) would only occur after large impacts.

References

G. S. Collins, H. J. Melosh, and R. A. Marcus. Earth Impact Effects Program: A Web-based computer program for calculating the regional environmental consequences of a meteoroid impact on Earth. *Meteoritics and Planetary Science*, 40:817–840, June 2005.

C. Covey, S. Thompson, P. Weissman, and M. MacCracken. Global climatic effects of atmospheric dust from an asteroid or comet impact on Earth. *Global and Planetary Change*, 9:263–273, 1994.

D. J. Erickson and S. M. Dickson. Global Trace-Element Biogeochemistry at the K/t Boundary: Oceanic and Biotic Response to a Hypothetical Meteorite Impact. *Geology*, 15:1014–1017, 1987.

D. A. Kring. Impact Events and their effect on the origin, evolution, and distribution of life. *GSA Today*, 10:1–7, 2000.

H. J. Melosh and A. M. Vickery. Impact erosion of the primordial atmosphere of Mars. *Nature*, 338:487–489, April 1989. doi: 10.1038/338487a0.

H. J. Melosh, N. M. Schneider, K. J. Zahnle, and D. Latham. Ignition of global wildfires at the Cretaceous/Tertiary boundary. *Nature*, 343:251–254, January 1990. doi: 10.1038/343251a0.

E. Pierazzo, D. A. Kring, and H. J. Melosh. Hydrocode simulation of the Chicxulub impact event and the production of climatically active gases. *Journal of Geophysical Research*, 103:28607–28625, December 1998. doi: 10.1029/98JE02496.

R. G. Prinn and B. J. Fegley. Bolide impacts, acid rain, and biospheric traumas at the Cretaceous-Tertiary boundary. *Earth and Planetary Science Letters*, 83:1–4, 1987. doi: 10.1016/0012-821X(87)90046-X.

T. L. Segura, O. B. Toon, A. Colaprete, and K. Zahnle. Environmental Effects of Large Impacts on Mars. *Science*, 298:1977–1980, December 2002. doi: 10.1126/science.1073586.

O. B. Toon, K. Zahnle, D. Morrison, R. P. Turco, and C. Covey. Environmental perturbations caused by the impacts of asteroids and comets. *Reviews of Geophysics*, 35:41–78, 1997. doi: 10.1029/96RG03038.

R. P. Turco, O. B. Toon, C. Park, R. C. Whitten, J. B. Pollack, and P. Noerdlinger. An analysis of the physical, chemical, optical, and historical impacts of the 1908 Tunguska meteor fall. *Icarus*, 50:1–52, 1982. doi: 10.1016/0019-1035(82)90096-3.

K. Zahnle. Atmospheric chemistry by large impacts. *Global catastrophes in Earth history: An interdisciplinary conference on impacts, volcanism, and mass mortality*, pages 271–288, 1990.

Palæobotanical Evidence for the K/T Impact
Diana E. Smith

A large bolide impact would produce lots of light-attenuating debris causing an "impact winter". In the K/T boundary section near Teapot Dome, WY, structurally deformed aquatic leaves were found and duplicated in extant aquatic leaves by experimental freezing. Based on the reproductive stages reached by the fossils, freezing and hence the impact winter took place in approximately June.
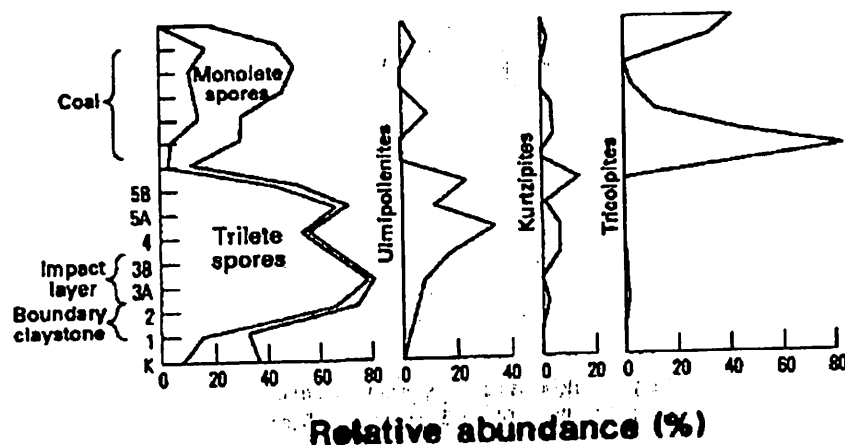
FIGURE 1: Palynomorph diagram of the Teapot Dome boundary interval.

- **Fern spores:** Trilete and Monolete. Fern spike of the clasts of bed 2 composed single type of fern spore. Fern abundance in the upper part of the coal composed of at least 5 spore types. (Sporing by plants grown from spores after impact winter over)

- **Deciduous plants:** Ulmipollenites, Kurtzipites, and Tricolpites. Abundance increases as relative abundance of fern spores decreases. Deciduous plants continue flowering after deposition of the impact layer. (Suggests impact winter did not result from second impact)

The Teapot Dome site preserves many leaves of aquatics in fine-grained, light-colored clay unlike characteristic carbonaceous mudstone of the lily pond before the boundary interval:

- Pond lily (*Paranymphaea*, allied to the extant *Nuphar* of Nymphaeaceae)
- Lotus (*Nelumbites*, allied to extant *Nelumbo* of Nelumbonaceae)

Fossils contain immature pollens of Nelumbonaceae and Nymphaeaceae, and since both occur in antherial masses, this suggests derivation from flowers at/near deposition site.

Leaf cuticles in bed 2 clasts and beds 3-5 have irregular folds that are not present in cuticles of bed 1. Experimental freezing with subsequent expansion produced these same folds, and unfrozen control and unfrozen dried leaves did not show these folds.

- At time of freezing, *Paranymphaea* had leafed out, bloomed, and produced seeds, whereas *Nelumbite* flowers were still immature.
- Today, *Nuphar* blooms and fruits before *Nelumbo*.
- Mature *Nelumbo* blooms develop approximately 2 months after the mean temperature reaches 16°C.
  - Mean temp of 16°C would have occurred in late April in Cretaceous Wyoming→Nelumbonaceae would bloom in late June→freezing would have been in approximately early June.
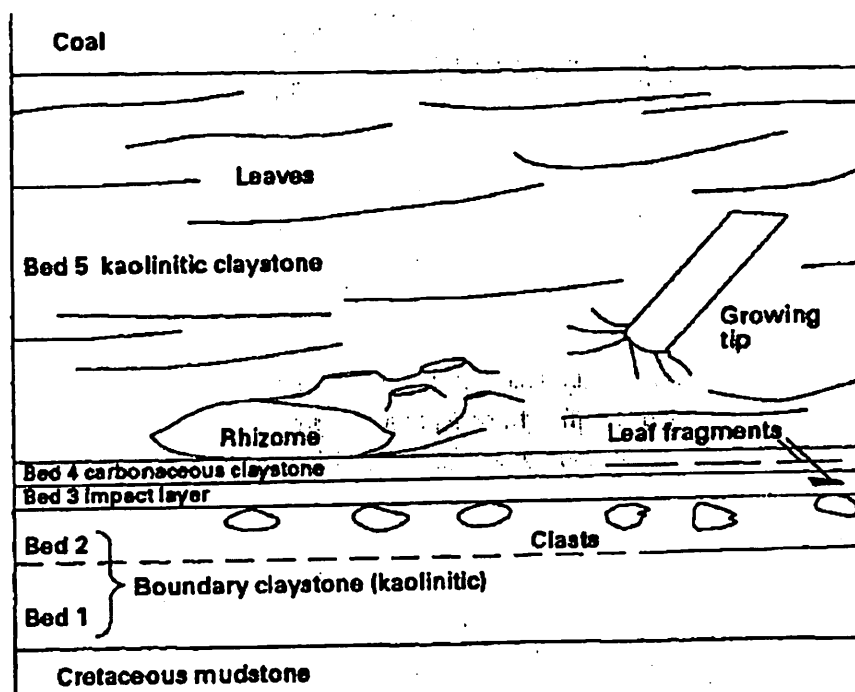
FIGURE 2: Diagram of the boundary interval at Teapot Dome.

TABLE 1	Suggested sequence of events represented in Teapot Dome K/T boundary interval
Bed 5	Finer debris from second impact falls on, and is washed into, pond; partially decayed, heavy *Nelumbites* rhizomes (Fig. 3*d*) deposited at base; decaying *Paranymphaea* leaves (Fig. 3*i*), pollen (Fig. 3*e*) and seeds (Fig. 3*k*), and *Nelumbites* leaves (Fig. 3*j*) and growing tips (Fig. 3*h*) randomly deposited; deciduous plants continue flowering: mean daily temperature 30 °C.
Bed 4	Little sedimentation; decaying debris falling to bottom is compacted, forming carbonaceous sediment.
Bed 3	Shock-metamorphosed minerals from second impact arrive; some decaying leaves deposited, forming layering; more deciduous plants begin flowering.
Bed 2	Mean daily temperature rises to 20 °C; fallout debris continues to be washed into pond; a single kind of fern reaches sporing stage; a few kinds of deciduous plants break dormancy and flower; mean daily temperature rises to 25–30 °C; spores and pollen fall on decaying leaves still covered with some fallout debris, which concentrates (with pollen and spores) as pods on cup-shaped *Nelumbites* leaves (Fig. 3*j*) and hardens in sun; some leaves decay further, releasing pods that, with some debris-filled petioles, fall on, and are incorporated in, upper part of bed 2; second bolide strikes; microtektite shower.
Bed 1	Mean daily temperature rises above 0 °C; rains begin; influx of water into pond area buoys solid ice upward, pulling growing tips of *Paranymphaea* rhizomes and *Nelumbites* off pond bottom and from upper part of Cretaceous pond sediment; ice melts rapidly, and fallout debris falls to bottom of pond; sediments rapidly wash in, unlayered, mostly comprising impact fallout but including some debris on land surface at time of impact (including remains of Cretaceous plants such as cuticles of '*Artocarpus*' *dissecta* and pollen of *Proteacidites*); a single kind of fern sends up new shoots from rhizomes.
Between latest Cretaceous carbonaceous shale and bed 1	Within a few days, mean daily temperature falls to −5 to −10 °C; pond freezes over (possibly to bottom); finer impact debris arrives after freezing, falling on ice and surrounding land; aquatic plants die, some frozen into ice and some falling on ice; many terrestrial plants, especially broad-leaved evergreens, die or are killed back, but some deciduous plants re-enter dormancy; no deposition on pond bottom.
Latest Cretaceous	Mean daily temperature ~19 °C; *Paranymphaea* flowering and fruiting, *Nelumbites* flower buds still unopened; pond also covered with abundant floating water-fern (*Azolla*); first bolide strikes, and microtektites arrive.

The time between initiation of the impact winter and the deposition of bed 5 was ~3-4 months. The impact winter lasted at least 1-2 weeks (time for fallout debris to occur in both hemispheres), but survival of large aquatic ectotherms suggests less than 2 months.

Impact Stratigraphy in the Umbria-Marche Region of Italy

Dave O'Brien

The Umbria-Marche Sequence

The Umbria-Marche (U-M) region is located in the northeastern Apennine mountains of Italy. From ~200 Ma through ~20 Ma, most of this region was a deep, pelagic (open-ocean) basin undergoing extensional tectonics and carbonate deposition. Following that phase, the region entered a compressional regime that built up the Apennine mountains and exposed the carbonate sequence, which provides a nearly uninterrupted record of the geologic, oceanographic, and biological processes that occurred in the region over the last 200 Myr. A number of impact signatures are recorded in the U-M sequence and have been extensively studied.

The K/T Boundary in the U-M Region

It was in an outcrop of the K/T boundary near in Gubbio where Walter Alvarez and his team first detected an Iridium enrichment in the boundary clay that was seen as a signature of a large extraterrestrial impact event. This iridium enrichment was subsequently detected in many other K/T outcrops in the region and throughout the world, in addition to other impact markers such as shocked quartz and impact microspherules.

The large number of K/T outcrops throughout the U-M region give an interesting perspective on the diversity of environments existing throughout the U-M basin around the time of the impact. I'll bring samples that I've collected from various locations in the U-M region and discuss some of the differences between the sections at **Gubbio** and **Frontale**, **Furlo** (Pietralata) and **Monte Conero** (Fonte d'Olio and Fornaci Quarry). In addition, I'll discuss the differences between the U-M sections in general and those of the Raton Basin.

The E/O Boundary and Late Eocene Record in the U-M Sequence

Massignano has been designated as the Global Stratotype Section and Point (GSSP) for the Eocene/Oligocene boundary. The E/O boundary and the late Eocene is well-recorded in the Massignano section, as well as in the Contessa section north of Gubbio and several other locations. These sections consist mostly of marly limestone occasionally interspersed with biotite-rich layers that can be radioactively dated. The Eocene/Oligocene boundary is located at the 19-meter point of the Massignano section, and by interpolating between radioactively-dated biotite-rich layers, its age is estimated as 33.7±0.4 Ma.

A prominent Iridium peak is found at 5.61 m in the Massignano section and has been dated to 35.7±0.4 Ma by interpolating between dated biotite layers. This layer also contains shocked quartz, extraterrestrial spinel, and microkrystites, all strongly suggestive of an impact event, and its age is consistent with the age estimates for both the Popigai (Siberia, 35.7±0.8 Ma) and Chesapeake Bay (35.5±0.3 Ma) craters, each of which are roughly 100 km in diameter. In addition, there is a broad peak in Helium-3 enrichment from about the 1-meter point to the 15-meter point of the section. The multiple large impact events occurring during the few Myr of He-3 enrichment at Massignano is seen as evidence for a comet shower occurring during the late Eocene (Farley et al. 1998).

There is also another significant Iridium peak at 10.25 m and a smaller peak at 6.2 m in the Massignano section, but I find no mention of shocked quartz, extraterrestrial spinel or microkrystites associated with those Iridium anomalies.

References

Farley, K., A. Montanari, E. M. Shoemaker and C. S. Shoemaker (1998). Geochemical evidence for a comet shower in the late Eocene. Science 280, pp. 1250-1253.

Montanari, A. and C. Koeberl (2000). Impact Stratigraphy: The Italian Record. Springer, Berlin.
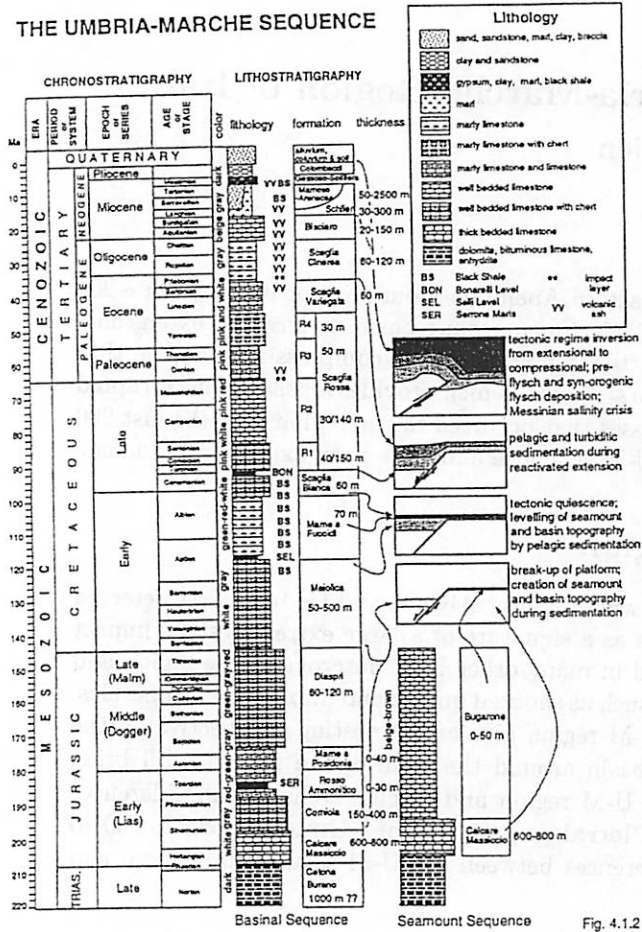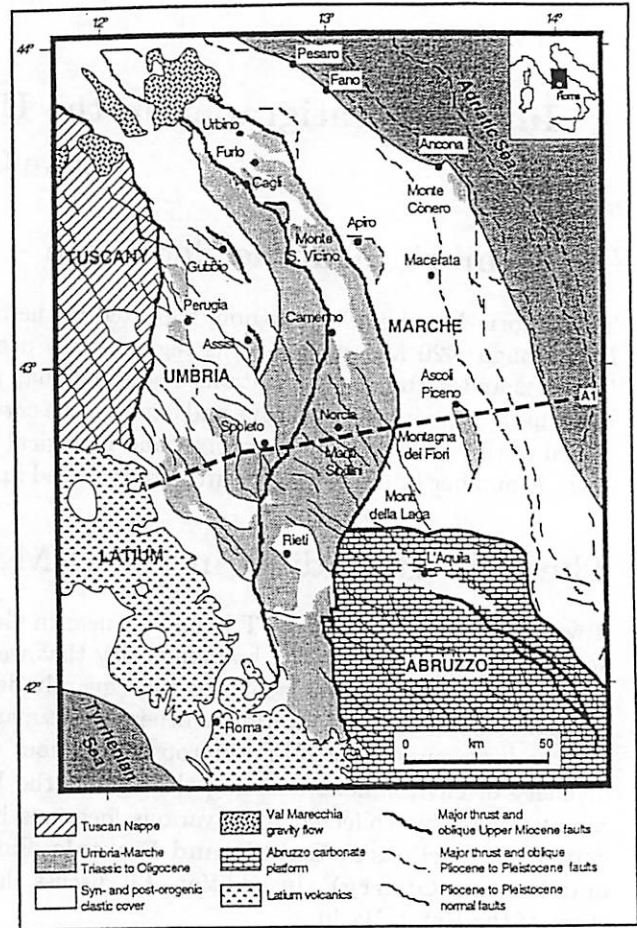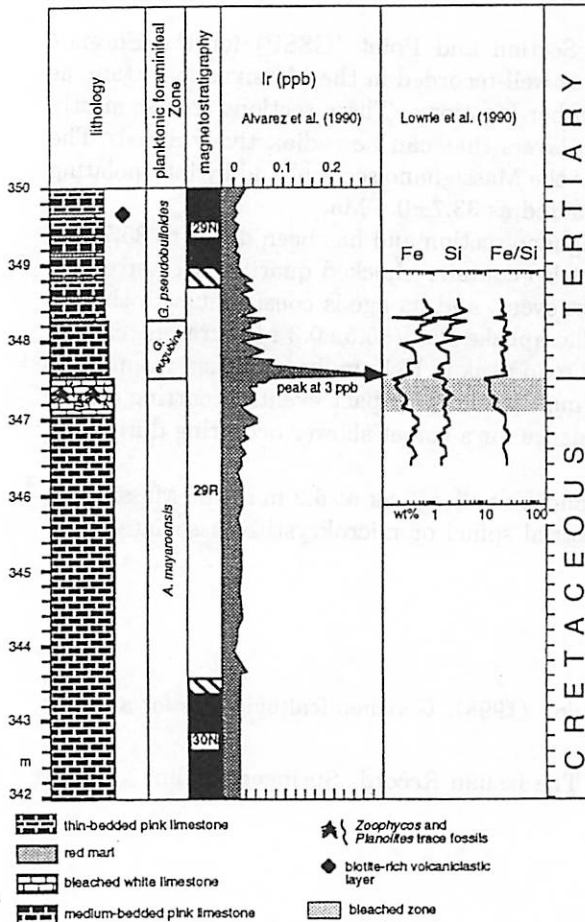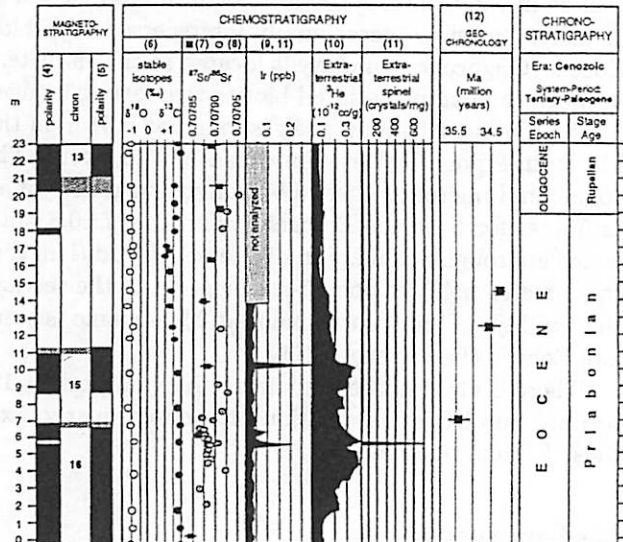
THE UMBRIA-MARCHE SEQUENCE

CHRONOSTRATIGRAPHY LITHOSTRATIGRAPHY

Lithology

	sand, sandstone, marl, clay, breccia
	clay and sandstone
	gypsum, clay, marl, black shale
	marl
	marly limestone
	marly limestone with chert
	marly limestone and limestone
	well bedded limestone
	well bedded limestone with chert
	thick bedded limestone
	dolomia, bituminous limestone, anhydrite

BS   Black Shale   ••   impact layer
BON   Bonarelli Level
SEL   Selli Level   VVV volcanic ash
SER   Serrone Marls

Chronostratigraphy / Lithostratigraphy columns:

QUATERNARY
CENOZOIC — TERTIARY — NEOGENE — Pliocene / Miocene
PALEOGENE — Oligocene / Eocene / Paleocene
MESOZOIC — CRETACEOUS — Late / Early
JURASSIC — Late (Malm) / Middle (Dogger) / Early (Lias)
TRIAS. — Late (Norian)

Formations / thickness:
Marne Amevecci (50-2500 m); Schlier (30-300 m); Bisciaro (20-150 m); Scaglia Cinerea (60-120 m); Scaglia Variegata (50 m); R4 (30 m); R3 (50 m); Scaglia Rossa R2 (30/140 m), R1 (40/150 m); Scaglia Bianca (50 m); Marne a Fucoidi (70 m); Maiolica (53-500 m); Diaspri (60-120 m); Marne a Posidonia (0-40 m); Rosso Ammonitico (0-30 m); Corniola (150-400 m); Calcare Massiccio (600-800 m); Cetona Burano (1000 m ??)

Seamount Sequence: Bugarone (0-50 m); Calcare Massiccio (600-800 m)

tectonic regime inversion from extensional to compressional; pre-flysch and syn-orogenic flysch deposition; Messinian salinity crisis

pelagic and turbiditic sedimentation during reactivated extension

tectonic quiescence; levelling of seamount and basin topography by pelagic sedimentation

break-up of platform; creation of seamount and basin topography during sedimentation

Basinal Sequence   Seamount Sequence   Fig. 4.1.2

Geographic map (Umbria-Marche region):

Cities/locations: Pesaro, Fano, Urbino, Furb, Cagli, Ancona, Monte Cònero, Monte S. Vicino, Apiro, Macerata, Gubbio, Perugia, Assisi, Camerino, MARCHE, UMBRIA, TUSCANY, Spoleto, Norcia, Monti Sibillini, Ascoli Piceno, Montagna dei Fiori, Monti della Laga, Rieti, LATIUM, L'Aquila, ABRUZZO, Roma, Adriatic Sea, Tyrrhenian Sea

Tuscan Nappe	Val Marecchia gravity flow	Major thrust and oblique Upper Miocene faults
Umbria-Marche Triassic to Oligocene	Abruzzo carbonate platform	Major thrust and oblique Pliocene to Pleistocene faults
Syn- and post-orogenic clastic cover	Latium volcanics	Pliocene to Pleistocene normal faults

km 0 — 50

BOTTACCIONE

lithology | planktonic foraminiferal Zone | magnetostratigraphy

Ir (ppb)
Alvarez et al. (1990)
Lowrie et al. (1990)

0   0.1   0.2

Fe Si Fe/Si

peak at 3 ppb

wt%   0.1   1   10   100

Zones: G. pseudobulloides, 29N, A. mayaroensis, 29R, 30N

TERTIARY / CRETACEOUS

350 – 342 m

	thin-bedded pink limestone
	red marl
	bleached white limestone
	medium-bedded pink limestone

Zoophycos and Planolites trace fossils

biotite-rich volcaniclastic layer

bleached zone

GLOBAL STRATOTYPE SECTION AND POINT FOR THE EOCENE-OLIGOCENE BOUNDARY: THE GSSP OF MASSIGNANO (1)

MAGNETO-STRATIGRAPHY			CHEMOSTRATIGRAPHY						(12) GEO-CHRONOLOGY	CHRONO-STRATIGRAPHY
			(6)	■(7) ○(8)	(9,11)	(10)	(11)			
polarity (4)	chron	polarity (5)	stable isotopes (‰)	$^{87}Sr/^{86}Sr$	Ir (ppb)	Extra-terrestrial ^3He (10^{-12} cc/g)	Extra-terrestrial spinel (crystals/mg)		Ma (million years)	Era: Cenozoic / System-Period: Tertiary-Paleogene
			$\delta^{18}O$ $\delta^{13}C$ -1 0 +1	0.70785 0.70790 0.70795	0.1 0.2	0.1 0.3	200 400 600		35.5 34.5	Series Epoch / Stage Age

Chron labels: 13, 15, 16

not analyzed

m scale: 23 down to 1

Era: Cenozoic; System-Period: Tertiary-Paleogene; Series/Epoch: OLIGOCENE (Rupelian), EOCENE (Priabonian)

REFERENCES

(1) Premoli Silva and Jenkins 1993
(2) Mattias et al. 1992
(3) Coccioni et al. 1988
(3a) Blow 1969; Berggren et al. 1985
(3b) Berggren et al. 1995
(3c) Berggren and Miller 1989
(3d) Martini 1971
(3e) Okada and Bukry 1980
(4) Bice and Montanari 1988
(5) Lowrie and Lanci 1994
(6) Odin et al. 1988
(7) Montanari et al. 1991
(8) Vonhof et al. 1998
(9) Montanari et al. 1993
(10) Farley et al. 1998
(11) Pierrard et al. 1998
(12) Montanari et al. 1985; Odin et al. 1988; Odin et al. 1991
(13) Clymer et al. 1996; Langenhorst 1996
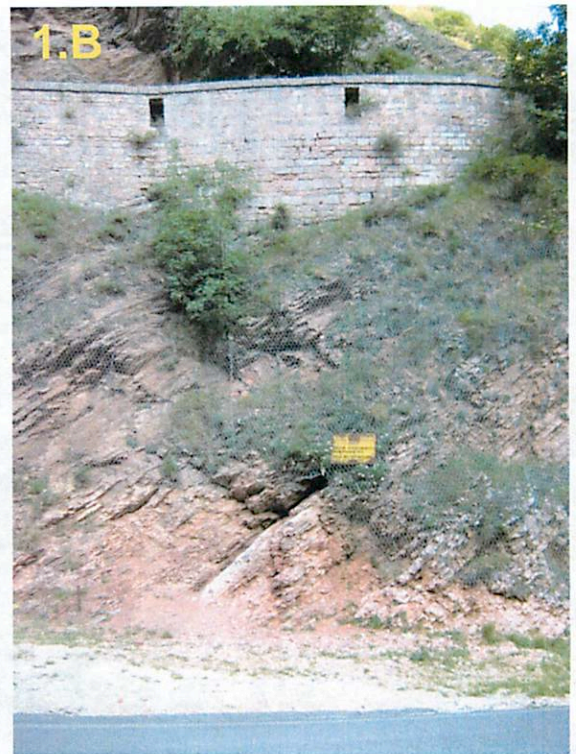
1.A,B) The 'original' K/T outcrop in the Bottacione gorge north of Gubbio, which lies along the road beneath a still-working 14th century aqueduct

2.A) The Frontale K/T outcrop, where samples were collected. For the most part it's similar to Gubbio sections

2.B) Planolite at the top of the K at Frontale

2.C) Zoophycos ~10 cm below the boundary at Frontale

3) The Fonte d'Olio outcrop (Monte Conero), with the K/T boundary marked by the pen.

4) The Fornaci East K/T outcrop (Monte Conero), where samples were collected—hard to get a good context image because it was blocked by trees.
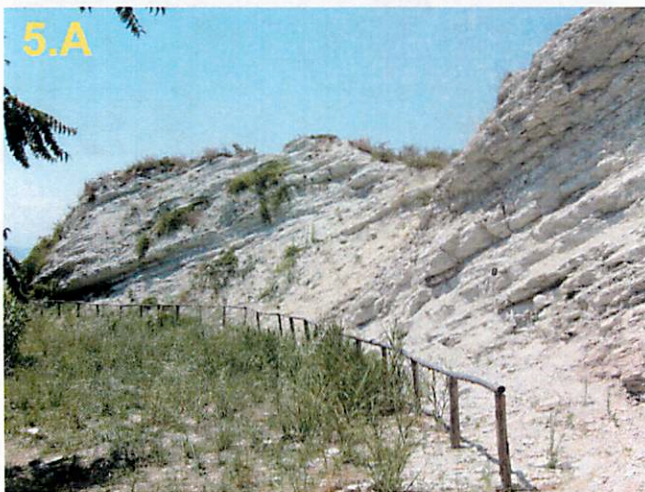
5.A,B) The Massignano section, which is the global stratotype for the Eocene/Oligocene boundary. The E/O boundary is towards the left of A at meter-marker 19. Samples were collected from the spot marked by the knife and pen in B, at the 5.6 meter point.

Impact Hazards
Comets vs. Asteroids and the Search for Near Earth Objects

David A. Minton

Introduction

The IAU Minor Planet Center (http://cfa-www.harvard.edu/iau/mpc.html) currently lists 799 "Potentially Hazardous Asteroids" (PHAs). All but a handful were discovered since 1990 and the majority of them discovered since the year 2000. Clearly we are only beginning to bet a quantitative idea about the impact risk the Earth faces. In many ways we have the Chixculub crater to thank for our increased understanding of this threat. The story of the demise of the dinosaurs from the effects of a massive impact of an object from outer space holds a great deal of popular appeal. Popular appeal harnessed into public funding has helped spur the search for any object that might have *our* name on it.

Steady state asteroid flux vs. comet showers

One of the great controversies surrounding mass extinction events, such as the K-T boundary impact at 65 Ma, is the idea that mass extinctions may be periodic. If large impacts trigger mass extinctions (another major controversy of its own), then the period of mass extinctions may be linked to periodic influxes of extraterrestrial material.

It has been suggested that the solar system's passage through the mid-plane of the galactic disk every ∼30 My, where there is a higher concentration of giant molecular clouds, could perturb the Sun's Oort cloud and send showers of comets into the inner solar system [1, 4, 13]. A periodicity of 28.4 Ma in mass extinctions events was reported by Raub [14]. Different statistical analyses by different groups on the cratering record seems to result in periods of either 26-32 My or 34-38 Ma [12, 15, 17].

Linking mass extinctions to impact events has not been very successful, except in the case of the K-T boundary [7]. Figure 2 is a compilation of dates (with uncertainties) of mass extinction events along side discovered impact structures and large scale igneous provinces. It should be noted that there are some significantly large impact structures that are separated in time by millions of years from any mass extinctions (i.e. Manicougagan crater, Popigai/Cheasapeake Bay, and others not listed in Figure 2 like Puchezh-Katunki, and 80 km diameter crater dated to 167±3 Ma). Based on the estimated cratering rate, large impacts seem to be more common than mass extinctions.

The statistical significance of the periodicity of impact events has met with a great deal of skepticism [9, 11]. Grieve and Shoemaker note that all statistical analyses are done on the terrestrial cratering record, which is quite poor due to Earth's active surface, and if one takes into account such biases the periodicity vanishes. From a steady state flux of material based on the terrestrial cratering rate, Grieve and Shoemaker estimate that we'd expect to see around 1 − 5 craters greater than 20 km in diameter every few million

years [8,9]. This view takes the K-T impact to be a rather ordinary occurrence in Earth's history, due to inevitable encounters between the Earth and a steady-state population of Near Earth Asteroids (NEAs).

One long standing problem in studies of NEA dynamics is their short dynamical lifetime. They are on terrestrial planet crossing orbits that are unstable on timescales of 10 Ma [6]. Therefore a source is needed to replenish them, but no obvious mechanism for their delivery from the asteroid belt was known. Yarkovsky, a Polish engineer, wrote a pamphlet in which he proposed a mechanism by which a rotating object in orbit and not in thermal equilibrium would radiate heat asymmetrically, thereby undergoing a small force that could change its orbital elements over time [5]. Now called the *Yarkovsky effect*, this slow change in semimajor axis can deliver asteroids from stable orbits into chaotic regions inside various mean motion or secular resonances.

Once inside a chaotic region, the asteroid can become Earth crossing in a relatively short time (< 1 My for the ν_6 secular resonance, for example). The maximum semimajor drift rate due to the Yarkovsky effect occurs for objects $\sim 1 - 10$ km in diameter, therefore the NEA population should have a size distribution that is more enhanced in small objects relative to the main belt population. This is seen in the normalized size frequency distribution shown in Figure 1. Also, the spectra of NEAs seems to be most similar to that of asteroids in the inner asteroid belt (dominated by S-type objects) [2].

The effect of Yarkovsky orbital drift has now been observed in at least one asteroid, 6489 Golevka [3].

Conclusion

The constant influx of asteroids from the main belt into terrestrial planet crossing NEAs due to the Yarkovsky effect seems to be more consistent with the idea of Earth impacts as being steady (as apposed to periodic) with impactors dominated by asteroidal material (as apposed to cometary). This view is supported by dynamical and spectral studies of the NEA population [2,6]. However this is by no means a settled issue. Whether any *particular* impactor, such as the one that formed Chixculub crater, was asteroidal or cometary is more difficult to determine. While the Ir enhancement has often been used as evidence than the Chixculub impactor was an asteroid, Jeffers has proposed that the Chixculub impactor was a Jupiter-family comet (JFC) from dynamical constraints and the estimated cratering rate due to JFCs vs. NEAs [10].
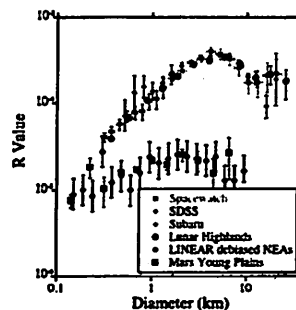

Fig. 4. The size distributions of the projectiles (derived from the crater size distributions), compared with those of the MBAs and NEAs. The red dots (upper curve) are for the lunar highlands (Population 1), and the red squares (lower curve) are for the Mars young plains (Population 2). The other colors and point styles are for the asteroids derived by various authors: in the upper curves, the light blue, the dark blue, and the green symbols are from Spacewatch (24), the Sloan Digital Sky Survey (25), and the Subaru asteroid surveys (26), respectively; the black dots in the lower curves are the debiased LINEAR NEAs (28). An arbitrary normalization factor was applied to obtain the R values for the asteroids. The MBA size distribution is virtually identical with Population 1 projectiles responsible for the LHB crater record. The NEA size distribution is the same as Population 2 projectiles responsible for the post-LHB crater record.

Figure 1: Figure from Strom, et al. (2005) [16]

Table 1
Comparison between ages of some epoch/stage boundaries, some asteroid/comet impacts and some Large Igneous Provinces (LIP) and Continental Flood Basalt (CFB) provinces

Epoch/stage boundaries and mass extinctions (EXT)	Asteroid/comet impacts (IMP)	Large Igneous Province (LIP, CFB)	Age overlaps
Mid-Miocene Langhian 15.97 Ma	Ries (24 km) 15.1 ± 1 Ma	Columbia Plateau Basalt 16.2 ± 1 Ma	
Eocene–Oligocene boundary 33.9 ± 0.1 Ma	Popigai (100 km) 35.7 ± 0.2 Ma; Cheasapeake Bay (85 km) 35.5 ± 0.3 Ma	Ethiopean Basalts 36.9 ± 0.9 Ma	IMP–CFB Near age overlap
KT boundary 65.5 ± 0.3 Ma	Chicxulub (170 km) 64.98 ± 0.05 Ma; Boltysh (25 km) 65.17 ± 0.64 Ma	Deccan Pleateau Basalts. 65.5 ± 0.7 Ma (pooled Ar ages — 65.5 ± 2.5 Ma)	IMP–CFB–EXT age overlap
Cenomanian–Turonian 93.5 ± 0.8 Ma	Steen River (25 km) 95 ± 7 Ma	Madagascar Basalts 94.5 ± 1.2 Ma	IMP–CFB Age overlap
Aptian (Lower Cretaceous) ·125–112 Ma	Carlswell (39 km) 115 ± 10 Ma; Tookoonooka (55 km), Tallundilli (30 kn) both 128 ± 5 Ma; Mien (9 km) 121 ± 2.3 Ma; Rotmistrovka (2.7 km) 120 ± 10 Ma	Ontong-Java LIP 120 Ma; Kerguelen LIP 120–112.7–108.6 Ma; Ramjalal Basalts 117 ± 1 Ma	Possible IMP (Carswell) – LIP age overlap
Jurassic–Cretaceous boundary 145.5 ± 4 Ma	Morokweng (70 km) 145 ± 0.8 Gosses Bluff (24 km) 142.5 ± 0.8 Ma; Mjolnir (40 km) 143 ± 2.6 Ma	Dykes SW India 144 ± 6 Ma	IMP–CFB–EXT age overlap
End-Pliensbachian 183 ± 1.5 Ma		Peak Karoo volcanism Start 190 ± 5 Ma; Peaks 193,178 Ma; Lesotho 182 ± 2 Ma	CFB–EXT age overlap
Triassic–Jurassic 199.6 ± 0.3 Ma	Manicouagan (100 km) 214 ± 1 Ma; Rochechouart (23 km) 213 ± 8 Ma; Saint Martin (40 km) 220 ± 32 Ma	Central Atlantic Igneous Province — 203 ± 0.7 to 199 ± 2 Ma; Newark Basalts 201 ± 1 Ma	CFB–EXT age overlap
Permian–Triassic 251 ± 0.4 Ma 251.4 ± 0.3 to 250.7 ± 0.3 Ma	Minor impact effects (possible pdf in detrital quartz grains, metal particles)	Siberian Norlisk 251.7 ± 0.4 to 251.1 ± 0.3 Ma	CFB–EXT age overlap
Late to end Devonian ~374–359 Ma	Woodleigh (120 km) 359 ± 4 Ma; Siljan (52 km) 361 ± 1.1 Ma; Alamo breccia (~100 km) ~360 Ma; Charlevoix (54 km) 342 ± 15 Ma	Rifting and 364 Ma Pirpyat–Dneiper–Donets volcanism	IMP–CFB–EXT age overlap over ~15 m.y.
End-Ordovician 443.7 ± 1.5 Ma	Several small poorly dated impact craters		EXT
End-lower Cambrian 513 ± 2 Ma		Kalkarindji volcanic Province, northern Australia 507 ± 4 Ma	CFB–EXT age overlap
~580 Ma	Acraman/Bunyeroo		IMP–EXT/ RADIATION age overlap

Sources of age data [1,17–19,22].

Figure 2: Table from Glikson (2004) [7]

67

References

[1] W. Alvarez and R. A. Muller. Evidence from crater ages for periodic impacts on the earth. *Nature*, 308:718–720, April 1984.

[2] R. P. Binzel, D. Lupishko, M. di Martino, R. J. Whiteley, and G. J. Hahn. Physical Properties of Near-Earth Objects. *Asteroids III*, pages 255–271, 2002.

[3] S. R. Chesley, S. J. Ostro, D. Vokrouhlický, D. Čapek, J. D. Giorgini, M. C. Nolan, J.-L. Margot, A. A. Hine, L. A. M. Benner, and A. B. Chamberlin. Direct Detection of the Yarkovsky Effect by Radar Ranging to Asteroid 6489 Golevka. *Science*, 302:1739–1742, December 2003.

[4] S. V. M. Clube and W. M. Napier. Comet capture from molecular clouds - A dynamical constraint on star and planet formation. *Monthly Notices of the Royal Astronomical Society*, 208:575–588, June 1984.

[5] P. Farinella, D. Vokrouhlicky, and W. K. Hartmann. Meteorite Delivery via Yarkovsky Orbital Drift. *Icarus*, 132:378–387, April 1998.

[6] B. Gladman, P. Michel, and C. Froeschlé. The Near-Earth Object Population. *Icarus*, 146:176–189, July 2000.

[7] A. Glikson. Asteroid/comet impact clusters, flood basalts and mass extinctions: Significance of isotopic age overlaps. *Earth and Planetary Science Letters*, 236:933–937, August 2005.

[8] R. A. F. Grieve, V. L. Sharpton, A. K. Goodacre, and J. B. Garvin. Periodic Cometary Showers: Real or Imaginary? In *Lunar and Planetary Institute Conference Abstracts*, pages 296–297, March 1985.

[9] R. A. F. Grieve and E. M. Shoemaker. The Record of Past Impacts on Earth. In T. Gehrels, M. S. Matthews, and A. M. Schumann, editors, *Hazards Due to Comets and Asteroids*, pages 417–+, 1994.

[10] S. V. Jeffers, S. P. Manley, M. E. Bailey, and D. J. Asher. Near-Earth object velocity distributions and consequences for the Chicxulub impactor. *Monthly Notices of the Royal Astronomical Society*, 327:126–132, October 2001.

[11] L. Jetsu and J. Pelt. Spurious periods in the terrestrial impact crater record. *Astronomy and Astrophysics*, 353:409–418, January 2000.

[12] W. M. Napier. Evidence for cometary bombardment episodes. *Monthly Notices of the Royal Astronomical Society*, 366:977–982, March 2006.

[13] W. M. Napier and S. V. M. Clube. A theory of terrestrial catastrophism. *Nature*, 282:455–459, November 1979.

[14] D. M. Raup and J. J. Sepkoski. Periodic Extinction of Families and Genera. *Science*, 231:833–836, February 1986.

[15] R. B. Stothers. The period dichotomy in terrestrial impact crater ages. *Monthly Notices of the Royal Astronomical Society*, 365:178–180, January 2006.

[16] R. G. Strom, R. Malhotra, T. Ito, F. Yoshida, and D. A. Kring. The Origin of Planetary Impactors in the Inner Solar System. *Science*, 309:1847–1850, September 2005.

[17] S. Yabushita. A spectral analysis of the periodicity hypothesis in cratering records. *Monthly Notices of the Royal Astronomical Society*, 355:51–56, November 2004.

68

Cancer from the Sky: Preventing Asteroids from Destroying Life on Earth

Rory Barnes

1 Introduction

Currently (as of September 20th, 2006) 4219 Near-Earth Objects (NEOs) are known [1], including 839 with a diameter larger than 1 km and 796 that are considered potentially hazardous to Earth. NASA is actively involved in decting the $\sim$ 1000 dangerous asteroids (objects that come with 0.05 AU of the Earth) by 2020 under the auspices of the Near-Earth Object Program. This pursuit is all well and good, but begs the question, "When we find the asteroid that will wipe out life on Earth, what the hell are we going to do about it?" Astronomers and planetary scientists could be responsible for informing every man woman and child of their death date, a dubious honor at best.

Although many of our colleagues enjoy rewarding careers studying asteroids, they are, nonetheless, the cancer of the cosmos. Like cancer, we know we might die from it, and early detection is critical to preventing them from having fatal consequences. Therefore, a plan is needed to save the Earth from this nuisance. Unfortunately there is no consensus on an appropriate course of action to save us, and most governments feel reluctant to commit the billions of dollars necessary to really prevent the devastation. Unlike cancer, the chances of regional or worldwide devastation from an asteroid in our lifetime is vanishingly small. However the possible ways to stop it are obvious, so let's figure out how to turn scientists into heroes!

2 The Celestial Mechanics of Asteroid Delfection

The first thing to remember is that the deadly asteroid is really just in orbit around the sun. Therefore we must change its orbital parameters with respect to the sun. There are several ways to do this: 1) push it with a rocket, 2) blow it to smithereens with nuclear weapons, 3) detonate a nuclear bomb next to it and let the subsequent radiation change the orbit, 4) ram something into it and hope for the best, 5) hitching a solar sail to the asteroid, 6) focusing

solar radiation onto the surface (somebody else on this field trip might know something about this), or 7) let the Earth do the work during an encounter prior to the collision (the lazy scientist's way out). Some of these options are good, some are bad and some are downright stupid. But which one is best?

In order to judge these possibilities, we must identify exactly what we need to do. The radius of the Earth is 4000 km, therefore we will need to change the position of an NEO by at most this much. Therefore let us adopt this distance as the minimum distance to safely save the Earth. The next most important item is how long do we have? An asteroid that will hit the Earth tomorrow would require an enormous impulse to move it $r_{crit} \equiv 4000$ km, but an object that will hit the Earth in 2106 doesn't need much of a nudge at all, a modified orbit will diverge from the dangerous one by an amount $\sim \Delta v \times t$. So when t is big, Δv can be small since r_{crit} is the same. For the sake of argument, let's assume that collision will occur in 20 years.

If an asteroid's speed could be altered by just 1 km/hr, then 20 years later, the asteroid's position would be changed by about 200,000 km. Clearly early detection is the key to preventing worldwide catastrophe. This seemingly small change, actually corresponds to a large amount of energy. A 1 km asteroid has a mass of 10^{13} kg. If we were to place a rocket on its surface and initiated a 1 hr burn, it would require 9.7×10^{10} N of force. For comparison, the solid rocket boosters of the space shuttle provide 3.25×10^7 N for 2 minutes. Therefore we would only need about 10,000 solid rocket boosters to effect this orbital change. This option falls in the "stupid" category.

Some of the options are based on non-gravitational effects, such as the Yarkovsky Effect [2]. The Yarkovsky Effect relies on differential radiative effects over the surface of the body. Since only one side of a body is illuminated by the sun, there is a net momentum change due to the radiation of photons from the surface. As you might expect, it takes a long time and a lot of photons to move a 1 km asteroid.

3 Options for Deflection

3.1 Nuclear Obliteration

Two options are available in this chemotherapy option: Surface or subsurface detonation. The major worry with this method is that the resulted pieces could still be deadly. Any piece greater than 35 m in size is still a threat (think Tunguska). So destruction would have to be total. Surface detontion would be cheaper, but if the asteroid is a rubble pile [3], then a considerable fraction of the energy could be absorbed during the crushing [4], see Fig. 1. Subsurface detonation is more likely to blast the rubble pile apart, but deploying a nucelar weapon to the center of an asteroid could be problematic. In both these scenarios, gravity could ultimately reassamble a signficant fraction of the asteroid (the cancer will have relapsed).
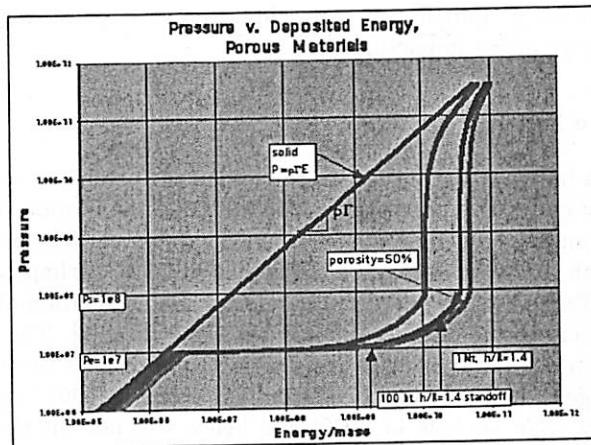
Fig. 1. The pressure in a body that has been instantly heated to a given energy per unit mass. In this model [4] additional energy from a nuclear explosion fails to increase pressure in a porous material. Without the additional energy, the particle will not vaporize and/or explode.

3.2 Radiative Deflection

The first option in this category still involves a nuclear device. If a nuclear weapon were detonated near an asteroid, but not so close to destroy it, the subsequent radiation field could induce a short-lived Yarkovsky Effect that could provide the requisite momentum. In principle a nuclear device could be as large as the amount of nuclear material that could be manufactured. Therefore an arbitrarily large radiation field could be generated.

Another option uses a mirror to deflect sunlight onto the surface of an asteroid to sublime any water ices that may be present on the surface [5]. This mechansism involves placing a mirror in orbit about an asteroid. The feasibility of such a method depends on the composition of the asteroid, but has the advantage that it launches mirrors into space, and does not involve a landing on the surface (not technologically difficult). It does, of course, require sufficient time for the deflection to be effective.

3.3 Kinetic Methods

A solar sail attached to the surface might provide the necessary momentum change to safe the Earth, but the size of the sail is enormous, and would have to be designed to always provide a force in the same direction, a tricky proposition on a rotating or tumbling body. A large mass could also be slammed into the asteroid, a lá *Deep Impact*. This would require precise modeling of the shape and rotation of the body, as well as an understanding of the tensile

strength of the body. Splitting the asteroid into several pieces might lead to one or more large pieces impacting the Earth.

3.4 Trust the Earth

Without multi-billion dollar initiatives to develop the preceding concepts, astronomers rely on precise observations to determine the motion of these asteroids in the multi-body environment of the Solar System (the homeopathic cure). Although an asteroid may be dangerous in 2036, perhaps a close approach to the Earth in 2029 will deflect the orbit. Determination of deflection relies on a precise orbit, usually defined by a "keyhole"[6]. The keyhole is a narrow region of space which, if the asteroid were to pass through, would critically change the probability of collision. For example, 99942 Apophis will miss its 400 m wide keyhole in 2029, and hence will not hit the Earth in 2036. Nonetheless, this asteroid will pass within the geostationary orbit of the Earth, and event that probably happens once every 1300 years [7].

3.5 Other Hair-Brained Schemes

How about sending miners to the asteroid to dig up and remove mass, and hence change the orbit (surgery)? What about putting a massive spacecraft near the asteroid and applying constant thrust to the spacecraft and let their mutual gravity interaction move the asteroid? Maybe we could cover the asteroid with a reflective coating to boost its Yarkovsky drift? They've been proposed, but probably would never be implemented.

References

[1] http://neo.jpl.nasa.gov
[2] Vokrouhlický, D. 1999 "Diurnal Yarkovsky effect as a source of mobility of meter-sized asteroidal fragments. I. Linear theory", *A&A*, **335**, 1093-1100
[3] Leinhardt, Z.M. et al. 2000 "Direct N-body Simulatons of Rubble Pile Collisions", *Icarus*, **146**, 133-151
[4] Holdsapple, K.A. 2002 "The Deflection of Menacing Rubble Pile Asteroids", Workshop, Scientific Requirements for Mitigation of Hazardous Comets and Asteroids. http://keith.aa.washington.edu/papers/mitigation.pdf
[5] Melosh, H.J., I.V. Nemchinov, & Zetzer, Y.I. 1994 "Hazards due to comets and asteroids", *Space Science Series*, Tucson, AZ: Edited by Tom Gehrels, M. S. Matthews. and A. Schumann. Arizona UP 111
[6] Milani, A. 2006 "Asteroid Impact Monitoring", *Serb. AJ*, **172**, 1-11
[7] http://en.wikipedia.org/wiki/99942_Apophis

The Rio Grande Rift

or, What Controls Rift Style

By: Mike Bland

Rift:

an elongate depression overlying places where the entire lithosphere has ruptured in extension.

Geography and Geology:

• One of the world's principle continental rift systems

• Runs from central Colorado, through New Mexico, into Texas and Chihuahua, Mexico: over **1000 km!**

• Series of asymmetrical grabens with as much as **6 km of structural vertical offset**.

• Part of a broad Region of "rift-like" late Cenozoic (last 30 million years) extensional deformation.

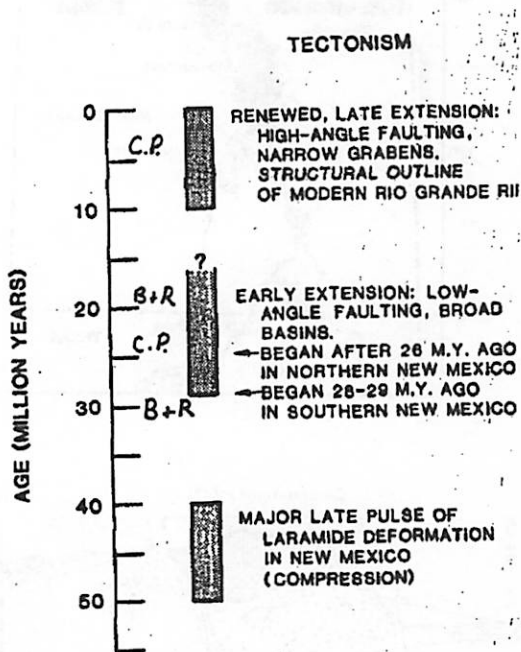• Part of the wide spread extensional event that formed the Basin and Range
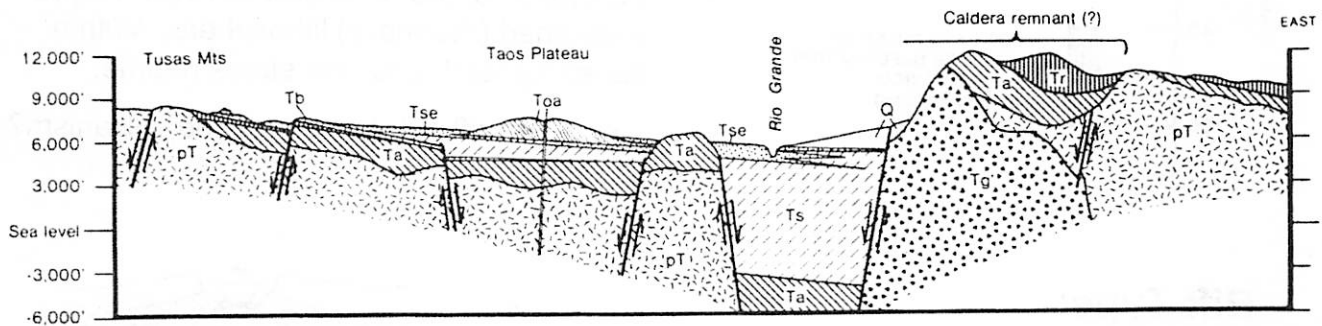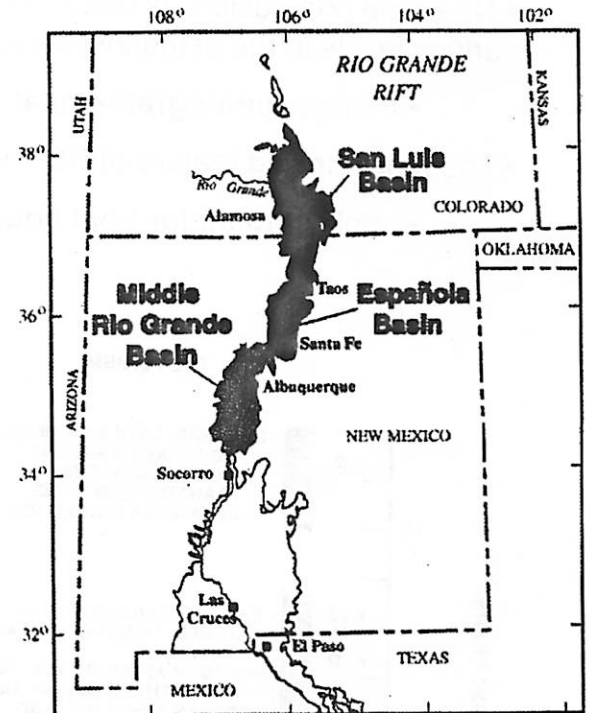
Geophysical Observations:

• Crust under the rift is thinned: depth to Moho is **~33 km** as opposed to 45 km under the Colorado Plateau and 50 km under the Great Plains – seismic profiles and gravity low

  • Suggests asthenosphere is in direct contact with the crust without any intervening mantle lithosphere.

• Abnormally **high crustal temperatures** - seismic velocities

• Mantle lithosphere deformation is distributed over a substantially greater lateral distance than the surface deformation.

Volcanism:

• Mostly **basaltic volcanism** from ~ 5 m.y. ago

• No single composition is dominant along the rift suggesting basalts were generated at various levels in the asthenosphere.

  • Implies **unintegrated heat source** with only local melting

• The most striking feature of RGR volcanism is that there really isn't any!!!

  • Implies **no major heat source** is associated with this rifting event.

TECTONISM

| AGE (MILLION YEARS)	
0	C.P. — RENEWED, LATE EXTENSION: HIGH-ANGLE FAULTING, NARROW GRABENS. STRUCTURAL OUTLINE OF MODERN RIO GRANDE RII
10	?
20	B+R — EARLY EXTENSION: LOW-ANGLE FAULTING, BROAD BASINS.
	C.P. — BEGAN AFTER 26 M.Y. AGO IN NORTHERN NEW MEXICO
30	B+R — BEGAN 28-29 M.Y. AGO IN SOUTHERN NEW MEXICO
40	MAJOR LATE PULSE OF LARAMIDE DEFORMATION IN NEW MEXICO (COMPRESSION)
50	

Rift Development:

• Rifting occurred in two phases:

  1. Early: low angle normal faulting throughout the rift area. Possibly involving up to 200% strain. – **Wide Rift**

  2. Late: High angle normal faulting producing large vertical offsets but low lateral strain. – **Narrow Rift**

• Formation of the rift seems to require a pre-weakened (thermally) lithosphere. With a superimposed tensional stress regime.

  • Pre-rift subduction related volcanism?

Rift Type:

• Rifts can (sometimes) be classified into either **a)** Active rifts, or **b)** Passive rifts.

• The RGR does fit either end member of the over-simplified "rift types"

• Delamination **(c)** may help explain some rift asymmetries.

• Rift Style Has Changed Over Time !!!

a) "ACTIVE"
b) "PASSIVE"
c) DELAMINATION

74

h = 40 km, Dry Quartz
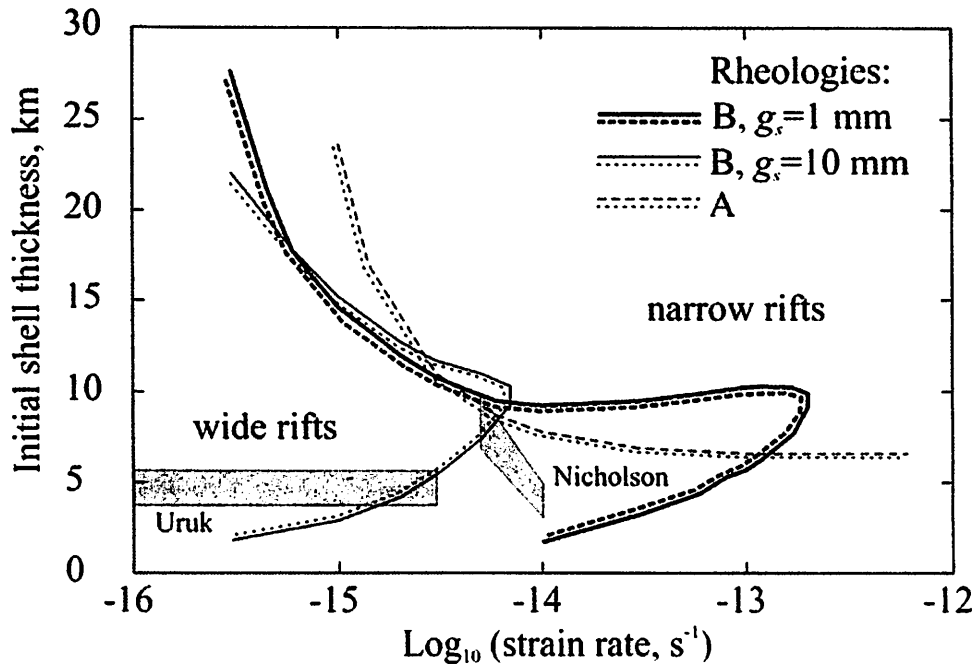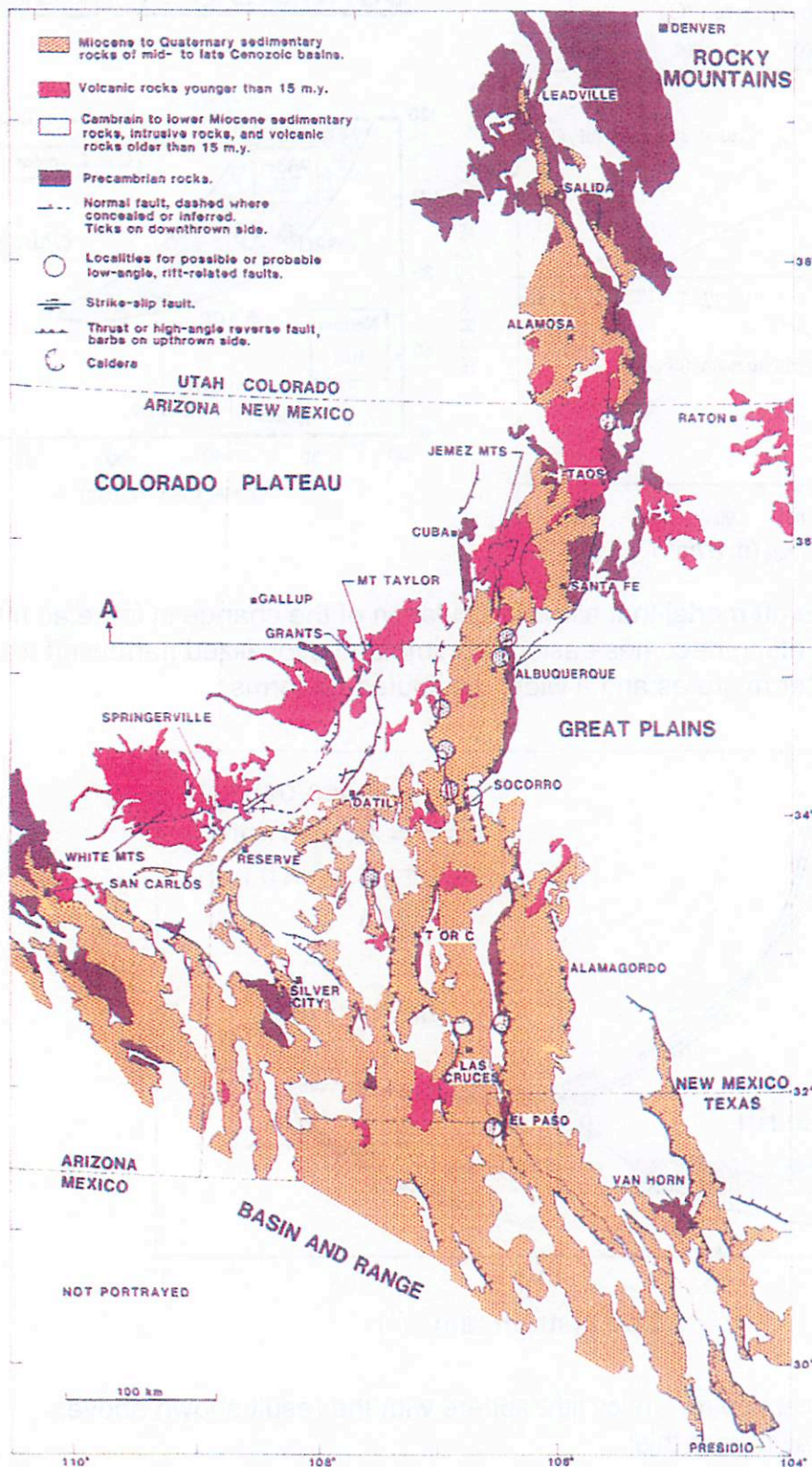
Moho Temperature (°C)
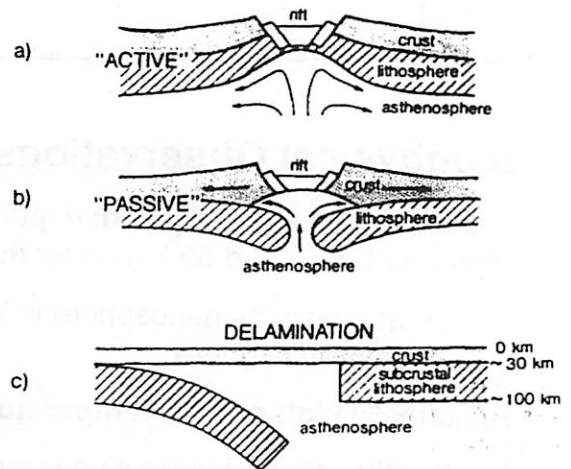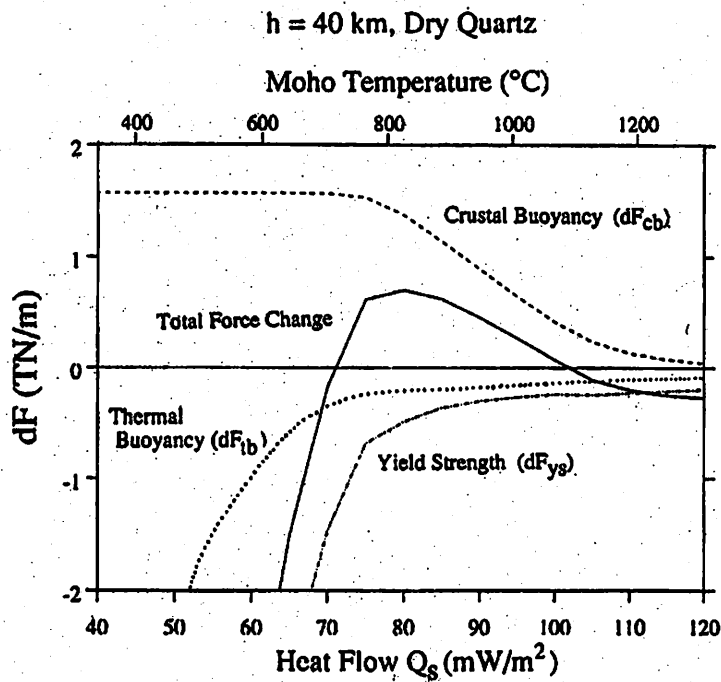
Controls on Rift Style:
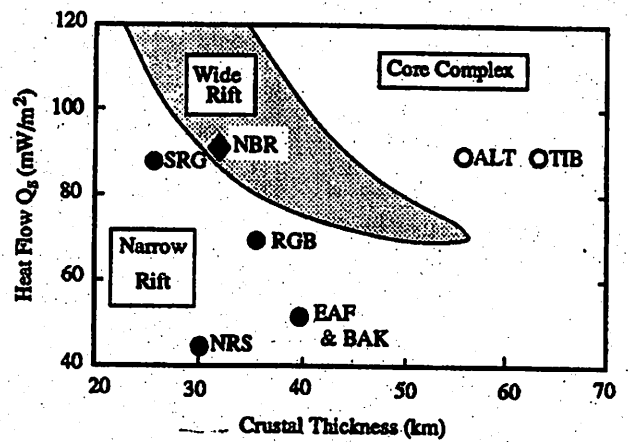
Buck (1991) developed a simple rift model that allows calculation of the change in force as rifting occurs. If the force decreases, rifting becomes easier with time and a localized narrow rift forms. If the force increases, the rift center migrates and a wide, distributed rift forms.

Nimmo (2004) repeated this exercise for an icy lithosphere with the result shown above. Several conclusions can be drawn from this:

• Narrow rifting (like Europa) is favored at large shell thicknesses or high strain rates and wide rifting (Ganymede) is favored at low strain rates.

• Implies that, at the time of rifting, shell thickness were probably larger on Europa than on Ganymede.

Legend:

- Miocene to Quaternary sedimentary rocks of mid- to late Cenozoic basins.
- Volcanic rocks younger than 15 m.y.
- Cambrian to lower Miocene sedimentary rocks, intrusive rocks, and volcanic rocks older than 15 m.y.
- Precambrian rocks.
- Normal fault, dashed where concealed or inferred. Ticks on downthrown side.
- ○ Localities for possible or probable low-angle, rift-related faults.
- Strike-slip fault.
- Thrust or high-angle reverse fault, barbs on upthrown side.
- C Caldera

Map labels: DENVER, ROCKY MOUNTAINS, LEADVILLE, SALIDA, ALAMOSA, UTAH COLORADO, ARIZONA NEW MEXICO, RATON, JEMEZ MTS, COLORADO PLATEAU, TAOS, CUBA, MT TAYLOR, SANTA FE, GALLUP, GRANTS, ALBUQUERQUE, SPRINGERVILLE, GREAT PLAINS, SOCORRO, DATIL, WHITE MTS, RESERVE, SAN CARLOS, T OR C, ALAMAGORDO, SILVER CITY, LAS CRUCES, NEW MEXICO TEXAS, EL PASO, ARIZONA MEXICO, VAN HORN, BASIN AND RANGE, NOT PORTRAYED, PRESIDIO

100 km

References:

Baldridge, W. A., K. H. Olsen, and J. F. Callender (1984). Rio Grande rift: Problems and Perspectives. *New Mexico Geological Society Guidebook, 35th Field Conference, Rio Grande Rift: Northern New Mexico.*

Basaltic Volcanism Study Project (1981). Basaltic volcanism on the terrestrial planets. Pergamon, New York.

Buck, W. R. (1991). Modes of continental lithospheric extension. *J. Geophys. Res.* **96**, 20161-20178.

Morgan, P. and M. P. Golombek (1984). Factors controlling the phase and styles of extension in the northern Rio Grande Rift. *New Mexico Geological Society Guidebook, 35th Field Conference, Rio Grande Rift: Northern New Mexico.*

Nimmo, F. (2004). Dynamics of rifting and modes of extension on icy satellites. *J. Geophys. Res.* **109**, E01003.

Olsen, K. H., W. S. Baldridge, and J. F. Callender (1987). Rio Grande Rift: An overview. *Tectonophysics* **143**, 119-139.

Wilson, D., R. Aster, M. West, J. Ni, S. Grand, W. Gao, S. Baldridge, S. Semken, and P. Patel (2005). Lithospheric structure of the Rio Grande Rift. *Nature* **433**, 851-855.

Map on page 1 courtesy of the USGS.

STRUCTURE OF THE CHICXULUB CRATER

by Priyanka Sharma

The structure of the Chicxulub crater has been actively investigated by potential field modeling, gravimetric and magnetic data analysis , seismic reflection and refraction surveys ,and drilling during the decade since its recognition as the crater responsible for mass extinction which terminated the Cretaceous Period .

In their cosmic hypothesis of 1980, Alvarez *et al.* had calculated from the amount of iridium dispersed around the globe that the source crater measured 150 to 200 km in diameter. In 1992, in order to better constrain the size and structure of the crater, Alan Hildebrand and geophysicist Mark Pilkington, compiled the existing gravimetric and magnetic data with seismic profiles across the basin , and the stratigraphic information provided by the C-1, S-1, Y-6 drill wells .
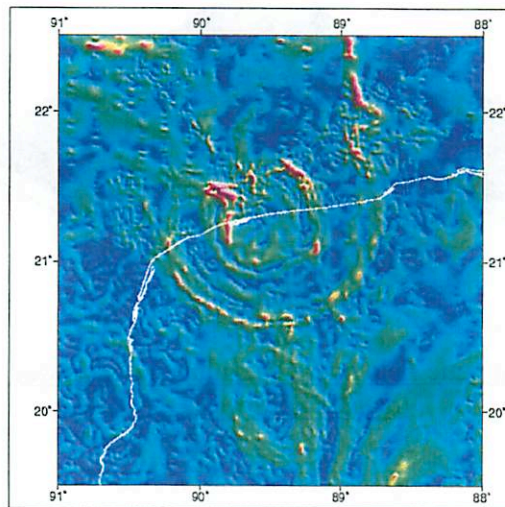
Horizontal Bouguer gravity anomaly
gradient over the Chicxulub crater.

Knowing the crater's size is necessary to quantify the lethal perturbations to the Cretaceous environment associated with its formation. The crater's size (and internal structure) is revealed by the horizontal gradient of the Bouguer gravity anomaly over the structure Horizontal gradient analysis of Bouguer gravity data objectively highlights the lateral density contrasts of the impact lithologies and suppresses regional anomalies which may obscure the gravity signature of the Chicxulub crater lithologies

Most prominent signature detected by Hildebrand et al. was the gravimetric signature of the crater . It showed a semi-circular outline, 180 Km. in diameter , opening up towards the north-west , in a horseshoe pattern (see figure 5.11). Gravity inside the crater was 30 milligals lower than the regional average, except for the very center of the structure where the gravity figures surged back up to a near absence of anomaly.

This bull's eye pattern is typical of impact craters and betrays the abnormal density of their rock units. Low gravity, 'negative' anomalies are believed to arise from the hundreds

of meters of shattered rock inside the impact basin: their density being lower than that of the surrounding, unbroken rock, one gets a lower reading for the local gravity field. As for the positive anomaly at the center of the structure, it is attributed to the uplift of dense basement rock close to the surface, that locally increases the gravity field.

The geometric center of the bull's eye pattern -and by inference of the crater itself-lies at 21.27°N and 89.60ow, near the small fishing village of Puerto Chicxulub. The southern half of the crater lies under the brush and agave plantations of the peninsula, while the northern half stretches under the shallow waters and sediments of the Gulf.

The periphery of the crater is highlighted by a string of cenote ponds , conspicuous in its south-western quarter . One interpretation is that the ring of cenotes is caused by a major fault –the crater's boundary fault –that intercepts the flow of groundwater of and causes it to upwell and undercut the surface .
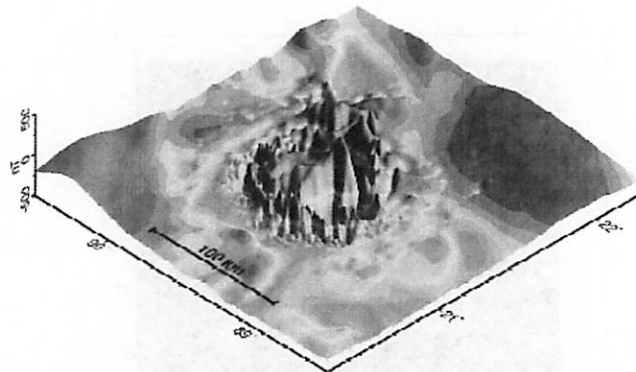
Three dimensional plot of magnetic field over Chicxulub crater viewed in perspective looking towards northwest .

Besides the gravity data which defines the overall geometry of the crater, the magnetic data further refines its structure by highlighting the boundaries of its buried impact melt. As it cools, molten rock indeed has the property of 'freezing' in place the magnetic field of the period. At Chicxulub, this 'ghost' field is all the more detectable in that the surrounding sediment is very weakly magnetized, which makes for a sharp contrast. Thus the central anomaly is clearly visible as a ring-shaped feature lying 20 to 45 km from the center of the crater. Processing the data shows that the source of the anomaly lies most likely at a depth of 1100 meters, which is indeed the depth at which impact melt shows up in the drill cores.
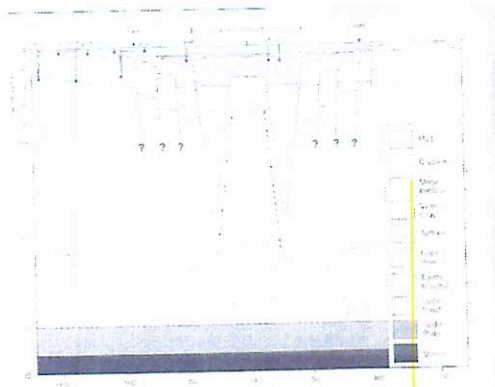
Figure 5.12 Cross-section of Chicxulub crater, constructed from well logs, cores and geophysical data. The vertical exaggeration is 8×. Exploratory wells by Pemex are drawn, as well as the inferred ring faults that bound the slump terraces (vertical lines with question marks). The model features a thick impact melt (hatched lines) covering the principal breccia units and the uplifted crustal rock. A ring of ejecta thins outwards, draping over the ring faults. (Courtesy of Mark Pilkington and Alan R. Hildebrand, Natural Resources Canada.)
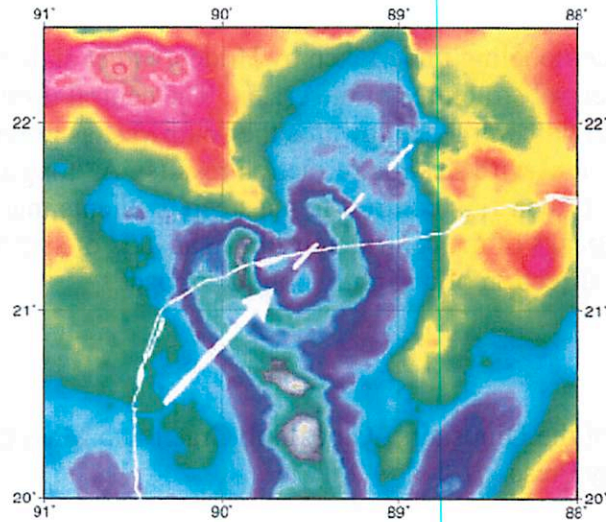
Gravity anomaly compilation over the Chicxulub crater; Bouguer gravity anomaly over land and free air anomaly offshore. Cool colours are lows, warm colours are highs; the coastline is indicated by a white line. White arrow indicates the direction of the non vertical motion of the impactor (from southwest to northeast).
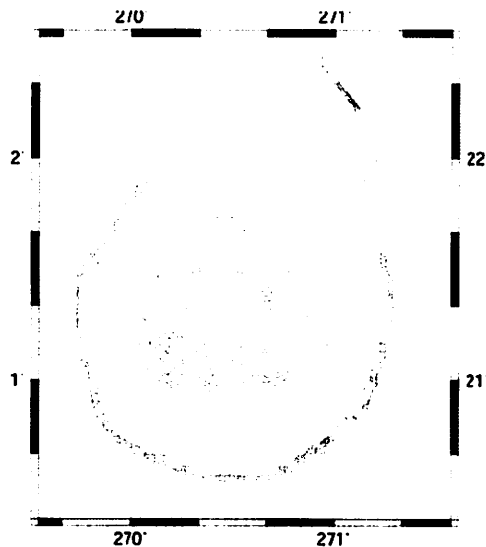
Results of 3D model calculation with same
colour convention.

The results of the 3-D modeling undertaken by Hildebrand et al. have been particularly informative for the central structures of the crater . The central uplift is revealed as a twin peaked structural high with vergence towards the southwest as previously indicated by 2D models and consistent with seismic refraction results . A "tongue" of the central uplift extends towards the northeast, in contrast to the steep gradients that bound it to the southwest. The twin peaks of the central uplift have an axis of symmetry oriented SW-NE, indicative of the direction of a slightly oblique impact.

References:

Frankel,C.,The End of the Dinosaurs –Chicxulub Crater and Mass Extinctions, Cambridge University Press

Hildebrand,A.R. ,Millar,J.D. , Pilkington, M .,2003. Chicxulub crater structure revealed by three-dimensional gravity filed modeling , Third International Conference on Large Meteorite Impacts, Nördlingen, Germany, abstract no.4121

Hildebrand,A.R. , Pilkington, M .,2003 . Three dimensional gravity field modeling of the Chixculub impact crater , Meteoritics & Planetary Science, vol. 38, Supplement, abstract no.5292

Hildebrand,A.R. , Pilkington, M ., 2001, Structure of the Chicxulub crater, International Conference on Catastrophic Events and Mass Extinctions: Impacts and Beyond, 9-12 July 2000, Vienna, Austria, abstract no.3153

Hildebrand,A.R. , Pilkington, M .,1995, Imaging the Buried Chicxulub Crater with Gravity Gradients and Cenotes , Meteoritics, vol. 30, no. 5, page 519

The History of the Santa Fe Trail
Ellen Germann-Melosh

Map Drawn by
Frank A. Cooper

Used with permission of
Velma Pauly
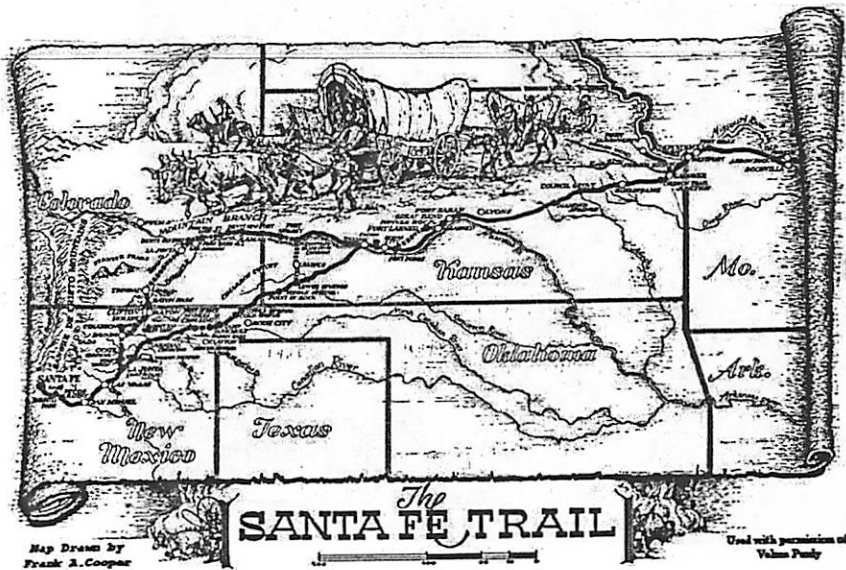
Between 1821 and 1880, the Santa Fe Trail was the main commercial "highway" connecting Missouri and Santa Fe, New Mexico. From 1821 until 1846, it was an international highway used by Mexican and American traders, since during these years Santa Fe was still part of Mexico.

During the Mexican American War of 1846 – 1848, the US Army of the West followed the Santa Fe Trail to invade the part of Mexico which eventually became New Mexico. When the Treaty of Guadalupe ended the war in 1848, the Santa Fe Trail became a national road connecting the United States to the new southwest territories.

In addition to commercial uses, the trial became the main passage for military freight to the southwestern forts. It was used as well during the gold rush by those seeking to make their fortunes in California and Colorado. People heading west to settle in the new southwest territories followed the route, making it the busiest route in the US during the years it was active.

In 1880 the railroad reached Santa Fe. Railroads provided easier and safer passage for both the people moving to settle the west and for the commercial transport, so the use of the trail began to fade into history.

A brief timeline for the Santa Fe Trail includes:

150 million years ago - Dinosaurs left footprints through what is now the Comanche National Grasslands

Pre 1540 – the Native Indian tribes established trade and travel routes along the trail

1540 – 1541 – Francisco Vazquez de Coronado explored from Mexico to Kansas

1601 – Juan de Onate spent 5 months traveling with wagons and artillery through the western plains

1739 – Paul and Peter Mallet made the first French trading venture to Santa Fe from Illinois

1792 – Pedro Vial traveled from Santa Fe to St. Louis for the Spanish government.

1821 – the Santa Fe Trail opened for legal trade between the US and Mexico with the welcome in Santa Fe of William Becknell's party from Missouri.

1825 – Senator Thomas Benton of Missouri arranged for the US government to survey the trail

1846 – US invaded Mexico – start of the Mexican-American War.

1848 – end of the Mexican_American War. The Treaty of Guadalupe Hidalgo resulted in almost half of Mexico's land being given to the United States, include what is today the state of New Mexico

1849 – 1852 – the Gold Rush in California increased the traffic on the Santa Fe Trail

1851 – Fort Union was established to help protect all travel on the Santa Fe Trail.